Investigation of the effects of drag reducing polymers on stratified flows

Ali Poursaeidesfahani

Master of Science Thesis

TU Delft Delft University of Technology

Investigation of the effects of drag reducing polymers on stratified flows

MASTER OF SCIENCE THESIS

For the degree of Master of Science in Mechanical Engineering at Delft University of Technology

Ali Poursaeidesfahani

August 18, 2014

Faculty of Mechanical, Maritime and Materials Engineering (3mE) · Delft University of Technology


TU Delft
Delft
University of
Technology


TNO
innovation
for life

DELFT UNIVERSITY OF TECHNOLOGY
DEPARTMENT OF
PROCESS AND ENERGY

The undersigned hereby certify that they have read and recommend to the Faculty of Mechanical, Maritime and Materials Engineering (3mE) for acceptance a thesis entitled

INVESTIGATION OF THE EFFECTS OF DRAG REDUCING POLYMERS ON STRATIFIED FLOWS

by

ALI POURSAEIDESFAHANI

in partial fulfillment of the requirements for the degree of

MASTER OF SCIENCE MECHANICAL ENGINEERING

Dated: August 18, 2014

Supervisor(s):

Prof.dr.ir. B. J. Boersma

Dr.ir. Jos van 't Westende

Pejman Shoeibi Omrani, MSc

Reader(s):

Dr.ir. C. Poelma

Dr. R. Delfos

Abstract

According to the increasing distance between the processing facilities and the oil and gas production sites, especially at subsea production sites (where multiphase flows commonly occur), innovative methods are demanded to help reducing the cost of multiphase flow transportation through the pipelines. In the past decades, Drag Reducing Polymers (DRPs) have been drawing attention in industry and academia. However, in these works it was predominately focused on single phase flows while limited attention was paid to multiphase flows.

In order to improve the understanding of the influences of the DRPs on horizontal stratified gas-liquid flows, a conventional air-water flow loop is used in this study. The "Conductance probes method" and flow visualization with high speed camera are used to examine the morphology of the gas-liquid interface. The conductance probe sensors and required electrical circuits are built as a part of this project. The stratified flow of gas and liquid provides the most suitable flow configuration to validate the equipment which was built to measure the time variations of the liquid film height. The effects of drag reducing polymers on stratified gas-liquid flows and particularly the effects of DRPs on the interfacial phenomena as the crucial characteristics of the stratified flows are discussed in this study.

Polyacrylamide with the molecular weight of 15000 kg/mol is used in this study. To get more insight on the rheological properties of polymeric solutions, the characteristics of solutions including static and dynamic surface tensions, dynamic and complex viscosities are measured. In order to find a link between these properties and the results obtained from the flow loop tests, the effects of polymer concentration on these properties are also investigated.

In this research the relevance of the gas and liquid flow rates to the drag reduction phenomenon is studied. The highest drag reduction observed in this study (about 55 percent) is obtained at the greatest liquid and gas superficial velocities. The maximum drag reduction of a stratified flow is compared with the one obtained from single phase flow of water.

Additionally, in this study it is tried to focus on the behavior of the interface between the gas and the liquid by adding polymers. Roll waves' frequency, velocity and shape as well as the influences of the drag reducing polymers on the roll wave's properties are discussed as well.

Finally a model is proposed to assess the drag reduction of stratified flows as a function of the changes in liquid holdup and the interfacial properties such as disturbances and the shape of the interface.

List of Symbols

Roman Symbols

Symbol	Description	Unit
a	Number of molecules in a single monomer	$[-]$
A	Cross-sectional area of the pipe	$[m^2]$
A_G	Cross-sectional area occupied by gas	$[m^2]$
A_L	Cross-sectional area occupied by liquid	$[m^2]$
D	Pipe diameter	$[m]$
D_G	Gas hydraulic diameter	$[m]$
D_L	Liquid hydraulic diameter	$[m]$
F	Force	$[N]$
f_{SG}	wall-gas fanning friction factor	$[-]$
f_{SL}	wall-liquid fanning friction factor	$[-]$
g	Gravitational acceleration	$[\frac{m}{s^2}]$
$G"$	Loss modulus	$[Pa]$
G'	Storage modulus	$[Pa]$
h	Liquid film thickness	$[m]$
Δh	Rms of liquid height fluctuations	$[m]$
h'	Modified rms of liquid height fluctuations	$[m]$
$\dot{m}_G$	Gas mass flow rate	$[\frac{kg}{s}]$
$\dot{m}_L$	liquid mass flow rate	$[\frac{kg}{s}]$
N	Number of repeating monomer	$[-]$
P	Pressure	$[Pa]$
r	Radius	$[m]$
T	Temperature	$[K]$
T_Z	Polymer relaxation time	$[s]$
S_G	Gas perimeter	$[m]$
S_L	Liquid perimeter	$[m]$
S_i	Interfacial perimeter	$[m]$
u_G	Gas actual velocity	$[\frac{m}{s}]$
u_L	Liquid actual velocity	$[\frac{m}{s}]$
u_{SG}	Gas superficial velocity	$[\frac{m}{s}]$

u_{SL}	Liquid superficial velocity	$[\frac{m}{s}]$
$U_{GS,2-D}$	Gas superficial velocity for transition to 2-D waves	$[\frac{m}{s}]$
$U_{GS,KH}$	Gas superficial velocity for transitional to long amplitude waves	$[\frac{m}{s}]$
u_τ	Friction velocity	$[\frac{m}{s}]$
u'	Streamwise velocity fluctuation	$[\frac{m}{s}]$
u_i^*	Frictional velocity at the interface	$[\frac{m}{s}]$
$\dot{V}_G$	Gas volume flow rate	$[\frac{m^3}{s}]$
$\dot{V}_L$	liquid volume flow rate	$[\frac{m^3}{s}]$

Greek Symbols

Symbol	Description	Unit
α_G	Gas holdup	$[-]$
α_L	Gas holdup	$[-]$
η^*	Complex viscosity	$[Pa.s]$
θ	Film wetted angle	$[rad]$
κ	Boltzmann constant	$[\frac{J}{K}]$
μ_s	Solution viscosity	$[Pa.s]$
ρ_G	Gas density	$[\frac{kg}{m^2}]$
ρ_L	Liquid density	$[\frac{kg}{m^2}]$
σ	Surface tension	$[\frac{N}{m}]$
τ_{WG}	Gas-wall shear stress	$[Pa]$
τ_{WL}	Gas-liquid shear stress	$[Pa]$
τ_i	Interfacial shear stress	$[Pa]$
$\overline{\tau_p}$	Polymer shear stress	$[Pa]$
v'	Normal velocity fluctuation	$[\frac{m}{s}]$
ω	Angular frequency	$[\frac{1}{s}]$

Abbreviations

Abbreviation	Description
DRP	Drag reducing polymer
DR	Drag reduction
FFT	Fast Fourier Transform
LDV	Laser Doppler Velocimetry
MDR	Maximum drag reduction
PAA	Polyacrylamide
PDA	Photochromic Dye Activation
PEO	Polyethylene Oxide
PIV	Particle Image Velocimetry
UCT	Ultrasound computerized tomography

Dimensionless groups

Dimensionless Group	Description
F_G	Gas densimetric Froude number
F_L	Liquid densimetric Froude number
Re_G	Gas Reynolds number
Re_L	Liquid Reynolds number
We_τ	Weissenberg number
X	Lockhart-Martinelli parameter

Contents

List of figures

Chapter 1: Introduction

The main focus of this chapter is on the formulation of the research and the objectives of this thesis. The first part is a description of the importance of the multiphase flows in the oil and gas industry as well as the motivations and goals of this study. The key concepts regarding the multiphase flows in horizontal pipes along with the classification of the stratified gas-liquid flow based on the shape of the interfacial phenomena are discussed in section 1.2. Thereafter, the scope of this work and the scientific questions are identified in section 1.3. Finally the methodology and the outline of this thesis are addressed in section 1.4 and 1.5 respectively.

1.1 Motivations and goals

In 1948 experiments conducted by Toms showed that the addition of 10 ppm of polymer (methyl methacrylate) into a turbulent flow of a Newtonian solvent (monochlorobeneze) can reduce the skin friction in pipe flow by up to 80%(Toms 1948). The oil and gas production industries have conventionally implemented the drag reducing polymers to reduce the pressure losses in the single-phase flows. The Trans-Alaska pipe line is one of the most famous examples of polymers' application in single phase flows. The drag reducing polymers were applied in the Trans-Alaska pipe line in 1979, where the flow rate has been increased by 32000 m^3 /d as a result of polymer addition(den Toonder 1996). DRPs have been considerably beneficial to increase the production rate and to reduce the frictional losses in single phase flows.

Oil-water-gas flows are common in petroleum production particularly when Enhanced Oil Recovery (EOR) techniques are used. These techniques may require injection of gas to reduce the well tubing static pressure (Gas Lift). It is usually neither practical nor economical to separate the oil-water-gas mixture at the production sites. Consequently, the multi-phase mixture is pumped through the pipelines to the separation/processing stations. The distance between the production sites and processing facilities are often many kilometers and the pressure drop of these pipelines is significant and an extremely cost effective item. Moreover, multiphase pipeline connecting remote wellhead platforms and subsea wells to the separation facilities are common features of offshore oil production in the North Sea. One of the greatest challenges in operating offshore production sites is reducing the pressure losses of the multiphase flow pipelines (Havre et al. 2000).

The increasing distance between the processing facilities and production sites, especially at subsea production sites, demands new methods to reduce the cost of the transportation. Although the DRPs are not specifically designed for the multi-phase flows, the use of DRPs in such applications could have some benefits. Besides, the effect of DRPs on flow regimes and required concentrations on an industrial scale are currently unknown and economic analyzes are impossible at this stage.

On the other hand, the pressure drop is not the only problem while dealing with multiphase pipelines. One of the most undesirable flow regimes in the transport lines is the slug flow. This flow pattern induces severe forces and stresses on the pipelines and downstream equipment. Large and rapid variations of flow rate and pressure in slug flow cause an unwanted flaring and reduces the production capacity. Moreover, severe slugging can even cause platform trip and plant shutdown.

Up until today, considerable effort has been spent in order to avoid problems associated with the slug flow. Examples of these works consist of installing slug catchers or increasing the size of the first stage separator to provide required buffering capacity. However, these solutions are inappropriate for compact separation units (Haandrikman et al. 1999). One solution could be to prevent or delay the onset of slug flow by applying the DRPs which could be helpful for reducing the mechanical stress fluctuation and the size and cost of equipment.

The benefits of using DRPs in existing systems include increasing the production, reducing the pipeline pressure for constant throughput and reducing the operational cost. The benefits of using the DRPs in multiphase pipelines can include preventing/postponing transition to slug flow as well as problems and damages induced by this flow regime in addition to the aforementioned merits.

There have been works in industry and in academia showing the benefits of using polymers to reduce the skin friction (mostly on single phase flows). However, there has not been a description explaining all of the aspects of drag reduction. Moreover, in industry the multiphase flows occur more regularly than the single phase flows do and the benefits of DRPs on the multiphase flows and underlying mechanisms for these benefits are not yet fully understood. All mentioned above provide a strong motivation to explore the effects of drag reducing polymers on the stratified gas-liquid flows and particularly the effects of DRPs on the interfacial phenomena as crucial characteristics of the stratified flows.

Therefore, the two goals of this study include: (i) increasing the understanding of the influences of drag reducing polymers on horizontal gas-liquid stratified flows and how they are affecting the pressure losses and fluctuations; and (ii) investigating the effects of drag reducing polymers on the interfacial phenomena and how these effects are related to the reduction observed in pressure losses and fluctuations.

1.2 Multiphase flows

Gas and liquid phases can adapt to a variety of geometrical configuration (known as flow patterns or flow regimes) in pipes. There are number of parameters that can play a role in determination of the flow patterns such as the volume flow rate of each phase, pipe characteristics (diameter, wall roughness, orientation and entrance condition)and fluid properties (density, viscosity and surface tension).

The flow patterns in horizontal pipes as the gas flux increases include:

1. Dispersed bubble flow, gas bubbles tend to flow at the top of the pipe.
2. Slug flow, long liquid slugs carry small bubbles and large gas pockets flow between the slugs.
3. Stratified flow, gas phase flows at top and liquid phase at the bottom of the pipe.
4. Annular dispersed flow, thin liquid film covers the entire perimeter of the pipe which is much thicker at the bottom due to the gravity.

Aforementioned flow patterns are presented in Figure 1.1:

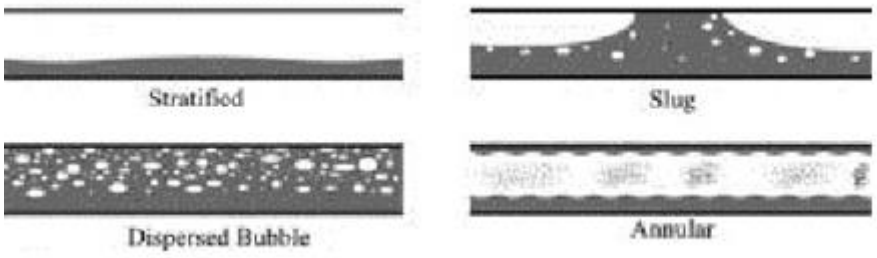

Figure 1.1: Representation of various flow patterns for gas-liquid flows in horizontal pipes

Lin et al. (1987) introduced another flow regime under the name "Pseudo-slug" where the disturbances have the appearance of slugs but they do not have the characteristic pressure fluctuations associated by the slugs. In contrast with the slugs, these disturbances do not travel with a velocity comparable to the gas phase velocity(Lin & Hanratty 1987).

As the pressure decreases towards the downstream of the line, the gas velocity increases along the pipe. Consequently, in long trunk lines used for simultaneous transportation of oil and gas all of the flow regimes may occur along the single pipe at the same time.

A flows pattern map is usually used to represent the boundaries between the various flow regimes. An example of a flow pattern map is introduced by Taitel and Dukler (1976) as shown in figure 1.2:

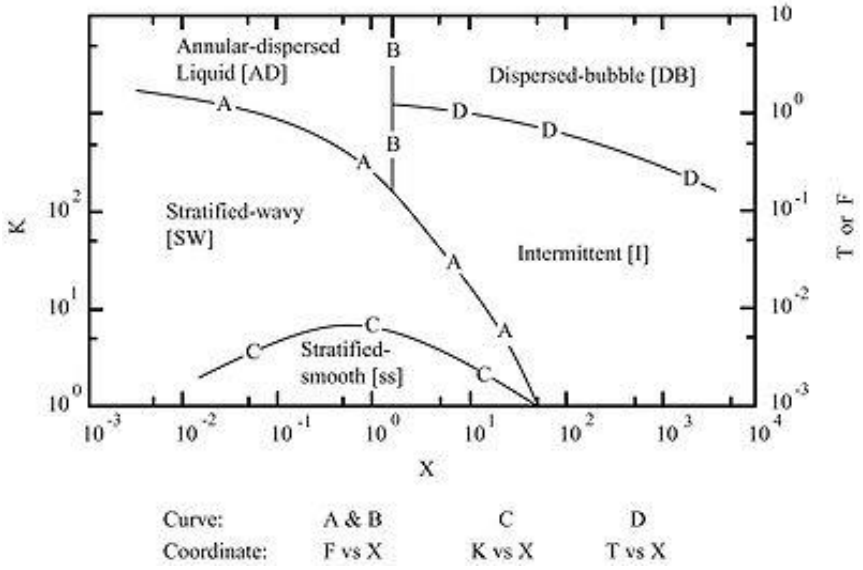

Figure 1.2: Taitel and Dukler flow pattern map.

Where the X on the horizontal axis is the Lockhart-Martinelli parameter defined as:

$$X = \left[\frac{(dp_F/dx)_{SL}}{(dp_F/dx)_{SG}}\right]^{1/2} = \left(\frac{f_{SL}F_L^2}{f_{SG}F_G^2}\right)^{1/2} \qquad Eq.1.1$$

In equation 1.1, f_{SG} *and* $f_{SL}$are wall-gas and wall-liquid fanning friction factors respectively and they are estimated from the Blasius equation or Poiseuille's law (see chapter 6). F_G *and* F_L are densimetric Froude numbers for two phases, which are defined by:

$$F_G = \sqrt{\frac{\rho_G}{\rho_L - \rho_G}\frac{u_{SG}^2}{gD}} \; and \; F_L = \sqrt{\frac{\rho_l}{\rho_L - \rho_G}\frac{u_{SL}^2}{gD}} \qquad Eq.1.2$$

Where ρ_G, ρ_L are the gas and liquid densities, and u_{SG}, u_{SL} are the gas and liquid superficial velocities. The superficial velocity is defined as the velocity which a phase obtains when flowing alone in a pipe:

$$u_{SG} = \frac{\dot{V}_G}{A} = \frac{\dot{m}_G}{\rho_G A} \; and \; u_{SL} = \frac{\dot{V}_L}{A} = \frac{\dot{m}_L}{\rho_L A} \qquad Eq.1.3$$

Here A is the cross-sectional area of the pipe.

As a result of slip between the fluids the local volume fraction of the liquid in the case of gas and liquid flow in a pipe is greater than that under the no-slip conditions. The lighter gas phase tends to flow much faster in comparison with the liquid phase. Hence, the liquid phase has a tendency to accumulate in horizontal pipes. As it is shown in figure 1.3, the liquid will occupy a part A_L of total cross section while the rimaining part A_G is avalable for the gas.

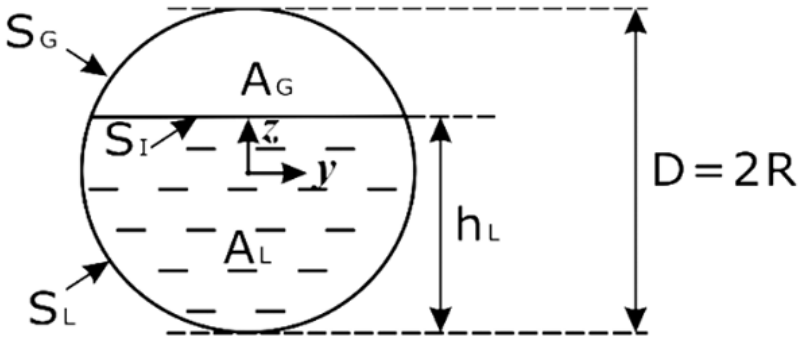

Figure 1.3: Representation of geometrical parameters for stratified gas-liquid flows in horizontal pipes.

The actual gas and liquid holdups (volume fraction) are shown by α_G *and* α_L and defined by:

$$\alpha_G = \frac{A_G}{A} \; and \; \alpha_L = \frac{A_L}{A} \qquad Eq.1.4$$

The average actual velocity of the gas and liquid are given by :

$$u_G = \frac{\dot{V}_G}{A_G} = \frac{\dot{V}_G}{A}.\frac{A}{A_G} = \frac{u_{SG}}{\alpha_G} \qquad Eq.1.5$$

$$u_L = \frac{\dot{V}_L}{A_L} = \frac{\dot{V}_L}{A}.\frac{A}{A_L} = \frac{u_{SL}}{\alpha_L} \qquad Eq.1.6$$

This study focuses on the stratified flow which is one of the typical flow regimes in horizontal wells and pipe lines connecting the offshore production wells to the onshore separator(Runge & Andersen 2007). Stratified flows can be further divided into different patterns based on the interfacial phenomena observed in each of them such as smooth stratified and wavy stratified. The precise predictions of stratified flow characteristics (e.g. liquid holdup, interface shape and

pressure drop) are not always possible. Andritsos et al. (1987) Provide the following classification for the observed sub-regimes of the stratified pattern in horizontal and nearly horizontal pipelines with respect to the interfacial behavior.

1. Smooth sub-region: when the gas and liquid superficial velocities are very low and the gas-liquid interface is smooth and flat.
2. Two-dimensional (2-D) wave region: in this region the gas-liquid interface is covered with small amplitude waves, also known as ripples. Ripples are periodic and distributed uniformly across the interface. Their amplitude and wavelength increase with the distance from the inlet. The required gas velocity for initiation of 2-D waves is highly dependent to the liquid viscosity. Greater liquid viscosity can shift the appearance of these disturbances to the higher gas superficial velocity. In this case the interface can still be considered flat.
3. Three-dimensional (3-D) waves, by further increase in the gas velocity the front of ripples will take a tortuous (or zigzag) shape. That is due to variation in the interfacial shear stress in crosswise direction. In this region as a result of wave spreading effect some liquid tends to climb up the pipe wall and a little curvature is seen at the interface near the pipe wall.
4. Large amplitude wave region, commonly known as roll waves: In this regime irregular roll waves with high amplitude and long wavelength can be observed passing the liquid film. Roll waves have a steep front followed by a long tail. Surface of roll waves are covered with smaller scale disturbances such as ripples. In this region much more liquid climb up the pipe wall and considerable concave down curvature is seen at the gas-liquid interface. This region was recognized even in early flow maps as the wavy region(Baker 1954).
5. Atomization (Entrained droplets) region, transition into this region is characterized by the observation of first droplet deposit on the top of the pipe. Droplets are separated from the crests of the large-amplitude waves. By increasing the gas velocity the liquid tend to spread more and more across the pipe perimeter and significant amount of liquid is transported by the gas phase in the form of droplet(Andritsos & Hanratty 1987).

Figure 1.4 represents the different sub-regions in wavy stratified gas-liquid flows.

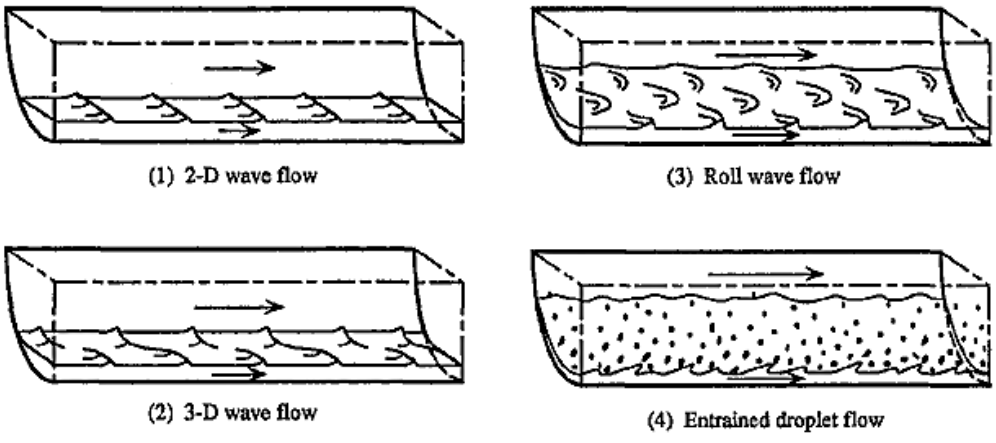

Figure 1.4: Sub-regions in wavy stratified gas-liquid flows (Cav & Brill 1997).

Similar to any other flow transition, the transitions between interfacial regimes in separated flows do not occur suddenly and at a completely defined condition but transitional zones are observed for each transition between the stratified flow sub-regimes. The height of the liquid waves increases by increasing the liquid flow rate and the transition to pseudo-slug and slug flow takes place when liquid waves touch the top of the pipe.

1.3 Scientific questions

Although the decline in the frictional losses after adding a minute amount of polymer to the pipe flow was observed for the first time by Toms in 1948 (Toms 1948), the underlying mechanisms for drag reduction are not completely understood yet. Exploring the benefits of the drag reducing polymers on multiphase flows (including the drag reduction and delaying the transition to slug flow), as well as finding the link between those and the flow properties provide the motivations to explore the effects of drag reducing polymers on the stratified gas-liquid flows. Aforementioned issues give rise to the following research questions:

- How different are the physical properties of the polymeric solutions (e.g. static and dynamic surface tension and complex and dynamic viscosity) as compared with water?
- How does the drag reduction change with the variation in the polymer concentrations and the gas and liquid flow rates?
- What are the influences of the drag reducing polymers on the interfacial disturbances and interfacial shear stress?
- In what ways are the roll waves influenced by the addition of drag reducing polymer?
- How different is the maximum drag reduction in the single phase and in the stratified gas-liquid flows?
- How can the drag reduction be explained by the observed changes in interfacial phenomena?

1.4 Methodology

In order to tackle the research questions of this study, at first some rheological measurements are conducted on the polymeric solutions with different concentrations in order to gain insight on their characteristics.

Furthermore, In order to explore the effect of drag reducing polymers on gas-liquid stratified flows, a conventional horizontal two-phase flow loop is designed and built. Three sets of conductance probes sensors along with their required electrical circuits are made and calibrated based on the method introduced by Koskie et al (1989). These sensors are verified with the high speed recordings (used to investigate the interfacial dynamics of stratified flows and the effects of DRPs on them) from the gas-liquid interface and used to gain information regarding the time variations of the liquid holdup.

Motivated by the experimental results, a model is developed to assess the contribution experimental findings to the drag reduction of the stratified flows.

1.5 Outline

Chapter 2 of this report addresses the literature study is performed about the drag reducing polymers and their applications in single phase and multiphase flows. Afterwards, the characterization of the polymer used in this experiment is presented in chapter 3, followed by a description of the experimental facility in chapter 4. The experimental results obtained in this work are presented in chapter 5. In this chapter explanation of the measurements' conditions and the method used to verify the sensors is presented. In the next parts of chapter 5 the drag reduction in stratified flows and the effects of different parameters on this phenomenon are discussed along with the effects of drag reducing polymers on the liquid height variations and wave dynamics. A recent model for prediction of the pressure drop in stratified flows is presented in chapter 6 and the measured pressure drops are compared with the values obtained by the model. Then this model is used to calculate the interfacial friction from the measured data. Chapter 6 is finalized by introducing a model based on the findings of this study to relate the changes in the interfacial phenomena to the drag reduction. Finally, conclusions of this study are drawn and recommendations for the future works proposed in chapter 7.

Chapter 2: Literature study

A literature review regarding the influences of drag reducing polymers on single phase flows and multiphase flows is presented in section 2.1. The most significant flow visualization techniques are reviewed in section 2.2. Finally the summary of the literature review and the relevance of this study are presented in section 2.3.

2.1 Drag Reducing Polymers

In this section the influences of the addition DRPs to the single phase and two phase flows are discussed and the relevant literature regarding the aforementioned subjects is briefly reviewed. A brief literature study on single phase drag reduction including the interactions between the polymers and turbulences, onset of drag reduction and the phenomenon of maximum drag reduction is provided in Section 2.1.1. The most recent scientific studies on the subject of drag reduction in gas-liquid flows are discussed in Section 2.1.2.

2.1.1 Single Phase flows:

2.1.1.1 Onset of Drag reduction

The drag reduction is defined by the percentual reduction of pressure drop due to the addition of polymer, at the same Reynolds number.

$$DR\% = \frac{\Delta P_N - \Delta P_P}{\Delta P_N} 100 \qquad \textit{Eq.2.1}$$

Suffixes 'N' and 'P' denote "Newtonian" and "polymeric" fluid, respectively. The onset of drag reduction is known as the point from which the pressure loss measured for the polymeric (non-Newtonian) solution deviates from the one for the solvent. The experimental works after Tom's discovery show that the underlying mechanisms for drag reduction involve dynamic interaction between the polymers and turbulence. There are two main evidences to support this hypothesis. First the laminar flow of polymeric solution has almost the same skin friction and pressure loss as the one measured for the Newtonian fluid and secondly the Reynolds number for which the drag reduction is observed for the constant pipe diameter is only dependent on the number of monomers at the long-chain polymer(type of polymer)(White et al. 2004).

Scaling analysis brought about the criterion that for the DR to occur, the relaxation time of the polymer should be greater that representative time scale of near-wall turbulence. Where the relaxation time of the polymer is defined as the time required by the stretched polymer to return to the coil configuration, defined as follows(Lumley 1948):

$$T_Z = \frac{\mu_s (N^{3/5} a)^3}{\kappa T} \qquad \textit{Eq.2.2}$$

Where N, a, κ, T *and* μ_s are the number of repeating monomer, the length of single monomer, the Boltzmann constant, the solution temperature and the solution viscosity respectively. According to equation 2.2 a higher molecular weight (the higher the number of repeating monomer or the longer the length of single monomer) results in a greater relaxation time of the polymer.

The representative time scale of the near-wall turbulence can be calculated as in equation 2.3(White & Mungal 2008):

$$T_T = \frac{\mu_s}{\rho {u_\tau}^2} \qquad \textit{Eq.2.3}$$

Where $u_\tau = \sqrt{\frac{\tau_w}{\rho}}, \tau_w \; and \; \rho$ denote the wall friction velocity, the shear stress at wall and the solution density. As it is presented in equation 2.3 the representative time scale of near-wall turbulences reduces by increasing the Reynolds number.

The above argument led to so-called time criterion for DR, stating that the drag reduction occurs when the ratio of the polymer time scale to flow time scale is greater than one this ratio is also known as the Weissenberg number :

$$We_\tau = \frac{T_Z \rho {u_\tau}^2}{\mu_s} > 1 \qquad \textit{Eq.2.4}$$

According to time criterion the onset of drag reduction is at lower Reynolds numbers for the polymers with greater relaxation times. Consequently, the effect of polymers with higher molecular weight can be observed at lower Reynolds number.

The lack of polymer concentration in time criterion is limiting its predictive capability. Experimental evidences proved that the onset of drag reduction systematically depends on the polymer concentration. The lack of well-known coupling between the turbulence and skin friction which is further coupled with the dynamics of long-chain flexible polymers has made the determination of exact mechanism of polymer drag reduction extremely difficult. There are currently two common approaches to explain the onset of drag reduction in details. The first one mainly focuses on the viscous effects of the polymers. It is argued that the vorticity field at the buffer layer is exactly suitable for the polymers to change their state from coil configuration to fully stretch. Stretching the polymers at the buffer layer (just outside the laminar sub-layer) results in significant increase in elongational viscosity leading to the extension of the buffer layer. This phenomenon can be seen as the laminarization of the flow at the near-wall region which brings about a reduction in skin friction(Lumley 1948). The advocates of this theory argue that the elongational viscosity will increase by increasing the polymer concentration.

Promoters of the second explanation believe that the strain rate at the buffer layer is high enough to stretch the polymers. However, it is fluctuating not only in time but also in space, consequently it can only cause the partial stretch of the polymers. The elastic theory predict the onset of the drag reduction when the cumulative elastic energy stored in polymers, as a result of partial stretch, becomes comparable with turbulent energy of some turbulence length scale larger than Kolmogorov scale. In this case the conventional Kolmogorov-type energy cascade will be terminated and the smaller scale turbulences will cut off and behave elastically(TABOR 1986). The advocates of this theory argue that the cumulative energy stored by polymers will increase by increasing the polymer concentration.

2.1.1.2 Drag reduction

For a Newtonian fluid the total shear stress for the turbulent flow is equal to the sum of the viscous shear stress and the Reynolds shear stress as it is illustrated in equation 2.5:

$$\tau_{(y)} = \mu_s \frac{d\overline{U}}{dy} - \overline{\rho u' v'} \qquad \textit{Eq.2.5}$$

Where, $\overline{\rho u' v'}$ is the Reynolds shear stress. $u', v'$are the streamwise and normal velocity fluctuations respectively and U is the average streamwise velocity.

For the polymeric solutions the experimental evidences show that the total shear stress is greater than the sum of the viscous shear stress and the Reynolds shear stress. This fact proves existence of another shear stress term for the case of polymeric solution called 'stress deficit' or in particular polymer shear stresses:

$$\tau_{(y)} > \mu_s \frac{d\overline{U}}{dy} - \overline{\rho u' v'} \qquad \textit{Eq.2.6}$$

$$\tau_{(y)} = \mu_s \frac{d\overline{U}}{dy} - \overline{\rho u' v'} + \overline{\tau_p} \qquad \textit{Eq.2.7}$$

Turbulence interacts with dissolved polymers in such a way that that additional stresses are introduced. Experiments of dilute polymeric solution show that $\overline{\tau_p}$ is equal to zero for laminar flows. The similar observations are noted in the laminar sub-layer of turbulent flows of dilute polymeric solution. However, just outside the laminar sub-layer finite values of $\overline{\tau_p}$ are measured. The addition of drag reducing polymers significantly reduces the Reynolds shear stresses and, in this way the total shear stress and consequently the friction losses are decreased(Warholic et al. 1999). It has been observed that the high shear stresses (above a certain threshold) at the buffer layer eventually break the polymers into smaller parts reducing their effectiveness. This process is known as the polymer degradation process.

The friction drag for the turbulent flow of Newtonian fluids can be predicted by Prandtl-Karman law. The onset of drag reduction can be defined as the point of departure from the Prandtl-Karman law for the polymeric solution. It has been noted that from this point, for a constant Reynolds number, increase in the polymer concentration results in increasing the drag reduction up to certain saturation value. The increase of the Reynolds number has a similar effect on the constant polymer concentration.

2.1.1.3 Maximum drag reduction (MDR)

The upper bound on drag reduction is known as Maximum Drag Reduction (MDR) or Virk asymptote(Virk et al. 1967). By increasing the Reynolds number or the polymer concentration the drag reduction is increased until it reaches its saturation value. The different trajectories of polymer drag reduction are shown figure 2.1:

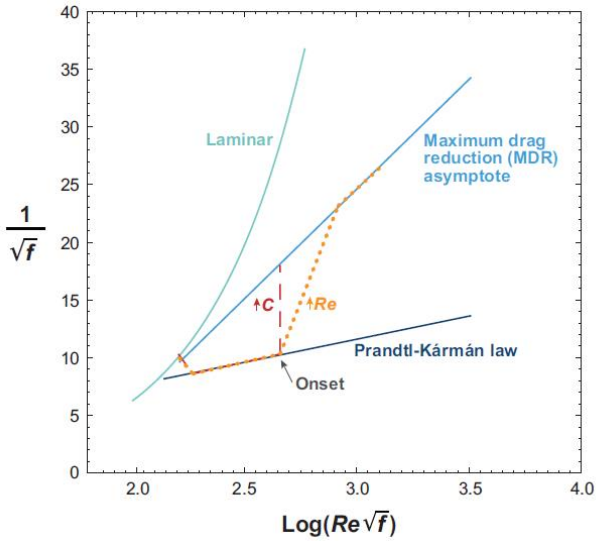

Figure 2.1: Schematic illustrations of the different trajectories of polymer drag reduction.

Due to the complexity of the interactions between the polymers and turbulence at different length scales, explanations for existence of certain bounding mechanisms for drag reduction remain mostly empirical and phenomenological. There are two hypotheses in this respect:

1. The maximum drag reduction occurs when the buffer layer is extended through the entire cross section. In the other words, the saturation limits on drag reduction is met when the effect of polymer is seen all over the cross section (Katerpallir & White 2000).
2. MDR occurs when the Reynolds shear stresses are mostly damped and the fluctuating polymer stresses are the main mechanisms that sustain the turbulence(Min et al. 2003).

These two theories have been constantly challenged by experimental observations. Polymer injection at the near-wall region showed high level of drag reduction close to the value expected by Virk asymptote while in this case the polymers are expected to stay mainly at the near-wall region and do not diffuse through the entire cross section(Fontaine et al. 2006).The prediction of MDR has had less success comparing to the prediction of onset of drag reduction.

2.1.2 Drag reduction in gas-liquid flows

As discussed in previous parts, in comparison with the single-phase flow, limited attention has been paid to the multiphase flows of polymeric solutions and academic works in this respect remains mainly experimental. A brief review of experimental works on the effects of drag reducing polymers on the gas-liquid flows is provided in this section to present the current status and advancements in the subject of DRPs on gas-liquid flows.

In one of the first experiments on gas-liquid drag reduction carried out by Oliver et al. (1668), Polyethylene Oxide (PEO) aqueous solution and air were used to investigate the characteristics of non-Newtonian liquid phase in slug and annular flows. They found out that the slug flow of polymeric solution has less circulation while the interface in annular flow is smoother(Oliver & A.Young 1968).

Polyhall295, polyacrylamide polymer is used to investigate the gas-liquid slug flow in 25 mm inner diameter pipe by Rosehart et al. (1972). In their experiments they kept the liquid Reynolds number constant and varied the gas Reynolds number. They concluded that the liquid drag reduction in gas-liquid can be greater than that of single phase liquid with the same superficial velocity. They separated the effect of liquid-wall friction and slug inertial on the total pressure gradient and noticed that in cases the slug inertia effect was greater than the liquid-wall friction effect (Rosehart et al. 1972).

Al-Sarkhi & Hanratty (2001) investigated the effect of Percol 727, a co-polymer of polyacrylamide and sodium-acrylate on annular water-air flow. They reached the drag reduction as high as 48% for concentration as low as 10-15 weight ppm. They also reported the change from annular flow to stratified flow for high drag reduction .They reported that high shear pump will degrade the polymers and should not be used to introduce the polymeric solution to the flow(Al-Sarkhi & Hanratty 2001).

Soleimani et ali. (2002) used an injection method to introduce a co-polymer of polyacrylamide and sodium-acrylate into the stratified water-air flow. They reported an increase in the average holdup, smoother gas-liquid interface and higher gas actual velocity and Reynolds number for same liquid and gas superficial velocities(Soleimani et al. 2002).

Al-sarkhi & Soleimani (2004) investigated the effects of addition of Percol 727, a co-polymer of polyacrylamide and sodium-acrylate on gas-liquid flow pattern map. Their experiments were

conducted in a 17 m long pipe with 25 mm inner diameter. They reported the change in flow pattern map and pressure drop occurs in almost all flow patterns. With their obtained results they suggested that maximum drag reduction occurs when the pseudo-slug, slug or annular flow is changed to stratified flow after addition of drag reducing polymers (Al-sarkhi & Soleimani 2004).

Daas & Bleyle (2006) studied the effects of drag reducing polymer on gas-liquid flow in 0.1 inner diameter pipe. They used two different type of oil with viscosity of 0.05 Pa.S and 0.0025 Pa.S as the liquid phase and carbon dioxide as the gas phase. They concluded that the difference between the pressure drops for the case with and without polymer was higher when the oil with higher viscosity (0.05 Pa.S) was used but the percentual drag reductions were greater when the less viscous oil was used(Daas & Bleyle 2006).

Fernandes et al. conducted an experimental work on the effect of drag reducing polymer on a two-phase vertical annular flow. The main motivation for this study was investigation of the possibility of using DRPs in high production rate gas-condensate wells where the friction is the limiting fact factor with respect to production rate. They concluded that addition of drag reducing agent can reduce the skin frictional component of total pressure drop up to 74%. However, the liquid holdup is increased in these cases resulting in an increase in the hydrostatic component of total pressure drop which reduces the effectiveness of DRPs in vertical gas-liquid flows(Fernandes et al. 2009).

Al-sarkhi et al. developed two correlations to predict the effect of drag reducing polymer on friction factor of gas-liquid and liquid-liquid flow for any pipe diameter. These correlations were verified for the air-liquid annular flow and oil-water flows in all flow regimes at the maximum drag reduction(Al-sarkhi et al. 2011). The obtained correlations and verification with experimental data are presented in figures 2.2 and 2.3:

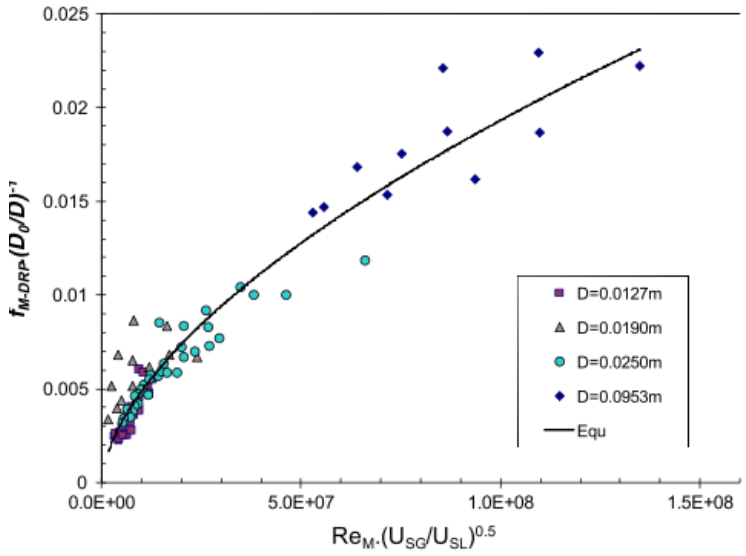

Figure 2.2: Fanning friction factor variation with the mixture Reynolds number times the square root of the superficial velocities ratio for different pipe diameters, D_0 = 0.0125 m (Al-sarkhi et al. 2011).

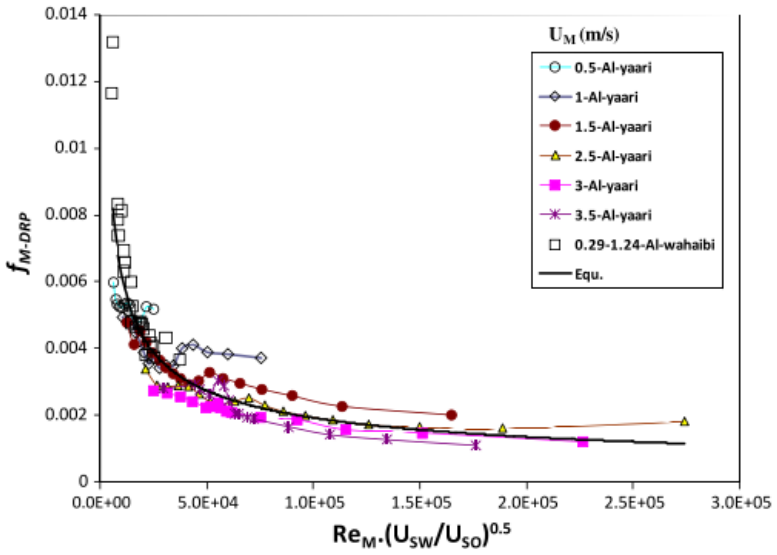

Figure 2.3: Fanning friction factor variation with the mixture Reynolds number times the square root of the superficial velocities ratio for different pipe diameters, oil viscosities and flow patterns(Al-sarkhi et al. 2011).

2.2 The-state-of the-art flow visualization methods

Considering the fact that the existence of waves can increase the interfacial shear stress dramatically in comparison with the smooth interface, sufficient understanding of the interfacial disturbances is required to assess the pressure drop in stratified flows. For quantitative investigation of liquid film topology an experimental method is required that can measure the liquid film thickness with high temporal and spatial resolution. In this section some of the proposed methods to investigate the gas-liquid interface topology in stratified flows are discussed.

2.2.1.1 High speed camera:

High speed cameras are widely used for observation and investigation of the flow patterns and large scale disturbances such as slugs and roll waves. An example of such investigations is the study of Al-Wahaibi et al. (2007) on the stratified oil-water flows. By using a light intensity filter in image processing it is possible to gain a black and white image (silhouette) with sharp separation between the liquid and gas, allows for measuring the exact position of interface. Yang et al. (2001) used high speed camera to investigate the gas-liquid flow pattern in small circular pipe. The main disadvantage of this method is the time consumption and difficulty of the post processing requiring complicated methods for image processing.

2.2.1.2 Conductance probes:

This method is based on the relation between the liquid film thickness and the electrical resistance of the fluid between the probes. It should be noted that the electrical resistance of water is a function of temperature and highly influenced by existence of impurities and especially ionic component. The probes are made of two thin parallel-wires stretched through the liquid film normal to the film flow direction. It is necessary to keep the wires taut and the wire spacing constant throughout the measurement. By the application of the parallel-wire probes method it is possible to measure the spatial average of the film thickness in the probe area(Koskie et al. 1989).

2.2.1.3 Ultrasound:

Ultrasound computerized tomography (UCT) is one of the important techniques by which it is possible to reconstruct the distribution of a gas/liquid two-phase flow over the cross-section of a pipe. It has been studied by several researchers since the early 1980s.Gia (1990) presented a circular transducer array involving multi-segment fan-shape beam transducers and an image reconstruction method based on judging the arrival or non-arrival of the transmitted pulse at a fixed time(Xu et al. 1997) (Gai 1990).

2.2.1.4 Photochromic Dye Activation (PDA):

A non-intrusive photochromic tracer technique can be used to visualize the instantaneous motion of the liquid in various two-phase flow regimes from near the pipe wall to the gas–liquid interface. In this measurement technique, a photochromic dye material is dissolved in a transparent liquid and irradiated with a beam of ultraviolet (UV) light. The dye molecules absorb the light's energy and temporarily change their molecular structure resulting a color change of the liquid containing the dye. It is a molecular tagging technique, so that there is no slip between the dye and liquid(Kawaji 1998).

2.2.1.5 Particle Imaging Velocimetry (PIV):

The technique of PIV (Particle Image Velocimetry) provides instantaneous whole field visualization in a plane of a flow field. This is achieved by projecting a plane of light into the flow. Two exposures are made to capture the images of particles within the plane using conventional photography. By measuring the distance between any pairs of particle double exposures, the velocity of the particle and therefore the fluid can be determined(Bryanston-Cross & Epstein 1990).

2.3 Summary

As presented in this chapter there is a limited understanding about the underlying mechanisms of drag reduction even in the single phase flows. There are some hypotheses about the onset of drag reduction and the maximum drag reduction in single phase flows. However, none of them can explain all of the aspects of these phenomena. The level of understanding is even lower about the gas-liquid flows and most of the scientific works on this subject are limited to observations. Several flow visualization techniques are presented to study the interfacial phenomena in stratified gas-liquid flows. Amongst the aforementioned methods, the high speed camera and conductance probes methods are chosen for application in this study. The main criteria for this selection include simplicity, high temporal and spatial resolution, safety, and feasibility. On the upcoming chapters an attempt is made to find the link between the observed drag reduction and changes in the interfacial phenomena. This could be the next step towards understanding the mechanisms of drag reduction in gas-liquid flows.

Chapter 3: Polymer Characterization

In this chapter the material and rheological properties of the polymeric solution used in this study are presented .The general information regarding the type of the polymer and the mixing method used to produce the solution are explained in section 3.1. Thereafter, the rheological properties of the solutions with different concentrations are discussed in section 3.2. The Static and dynamic surface tensions of the polymeric solution are compared with water in section 3.3 and finally a summary of the results obtained in this chapter along with the main findings are presented in section 3.4.

3.1 Polyacrylamide

Polyacrylamide with a molecular weight of $(15 \times \frac{10^6 g}{mol})$ is used in this experiment. Polyacrylamide is not toxic and it is highly water-absorbent. This kind of polymer showed considerable resistance to the mechanical degradation as a result of high shear stress. The powder of the polymer used in this work is produced under the commercial name "Superefloc A 110" by CYTEC.

The master solution is made by mixing a specific amount of (5 g) of Superfloc A 110 into the specified amount of tap water (495 g) to create the solution with a concentration of 1000 ppm by weight. Then by diluting the master solution with certain amount of water it is possible to make the polymeric solutions with any concentration lower than 1000 ppm. The process of making the master solution includes gently mixing the polymer powder with water. In order to prevent polymer degradation the lowest possible rotational speed for the mixer is selected and the mixture is stirred for about 12 hours to obtain a homogeneous solution.

3.2 Viscosity

Lin and Hanratty(1986) showed that the effect of viscosity cannot be ignored while dealing with long waves. They predicted the transition to slug flow by determining the condition in which small amplitude long wavelength disturbances introduced at the gas-liquid interface become unstable and can grow until they cover the entire cross section of the pipe and form slugs. They considered the viscous effect in their calculations and their prediction showed sufficient precision in comparison with experimental data. They conclude that higher viscosity postpones the transition to slug flow to the higher liquid velocities(Lin & Hanratty 1986).

As a result the viscous effects are considered to play an important role in initiation of the long amplitude waves. Consequently, any difference in the viscosity of the polymeric solution and water can be used to explain the different interfacial phenomena observed after the addition of the polymers to the stratified gas-liquid flows.

3.2.1 Dynamic viscosity

The addition of a limited amount of long chain molecules such as polyacrylamide to the water changes the Newtonian properties of the solvent and brings about considerable non-Newtonian behavior. A Newtonian fluid has a constant viscosity at any shear rate. The viscosity of the polymeric solutions are measured at different shear rates (with a rotational cylinder rheometer) to investigate the effect of the shear rate on solutions' viscosity. The viscosity of the

polymeric solutions with different concentrations at different shear rates and stresses are shown in figures 3.1 and 3.2 respectively:

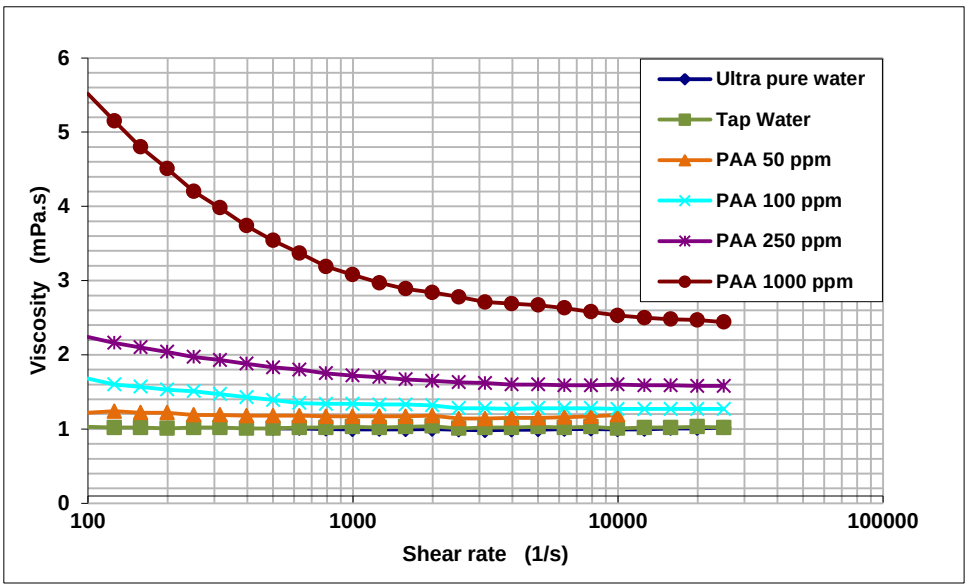

Figure 3.1: Viscosity as a function of shear rate for different polymeric solutions.

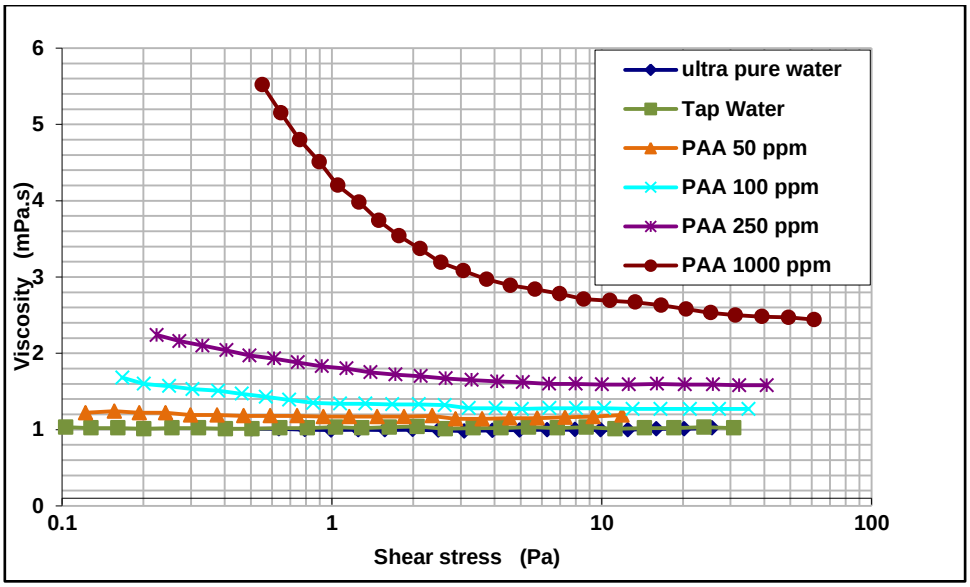

Figure 3.2: Viscosity as a function of shear stress for different polymeric solutions.

As shown in figures 3.1 and 3.2 the viscosity of the polymeric solution increases by increasing the concentration. On the other hand, the viscosity of the polymeric solution decreases by increasing the shear rate. This phenomenon is known as “shear thinning” which is an indication of the deviation from the Newtonian behavior. When the shear rate approaches to infinity, the viscosity of the polymeric solution approaches the viscosity of water at that temperature regardless its concentration.

3.2.2 Complex viscosity

As discussed in chapter 2, the polymeric solutions tend to show an elastic behavior. Promoters of elastic theory believe that this is the most important characteristic of polymers in their interaction with turbulences. The complex viscosity is an adequate measure to examine the viscoelastic behavior of the polymeric solutions.

The complex modulus is defined as the total resistance of the fluid to the deformation, regardless whether this deformation is recoverable (elastic) or non-recoverable (viscous). Complex modulus is a property of fluid directly quantifying the rigidity of a material. As a result, it is an adequate indicator of the flexibility and the stiffness of a fluid. The complex modulus is consisting of the storage modulus (G') (imaginary part) and loss modulus (G") (real part). The storage modulus is a measure of the energy stored in a material and loss modulus is a measure of the energy dissipated in a material. The complex viscosity is defined as the complex modulus divided by the angular velocity. The relation between the complex viscosity and storage modulus (G') and loss modulus (G") is presented as following:

$$|\eta^*| = \sqrt{\left[\frac{G'}{\omega}\right]^2 + \left[\frac{G''}{\omega}\right]^2} \qquad \textit{Eq.3.1}$$

Where: ω is the angular frequency (Hz).

When the storage modulus is zero, the complex and dynamic viscosities are equal. The viscoelastic properties (complex modulus) of a material are measured in an oscillation test. Oscillation is the technique whereby a sinusoidal stress or strain is applied to the fluid. In this manner, the sample is continuously excited. In case of the overstraining the sample, the elastic structure will be destroyed and this can be noticed by a sharp drop in the elastic modulus. While the sample structure is maintained, the complex modulus is constant; when the applied stress becomes too high, breakdown occurs and the modulus decreases.

The measured complex viscosity along with the storage and loss moduli for different polymer concentrations are presented in figures 3.3 to 3.4:

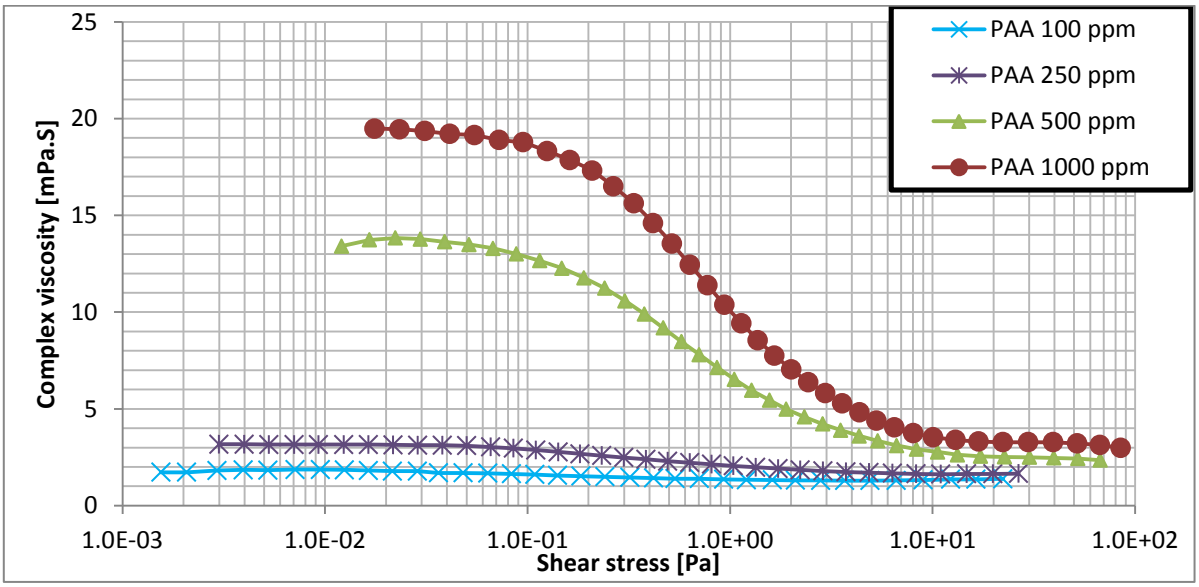

Figure 3.3: Complex viscosity as a function of shear stress for different polymer solutions.

It is not possible to measure the complex viscosity of water with oscillatory test due to its low viscosity and lack of structure. The results for 50 ppm solution were unrepeatable; consequently they are not shown in figure 3.3. As it is shown in figure 3.3 complex viscosities of polymeric solutions are greater than their dynamic viscosity and that is because of the existence of the storage modulus. By comparing figures 3.3 and 3.4 it is concluded that the proportion of storage modulus increases by increasing the concentration. This can be interpreted as a more robust structure that polymers form in solution.[1]

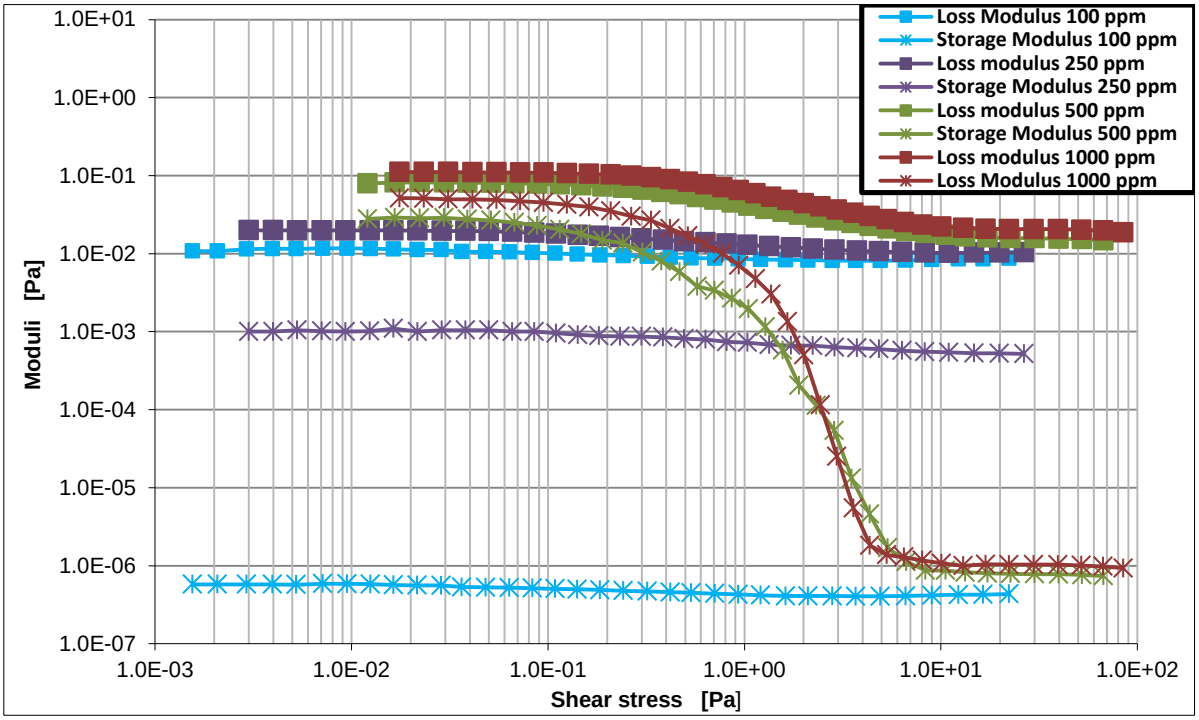

Figure 3.4: Storage and loss modulus as a function of shear stress for different polymer solutions.

As shown in figure 3.4, there is a sharp decrease in the elastic modulus of polymeric solutions with high concentrations (500 ppm, 1000 ppm). The most interesting point about this measurement is that although the elastic modulus of the solutions with lower concentrations (250 ppm, 100 ppm) is less than the same component for higher concentrations (500 ppm, 1000 ppm), it remains roughly constant for the whole range of shear stresses.

3.3 Surface Tension

Surface tension is one of the most important parameters when dealing with flow instabilities. The formation of waves in an inviscid flow is traditionally explained with Kelvin-Helmholtz instability theory. In this theory the gravity and surface tension are considered as the stabilizing forces while the inertia is known as the destabilizing force. Consequently any difference in the surface tension between the surface tension of the polymeric solution and water can be used to possibly explain the different interfacial phenomena observed after addition of polymers to the stratified gas-liquid flows.

[1] These measurements are conducted at a constant frequency of 1 Hz.

In order to compare the surface tension of water with of the polymeric solutions with different concentrations, first the well-known du Noüy ring method is used to measure the static surface tension. This method along with the results obtained from the measurement is explained in part 3.2.1. Then the dynamic surface tensions are measured by bubble pressure tensiometer (section 3.2.2).

3.3.1 Static surface tension (du Noüy ring method)

This method was proposed for the first time by Pierre Lecomte du Noüy in 1925. The method consist of immerging a platinum ring with extremely precise geometry into the liquid, Then slowly lifting it out of the fluid the fore on the ring is measured while it is raised from the liquid surface. This force is related to the liquid surface tension according to equation 3.2:

$$F = 2\pi(r_i + r_o)\sigma \qquad Eq.3.2$$

Where $F, r_i \; and \; r_o$ are the required force for lifting the pelatinum ring, inner and outer radius of the ring respectively.σ denotes the surface tension of the liquid. The schematic representation of the du Noüy ring is presented in figure 3.5:

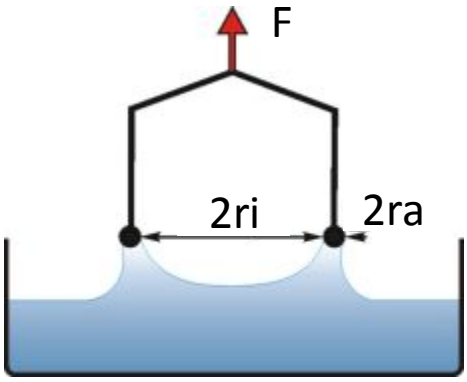

Figure 3.5: Schematic representation of du Noüy ring device.

In order to calibrate the equipment, first the surface tension of the ultra-pure water was measured and then it was compared with the available data in literature for the measurement temperature[2]. Afterwards, the surface tension of the tap water and polymeric solutions with high concentrations (250 ppm and 1000 ppm) are measured. Each measurement takes place twice to ensure the repeatability of the results. The results of the static surface tension measurements with du Noüy ring method are presented in figure 3.6:

[2] All the measurements in this section are conducted at the temperature of 23° C.

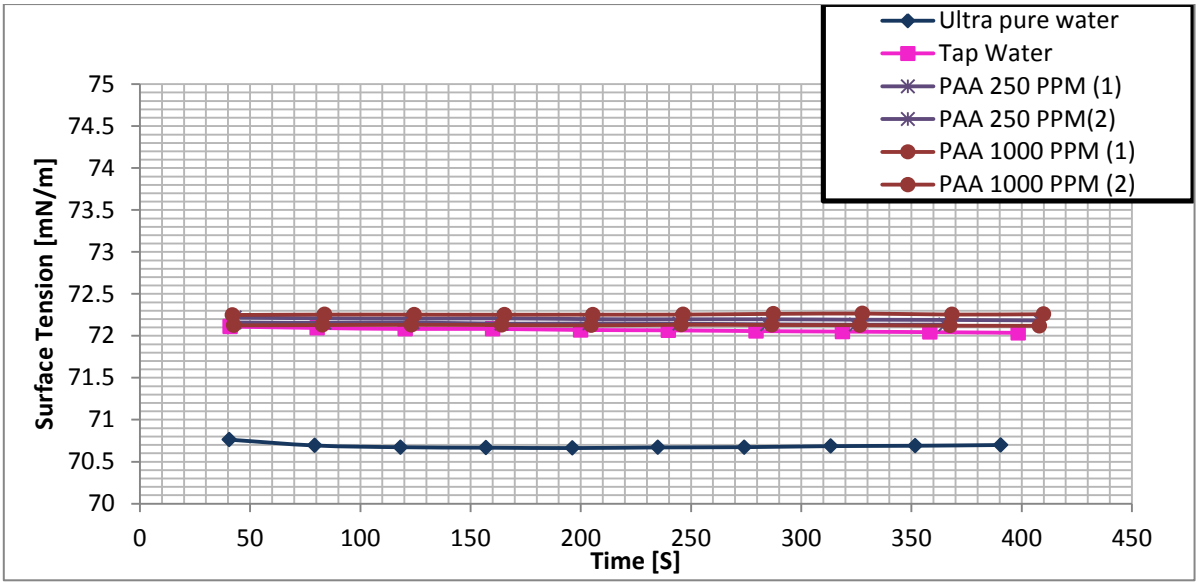

Figure 3.6: Comparison between static surface tension of polymeric solutions with different concentrations.

As shown in figure 3.6, the value measured for the surface tension of the polymeric solution even at the high concentrations is similar to the values obtained for tap water. These measurements show that the addition of polymers even with a high concentration of 1000 ppm does not influence the static surface tension.

3.3.2 Dynamic surface tension

When polymers are added to the flow certain time is required for the surface to reach the static equilibrium state. Since in the gas-liquid flows -as a result of dynamic interaction between the two phases- the interface is produced considerably fast, there may not be enough time for the molecules to reach their equilibrium configurations. Consequently, the surface tension measurements based on dynamic equilibrium could be used for taking the effect of surface age into account. In the dynamic surface tension measurement the surface is made at different rates and the value of surface tension is measured for each surface age separately. The value of dynamic surface tension strongly depends on the mobility of the polymer molecules in water.

Bubble pressure tensiometer is used to compare the dynamic surface tension of water with polyacrylamide solutions with various concentrations. The method is based on the measurement of the maximum internal pressure of a bubble as it grows with different rates.

The "Young-Laplace" equation states that the internal pressure of the spherical bubble is a function of the surface tension of the fluid and the radius of the bubble:

$$P = \frac{2\sigma}{r} \qquad Eq.3.3$$

By producing a gas bubble at the tip of a capillary, the curvature increases at first and then after reaching a certain value it decreases. The internal pressure reaches its maximum when the curvature has its maximum value. As it is shown in figure 3.7 the maximum value for curvature occurs when the diameter of the gas bubble is equal to the inner diameter of the capillary:

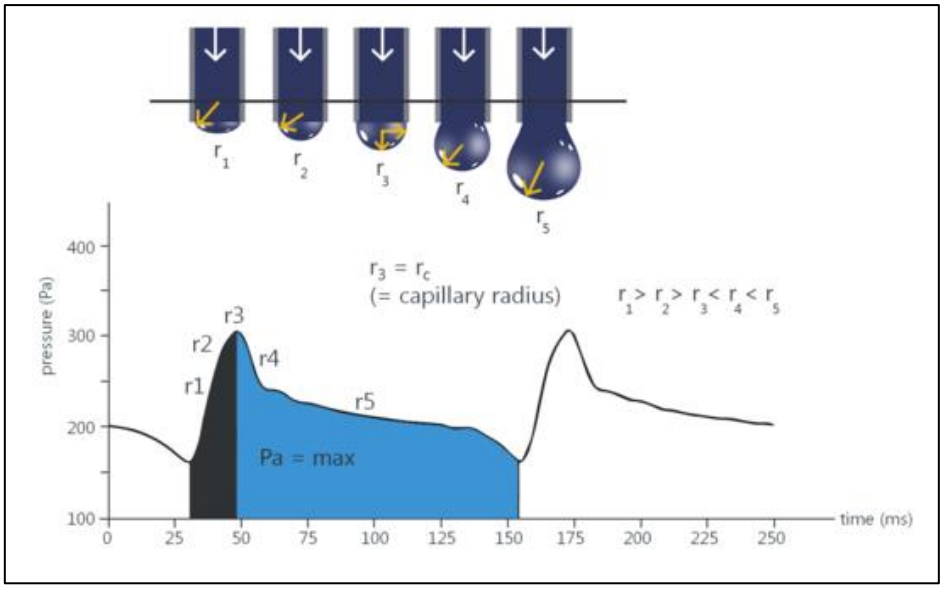

Figure 3.7: Pressure characteristic for bubble pressure measurement.

By knowing the capillary diameter, the surface tension can be calculated for measuring the maximum internal pressure of the bubble. Since the capillary is immerged in the liquid, as it is presented in equation 3.4, the hydrostatic pressure of the liquid above the capillary should be subtracted from the measures of internal bubble pressure.

$$\sigma = \frac{(P - P_0) r_{cap}}{2} \qquad Eq.3.4$$

The measured dynamic surface tension corresponds to the certain surface age which is defined as the time from the formation of the bubble to occurrence of maximum pressure. The surface age is controlled by the gas flow rate into the gas bubble. The results of the dynamic surface tension measurements with bubble pressure tensiometer are presented in figure 3.8.

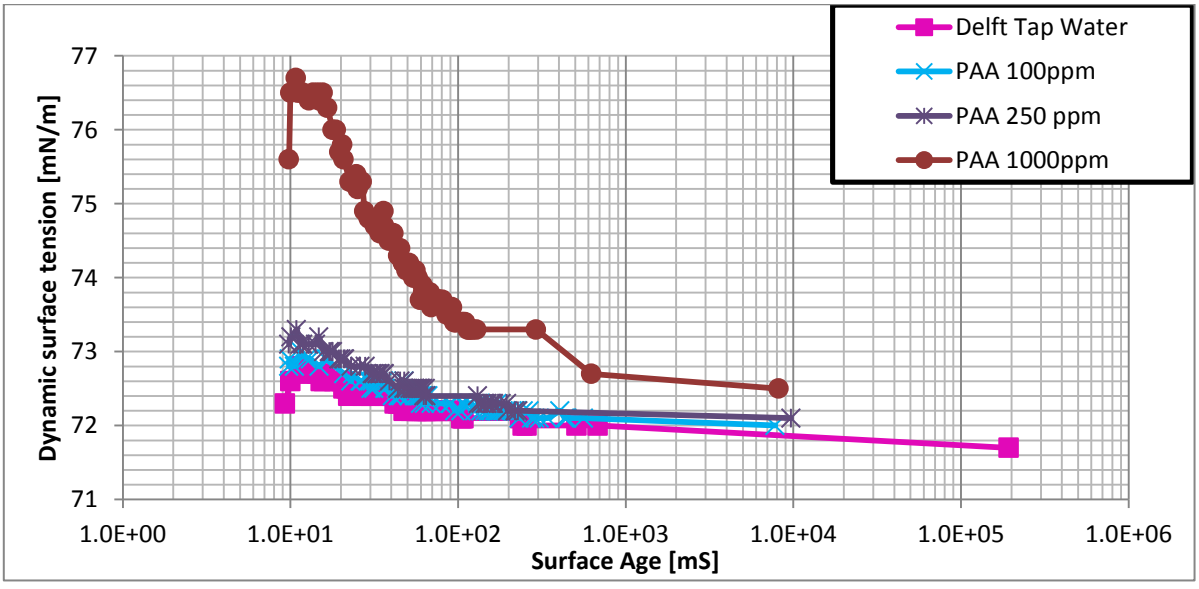

Figure 3.8: Comparison between dynamic surface tension of polymeric solution with different concentrations.

As it is illustrated in figure 3.8, dynamic surface tension increases by increasing the polymer concentration. The effect of addition of the polymer is only clearer when the polymer concentration is high (1000 ppm). By increasing the surface age the dynamic surface tension of polymeric solutions approaches the static surface tension of water. Such a behavior may exist due to a certain time that is required for the surface to reach its static equilibrium configuration.

3.4 Summary and conclusions

The dynamic viscosity of the polymeric solution rises by increasing the polymer concentration. In contrast with the Newtonian fluids, polymeric solutions show the shear thinning behavior (see section 3.2.2). The Addition of polymers to water results in a viscoelastic behavior proving that the polymer molecules are capable of storing and then releasing the energy after an applied shear force is removed. There is a congruency among a group of scientists that the viscoelastic behavior of polymers is the main reason for the interactions between the polymers and turbulences (in single phase flows) resulting the drag reduction. Damping of the wave turbulences and the turbulences at the liquid phase might also be a mechanism for the drag reduction in stratified flows.

A portion of energy that is stored by polymers is measured by storage modulus and a part of energy which is dissipated is measured by loss modulus. The viscoelastic behavior of the polymeric solution is a function of the shearing cycle frequency and the polymer concentration. In this study the viscoelastic behavior of the polymeric solutions has been examined at a frequency of 1 Hz. More solid conclusions can be drawn when the similar measurements are conducted at the frequencies corresponding to different turbulent scales.

The static surface tension of water is not considerably affected by the addition of the polymers. However, when the surface is formed quickly there is a clear difference between the surface tension of water and polymeric solution with a high polymer concentration (1000 ppm).

The influences of the addition of polymers on the dynamic surface tension are only considerable when the polymer concentration is higher than 250 ppm. Consequently, it could be argued that for the polymeric solutions with concentration lower than 250 ppm the effect of the addition of polymers on surface tension is negligible. Hence, for these polymer concentrations the contribution of the changes in surface tension to drag reduction in stratified flow is negligible.

The drag reduction in stratified flows with polymer concentrations of 20-100 ppm is investigated in chapter 5.

Chapter 4: Experiment Setup

In this chapter a description of the conductance probes method, implemented to measure the liquid film thickness is shortly explained in section 4.1. Afterwards, the methods utilized to verify the liquid film thickness measurements are described (section 4.2).The experimental facility applied during this study is presented in section 4.3 as well as the configuration of flow loop.

4.1 Conductance probes method

The method proposed in this work is based on the relation between the liquid film thickness and the electrical resistance between the probes. The reasons for selecting this method includes: simplicity, high temporal and spatial resolution, safety, and feasibility. The probes are made of two thin parallel-wires stretched through the liquid film normal to the film flow direction. It is necessary to keep the wires taut and the wire spacing constant throughout the measurement.

The use of parallel-wire probes method allows measurement of the spatial average of the film thickness in the probe area. The probe area is the area around the wires which has a significant effect on the resistance between them. Reducing the wire spacing will reduce the probe area and consequently increase the spatial resolution of the conductance probes measurement. The wires should be made of material with extremely high conductivity, so that the liquid resistance can be considered as the only resistance in the circuit. The wire diameter should be as large as possible to reduce the resistance; on the other hand, it should be as small as possible to prevent flow distortion and to avoid vortex shedding(Koskie et al. 1989).

In order to compensate the variations in liquid conductivity as a consequence of changes in liquid temperature or composition, a set of reference probes is located upstream of the liquid supply line. These probes use the same circuit as the thickness probes but are connected to a pipe with a single phase liquid flow. The output of the film thickness probes is non-dimensionalized by dividing it by the signal from the film reference probes. The electrical circuit and the calibration steps are explained in appendix A.

When the electrical resistance between the wires is much greater than the electrical resistance of the wires, the dimensionless output of the film thickness probes varies linearly with the film thickness. Consequently, if the liquid conductivity decreases or if the conductivity of the wires increases, the linearity of the calibration curve will improve.

In view of the fact that the parallel-probes method measures the liquid film thickness based on the wetted length of wires, it cannot fully resolve the waves with folding fronts.

4.2 Verification

In this part an attempt is made to verify the conductance probes method for holdup measurements with the high speed camera recordings. First the interface detection technique utilizing the high speed camera is explained and then a comparison is made between the results obtained from the two methods.

4.2.1 Time slice with high speed camera

In this method a high speed camera with the specifications described in Appendix B is placed perpendicular to the pipe. The camera is positioned in such a way that a set of conductance probes is at the middle of the field of view. In order to allow for the highest image resolution, images were taken at the rate of 250 frames per second. The field of view of the camera in this situation is about $25 \times 115\ mm$ which is formed by a matrix of 140×640 pixels. The detail specifications of the high speed camera used in this study are presented in appendix B

This interface detection method measures the liquid height at the fixed position and at the consecutive sampling times by utilizing the high speed camera. Each frame consists of several vertical arrays of pixels. Each array can be used as the representation of a line perpendicular to the flow direction passing the center of all pixels in the array. By collecting the vertical arrays of pixels with the same position in consecutive frames, it is possible to analyze the videos at a certain fixed position in varying time.

In order to conduct the two measurements at the same location, the position of the conductance probes in the field of view is registered then, the closest vertical array of pixels to this position is taken from each frame.

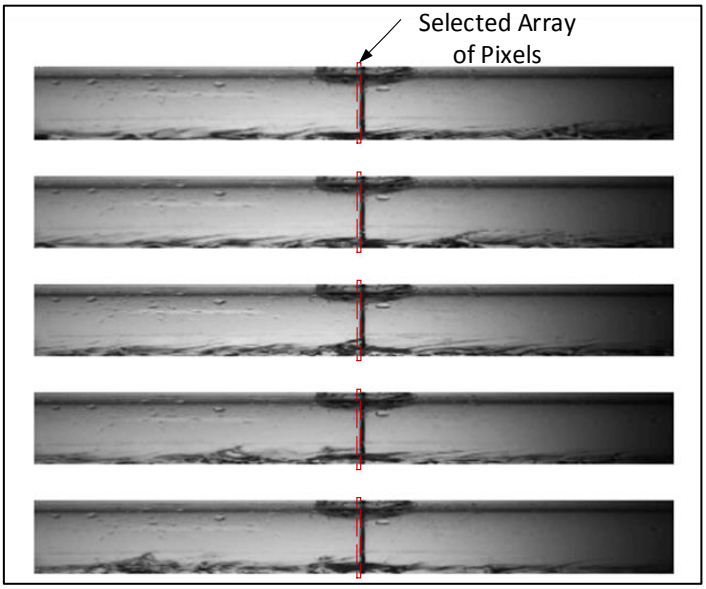

Figure 4.1: Representation of the selected vertical array of pixels in the consecutive frames.

As shown in figure 4.1 according to the shadow of the conductance probes in this location, the interface can be recognized by the dark line separating the gas phase from the liquid phase. Consequently, the position of the interface is approximated by the position of the pixel with the lowest light intensity. The accuracy of this method is highly related to the size of the pixels. In this case, there are 140 pixels in the vertical direction.

Figure 4.2 is obtained by positioning the consecutive time slices one after the other. This picture can be used to roughly estimate the average liquid holdup. The dark part that appears in figure 4.2 at the dimensionless height of about 0.75 and after 10 seconds, represents an almost stationary droplet.

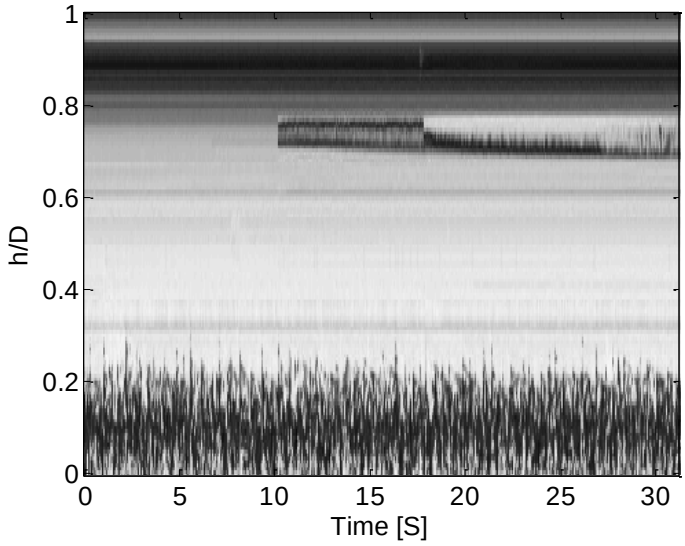

Figure 4.2: Representation of the time slice method with camera.

The main disadvantages of the time slice method are the following limitations. It is not possible to apply this technique when the atomization is the dominant sub-region of the stratified gas-liquid flows. When the surface of the waves is filled with ligaments and there are several sharp corners at the interface, this method fails to estimate the position of the interface accurately. This method is more suitable for the applications when a clear interface is present between the two phases.

4.2.2 Comparison between the conductance probes and high speed recordings

Considering the fact that the sampling rate of the conductance probes is 1 KHz and the frame rate of the camera is 250 fps, corresponding to each time slice there are four values measured by conductance probes. Consequently, the average of these four values is used to make the comparison between the two methods.

The average error amongst the obtained values is about 1 percent of the pipe diameter (is in this case about five percent of the range of liquid film thickness variations (peak-to-peak). The average liquid height measured with conductance probes is 3.1 mm while the one measured with high speed camera is 2.95 mm. The standard deviation of obtained signals from conductance probes and high speed camera are 0.645 mm and 0.61 mm respectively. In Figure 4.3 it is tried to compare the liquid holdup measured by the time slice method and the conductance probes. As discussed above and shown in figure 4.3 there is a qualitative agreement between the two techniques. The curvature of the pipe and the difference between the reflective indexes of air and Perspex might be a source of error in the time slice method. Moreover, the fact that the conductance probes method measures the average liquid height at the probes area (see section 4.1), while the time slice method measures the liquid height based on the one-dimensional representation of cross section (one array of pixels) may also cause a differences between the two methods.

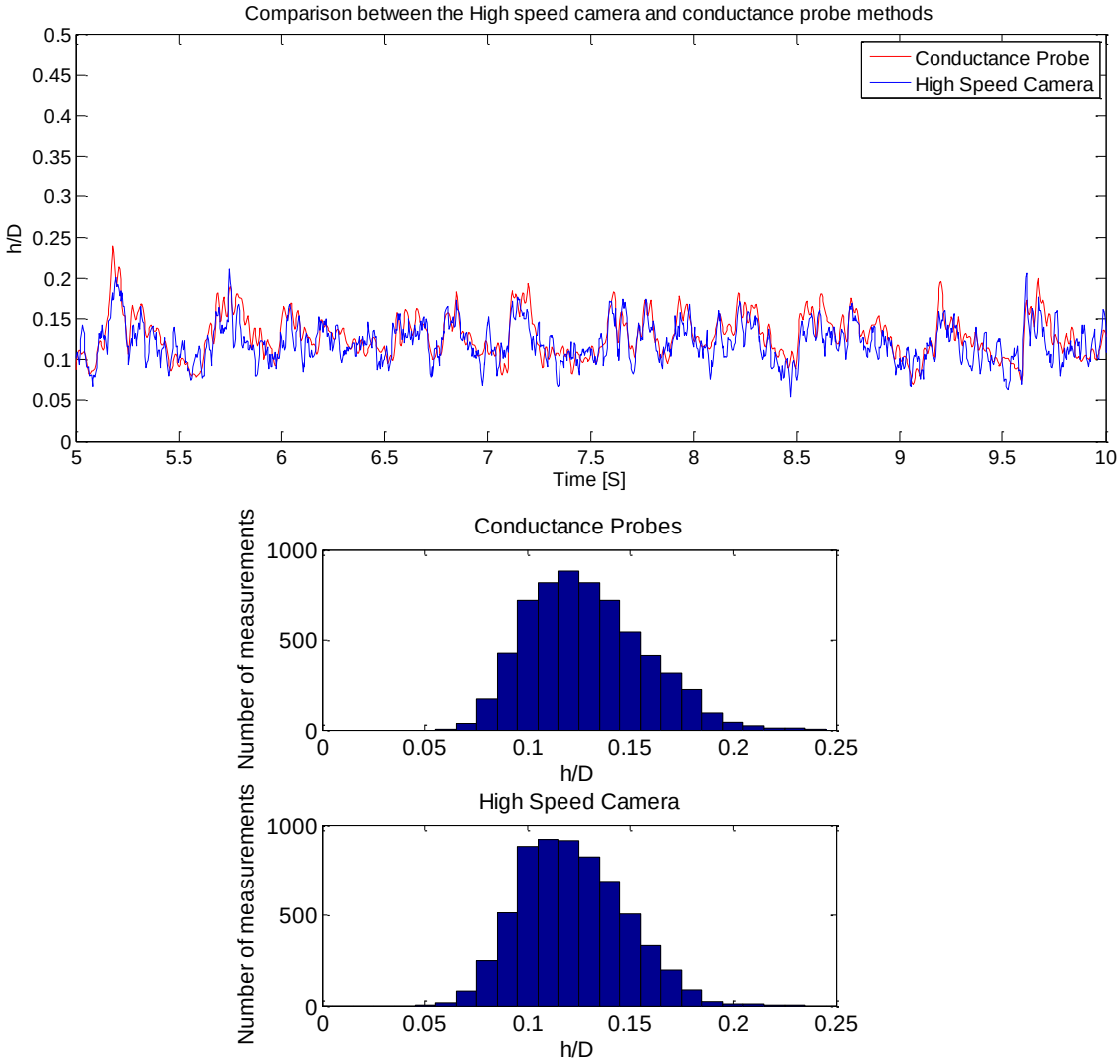

Figure 4.3: Comparison between the high speed camera and the conductance probes methods. Upper figure: h/d variations, lower figure histograms.

4.3 Flow loop

A transparent pipe with inner diameter of 24 mm and length of 3.6 m was set up from joining shorter sections of Perspex (PMMA) pipes. Pipes are fixed on an experimental table to ensure that the pipes are levelled horizontally.

Air and water are introduced to the pipe through a Y-shaped entrance. Air brought into contact with water from 30° above and water is entered horizontally. Two phase flow is developed over a length of 125D (3 m) before reaching the test section. After the test section there is another 25D (0.6 m) before the two-phase flow being discharged freely into an open container. Pressure gradients are measured at the last 0.1 and 1.7 m (see figure 4.4) of the pipe using a differential pressure transducer and a pressure transducer.

Tap water is used in this experiment in order to provide the required conductivity for the liquid film thickness measurement using conductance parallel wire probes. Water flow rate is

controlled by a rotameter and a needle valve while the Air flow rate is controlled by an air flow controller.

A pressurized tank is filled with diluted master solution with concentration of 120-400 ppm (depending on required final concentration) of polyacrylamid. In order to prevent polymer degradation as a result of shear stress in commonly high shear pumps, solution is forced towards the main line by compressed air through an 8 mm flexible pipe. A rotameter and a needle valve are placed in this line to allow adjustment of the master solution flow rate based on the water flow rate to achieve a certain final concentration in the main line.

Water and master solution are mixed together in a tee junction located prior to the gas phase introduction point. In order to ensure that the master solution and water are fully mixed and a homogeneous solution will reach the test section a long flexible pipe with small diameter is used[3] . In this way the Reynolds number of the liquid mixture is increased, accompanied by the higher turbulence level resulting in a more effective mixing. Concentration of final solution is checked by comparing the viscosity of samples from outlet of the setup with homogeneous solutions with known concentrations. The experiment flow diagram is shown in figures 4.4 and 4.5:

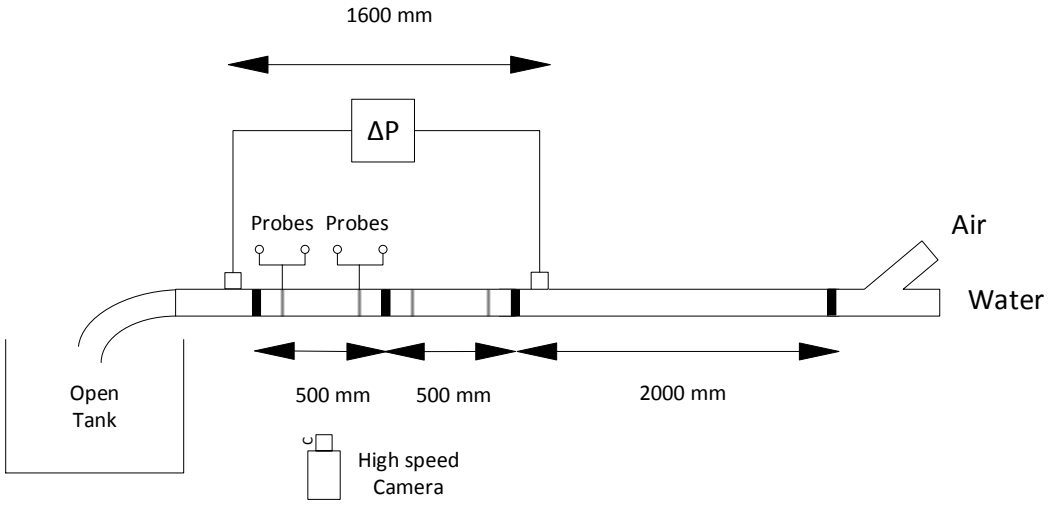

Figure 4.4: Schematic representation of the main pipe and test section.

[3] The diameter of flexible pipe is reduced from 8 mm before the first tee junction to 4 mm.

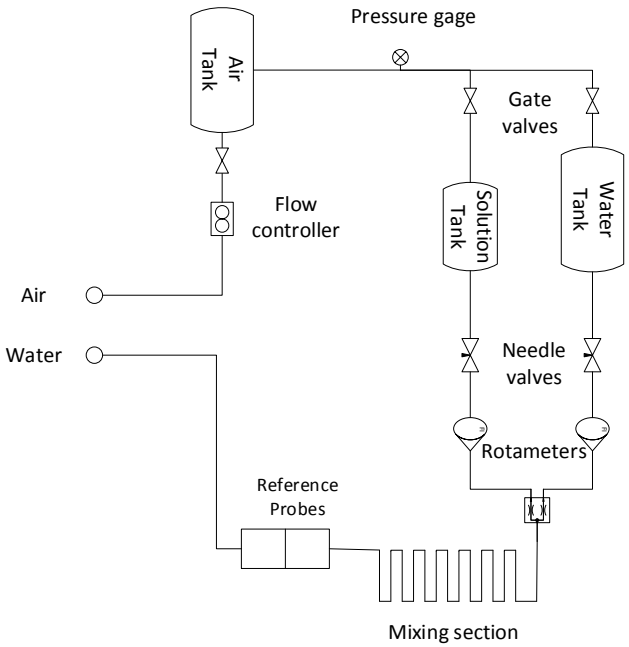

Figure 4.5: Schematic representation of the experimental facilities before the main pipe.

The test section consists of two sets of conductance probes. Conductance probes are used to measure the water film thickness with considerably high spatial and temporal resolution. In order to compensate for the variations in water conductivity as a consequence of changes in water composition and temperature, another set of conductance probes (reference probes) is placed upstream the air introduction point. Reference probes are placed where the water-polymer mixture occupies the entire pipe cross-section and the signal from this set is used as a reference to measure the film's thickness at test sections. Schematic representation of the test section is presented in figure 4.6:

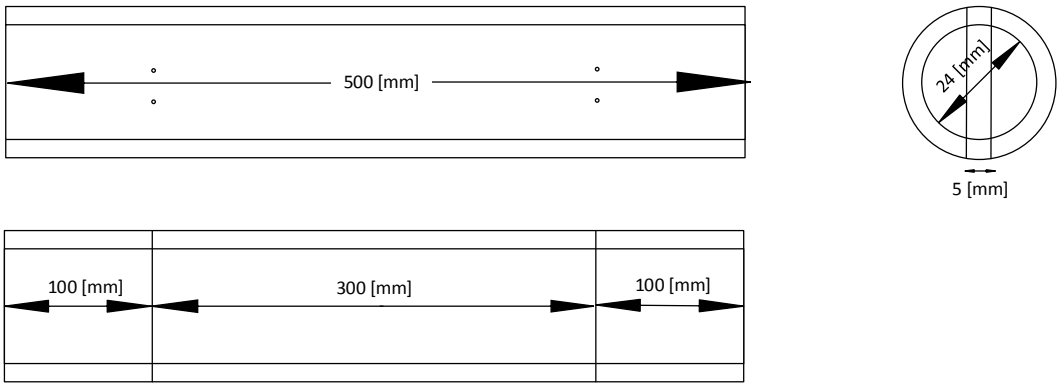

Figure 4.6: Top, side and front views of the test section.

A high speed camera is implemented in this experiment which is placed perpendicular to the pipe axis at test section in horizontal plane to visualize the flow. The curvature of pipe makes it difficult to estimate the liquid height from the recordings when the liquid holdup is extremely low.

Chapter 5: Experimental results

This chapter opens with the information regarding the test conditions as well as the polymer concentrations used for the experiments. In section 5.2 the pressure losses and the drag reductions for different polymer concentrations are presented as well as the effects of gas and liquid flow rates on them. Then, the maximum drag reduction in the single phase flows is compared with the stratified gas-liquid flows in section 5.2. Thereafter, the time variations of liquid holdup and the influence of the DRPs on them are explained in section 5.3. That is followed by the analysis of the DRPs' effects on wave dynamics (section 5.4).

5.1 Measurement conditions

Air and water flow rates are selected based on the flow map provided by Al-Sarkhi et al. (2004) for the air-water flows in a smooth horizontal pipe with inner diameter of 25.4 mm. Measurements were performed for a wide range of liquid and gas superficial velocities corresponding to the stratified gas-liquid flow regimes. Table 5.1 presents the gas and liquid superficial velocities as well as the polymer concentrations used for the measurements:

Table 5.1: Gas and liquid superficial velocities and polymer concentrations used in the experiments.

Variable	Range	Step
U_{SG}	5-15 [m/s]	2 [m/s]
U_{SL}	0.03-0.15 [m/s]	0.03 [m/s]
Polymer Concentration	0-100 (up to 400 for MDR) [PPM]	-

5.2 Pressure drop & Drag reduction

5.2.1 Pressure drop and drag reduction in stratified flows

In this section the effect of the addition of the drag reducing polymers on pressure drop is discussed. In Figure 5.1 the pressure gradient for different polymer concentrations for the superficial gas velocity of 9 m/s is shown.

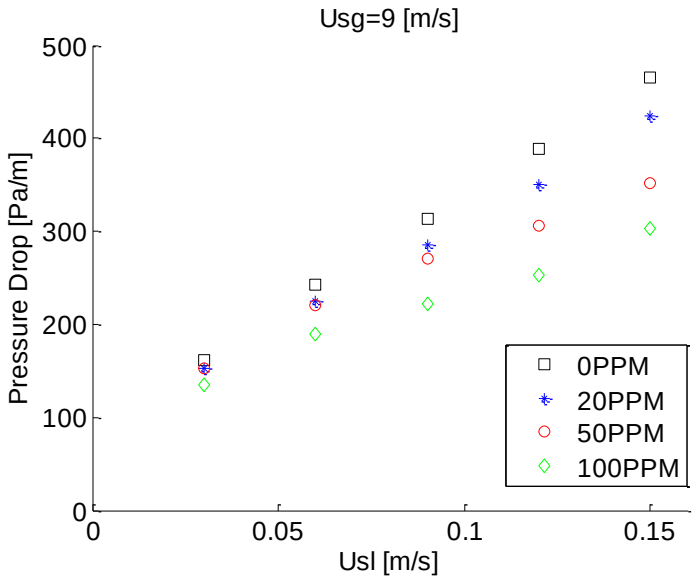

Figure 5.1: Measurements of the effect of Usl and polymer concentration on pressure gradient for Usg= 9 m/s.

As presented in figure 5.1, pressure gradient is observed to decrease by the addition of polymers. Comparing the pressure losses for the constant gas and liquid flow rates, it can be clearly seen that the reduction in the pressure drop increases by increasing the polymer concentration. At the lower liquid flow rates the range of the variation in drag reductions (for different polymer concentrations) is smaller. It is suggested that that increasing the polymer concentration has less influence at lower liquid flow rates. Increasing the liquid superficial velocity is accompanied by an increase in the drag reduction. In previous studies on single phase flows, it is claimed that an increase in Reynolds number leads to a higher drag reduction (see section 2.1). In stratified gas-liquid flows, higher liquid velocity, with constant gas velocity, means higher liquid Reynolds number which increases the drag reduction as well (see figure 5.1).

On the other hand, increasing the gas superficial velocity results in a reduction of the liquid holdup associated with the higher interfacial shear stresses at the higher gas velocities. When the liquid holdup is reduced for a constant liquid superficial velocity, the actual liquid velocity is increased according to the equation 1.6. Consequently, an increase in the gas superficial velocity is also accompanied by an increase in the liquid Reynolds number and higher drag reduction is expected at the higher gas superficial velocities. In figure 5.2 the pressure losses for different polymer concentrations for superficial liquid velocity of 0.09 m/s are shown:

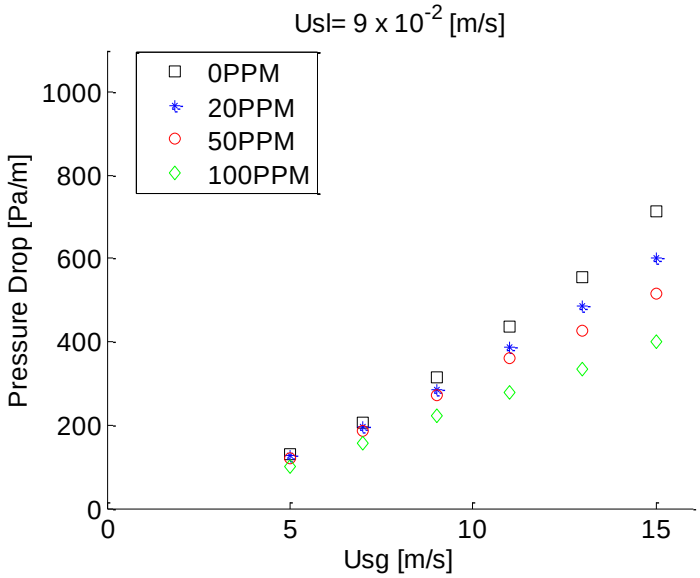

Figure 5.2: Measurements of the effect of Usg and polymer concentration the on pressure gradient for Usl= 0.09 m/s.

As it is presented in figure 5.2, the reduction in pressure losses increases by increasing the gas superficial velocity. The measured pressure losses for different gas and liquid superficial velocities are presented in appendix E.

The effects of the superficial gas and liquid velocities on the drag reduction are presented in figure 5.3:

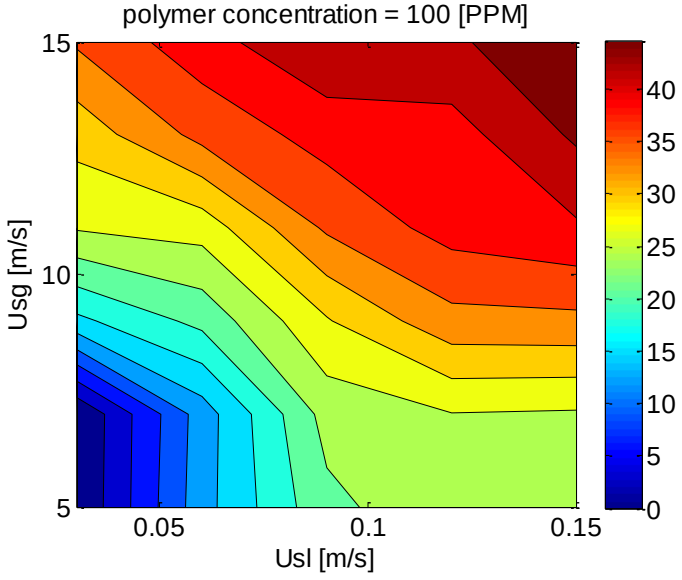

Figure 5.3: Measurements of the effect of liquid and gas superficial velocities on the drag reduction.

As shown in figure 5.3, the drag reduction is increased by increasing the liquid and gas superficial velocities. Hence, the highest drag reduction observed in this study (about 55 percent) is obtained at the greatest liquid and gas superficial velocities. Drag reductions up to 55% are obtained by using the polymer concentrations as low as 100 ppm. Since at these

concentrations the dynamic and the static surface tensions of polymeric solutions are roughly equal to the ones for water (see section 3.3), it could be argued that the contribution of surface tension to drag reduction is negligible.

5.2.2 Maximum Drag Reduction

In this section an attempt is made to compare the maximum drag reduction in single-phase flows and stratified gas-liquid flows. Al-sarkhi et al. (2011) showed that in stratified gas-liquid flows the drag reduction increases by increasing the polymer concentration until it reaches the certain saturation point from this point (alike the single-phase flows) addition of more polymers does not lead to further increase in the drag reduction(Al-sarkhi et al. 2011). In This section it is tried to compare the maximum achievable drag reduction in the single-phase and stratified gas-liquid flows and their corresponding polymer concentrations.

5.2.2.1 Single phase

In order to make a comparison between the drag reduction curve in the stratified air-water and in the single phase water flows, the experimental data for exactly the same type of polymer was required which could not be found in the available literature. Consequently, a simple experimental setup was built to measure the required data (see Appendix C).

The drag reduction curves for the single phase flow of water and different Reynolds numbers are shown in figure 5.4:

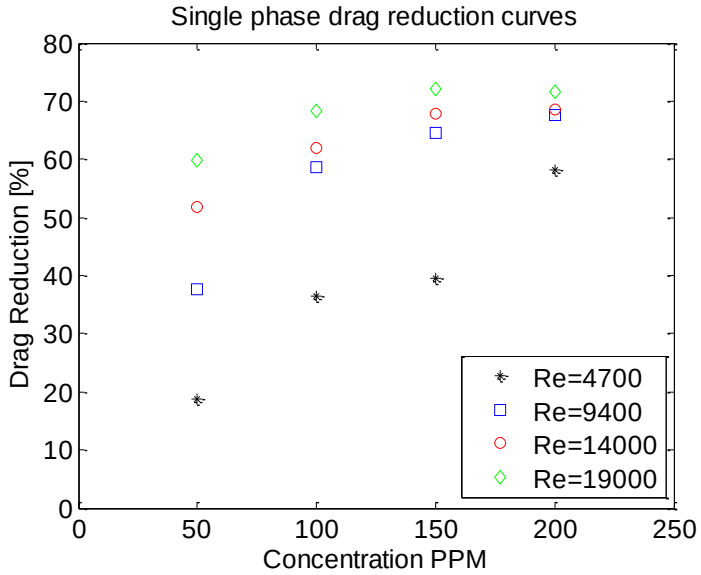

Figure 5.4: Drag reduction curve for the single phase flow of water at different flow rates.

As shown in figure 5.4, the drag reduction of the single phase flow increases by increasing the Reynolds number. The drag reduction curves for the higher liquid flow rates (Re=9400, 14000, and 19000) reach their maximum with the polymer concentration of about 150-200 ppm. While adding more polymers may lead to a higher drag reduction for the single phase flow with the lowest Reynolds number considered in this study.

5.2.2.2 Stratified air-water

In order to assess the maximum drag reduction in stratified gas-liquid flows, the gas and liquid superficial velocities are kept constant at 13 m/s and 0.12 m/s respectively and the polymer concentration is increased until the drag reduction curve reaches its maximum. The drag reduction curve for these measurements is presented in figure 5.5:

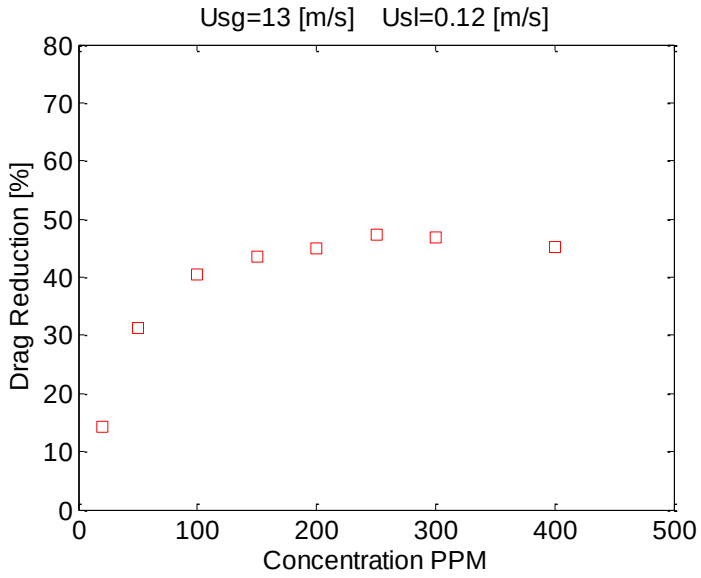

Figure 5.5: Drag reduction curve for the gas superficial velocity of 13 m/s and the liquid superficial velocity of 0.12 m/s.

As it is presented in figure 5.5 the drag reduction increases by increasing the polymer concentration until the certain saturation point. In this case the maximum drag reduction of about 50% is measured at the polymer concentration of about 200-250 ppm. The Reynolds number of the liquid phase based on the liquid actual velocity -without polymers and with the aforementioned gas and liquid superficial velocities- is about 16000. It should be mentioned that increasing the polymer concentration increases the liquid holdup (see section 5.4). Consequently, by increasing the polymer concentrations, the actual liquid velocity and the liquid phase Reynolds number are reduced. Moreover, increasing the polymer concentration increases the liquid phase viscosity (see section 3.2) which results in a reduction of the liquid's Reynolds number in single phase and stratified flows.

5.2.2.3 MDR in single phase and stratified flows

In order to take the liquid Reynolds number variations of the stratified flow into account, the maximum drag reduction in stratified flows is compared with a range of Reynolds numbers in single phase flows (Re=9400-16000).

The measured pressure losses for the single phase and stratified flows show that the drag reduction of single phase flows is higher than the one of stratified gas-liquid flow for the same range of Reynolds numbers. The maximum drag reduction achieved in the single phase flow is greater than the value obtained for the stratified gas-liquid flow for the same range of liquid Reynolds numbers. Moreover, the concentration at which the drag reduction curve approaches its plateau is lower for single phase flows.

Rosehart et al. (1972) obtained higher drag reduction in gas-liquid flows than the one measured for the single phase flow with the same liquid superficial velocity(Rosehart et al. 1972), which is in contrast with the findings of this study. This shows that the conclusions are influenced by the parameter used to draw the analogy between the single phase and gas-liquid flows. Neither the constant superficial liquid velocity (used by Rosehar et al. (1972)) nor the constant the Reynolds number (used in this study) can define an exactly similar situation for both types of flows. There are several features of stratified flow (e.g. air-water interface, waves, entrainments, etc.) which do not exist in the single phase flows. Choosing each parameter is accompanied by several assumptions. When the constant Reynolds number is selected, it is assumed that the liquid flow in the stratified gas-liquid flow is similar to the single phase flow of liquid with the same flow rate inside the pipe with a diameter equal to the liquid phase hydraulic diameter. In this way, interface effects, waves, the shape of cross sectional area occupied by liquid, etc. are ignored in the comparison. Moreover, the drag reduction is considerably influenced by the size of the pipe. Consequently, more solid conclusion can be made if both of the experiments were conducted with the same pipe.

Effects of DRPs on different aspects of stratified gas-liquid flows are investigated in following sections.

5.3 Measurements of the holdup

5.3.1 Tracings of time variation of h/D

Liquid holdup and interfacial shear stresses have a considerable contribution to the pressure loss of stratified flows and changes in either one of them could result in variations in the pressure losses. In this section the effects of addition of DRPs on the liquid holdup variations are discussed.

Tracings of the time variation of h/D for tap water and 100 ppm solution are presented in figure 5.6. For both of the cases the gas and the liquid superficial velocities are 15 m/s and 0.09 m/s respectively. Note that these representations of the tracings are considerably compressed and it is not possible to obtain a true geometrical representation of the waves from them. Based on the criterion introduced by Andritsos & Hanratty (1987)[4], the large scale structures of the tracings are characterized as roll waves. These structures can be easily seen in the tracings of the polymeric solution in figure 5.6. It can be seen that the occurrence of the roll waves and their shapes are more regular for the case of polymeric solution. Issues regarding the wave shapes and their frequencies are discussed in detail in section 5.5.

[4] . roll waves have a steep front and a long wavelength (Andritsos & Hanratty 1987).

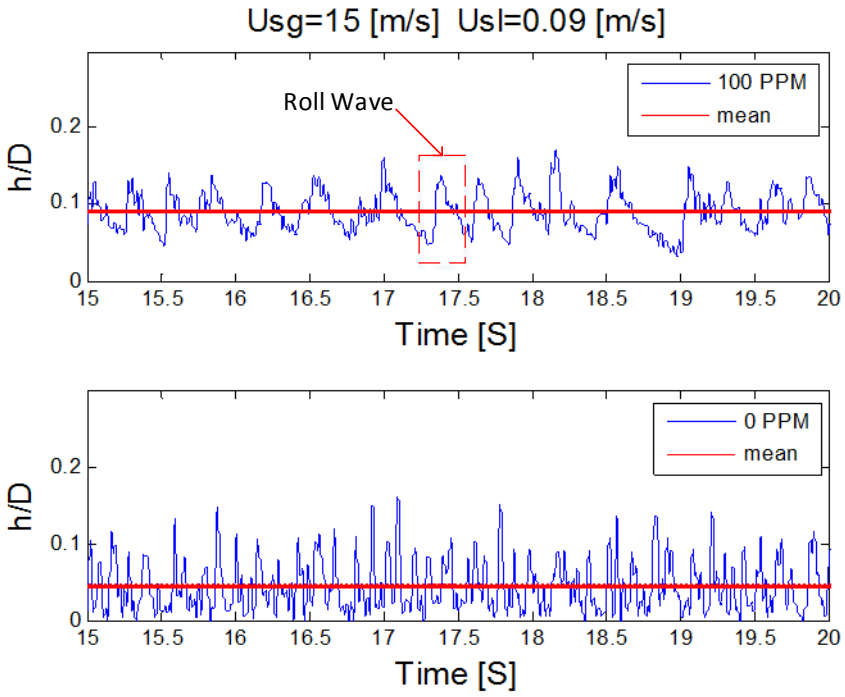

Figure 5.6: Measurements of the time variation of h/D for water and 100 ppm solution.

As shown in figure 5.6, the interfacial disturbances are more concentrated in absence of polymers and the average liquid holdup is increased by addition of the polymer. The latter has also been observed by Al-sarkhi et al. (2004). Moreover, visual observations suggest that addition of polymers affects the shape of the gas-liquid interface. For the gas superficial velocities higher than 7 m/s the gas-liquid interface has a significant curvature, while by increasing the polymer concentration the curvature of interface is reduced. The reduction in the curvature of the interface causes a reduction in the interfacial area which might be a reason for reducing the effect of the interfacial shear stress on the frictional pressure losses. The importance of the shape of the interface on the pressure drop is assessed in chapter 6.

The statistical analysis of the measured liquid film thicknesses for different polymer concentrations over a period of one minute is presented in figure 5.7. The gas and liquid superficial velocities are 15 m/s and 0.09 m/s, respectively for all of the cases.

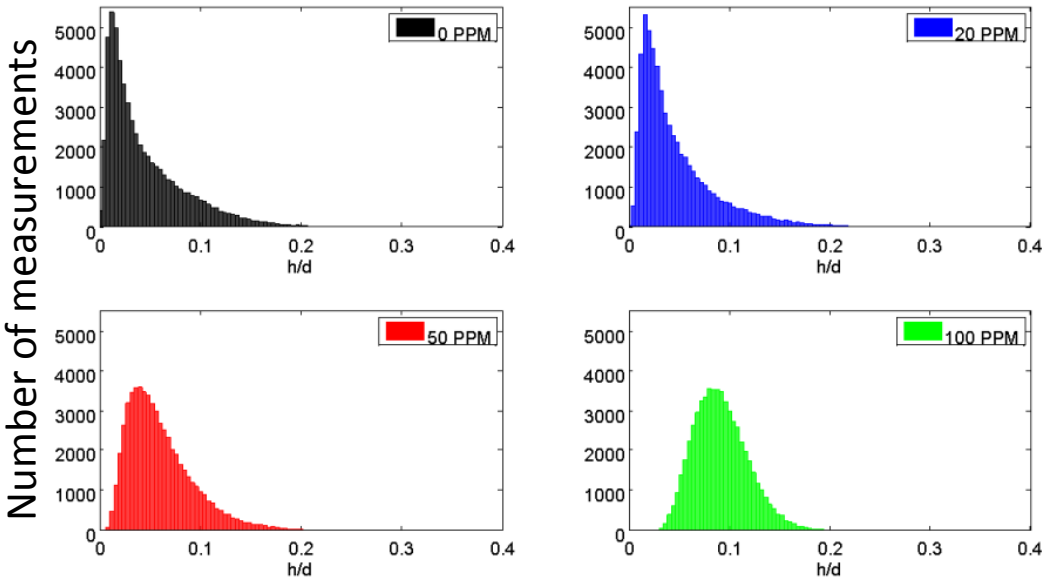

Figure 5.7: Statistical representation of the measured holdups for different concentrations.

It is illustrated in figure 5.7 that by increasing the polymer concentration, the mean value of the measured liquid height data is shifted towards higher values. This is an indication of an increase in the average holdup. It is assumed that increasing the slip velocity at the interface as a result of reduction of the interfacial shear stress is the main reason for that. Of a particular interest is the shape of the histograms for different polymer concentrations. In absence of polymers, most of the measured holdups are distributed at the left side of the diagram and the bar with greatest occurrence frequency is representing the holdups close to zero. While by increasing the polymer concentration the maximum is shifted towards the right, the measured holdups are distributed more and more equally around the maximum and the distance between the tails of the histograms is significantly reduced (data are distributed along the narrower range). This shows that at high polymer concentration the disturbances occur with lower amplitude around the mean value of the liquid height, while disturbances with larger amplitude pass over a thin layer of liquid in absence of polymers. This means that by addition of polymers, some of the interfacial disturbances are damped and the gas-liquid interface becomes smoother. Damping of the interfacial disturbances results in a reduction of the interfacial friction factor and the interfacial shear stress (see chapter 6.2).

5.3.2 Frequency domain

The measurements of the time variation of h/D are transferred from the time domain into the frequency domain to gain a better insight on the effects of DRPs on the occurrence and regularity of the dominant interfacial disturbances. This is done by applying the Fast Fourier Transform function (FFT) to the time discrete signals, obtained from the conductance probes. First signals are divided into ten parts and then a window function with an isosceles trapezoid shape is applied to each part. Thereafter, the fast Fourier transform is applied to each part and the final frequency domain signal is measured by averaging over all of the sections. Finally a moving average window is applied to the frequency domain signals to clear the existing noise.

The frequency domain signals of liquid holdup data for different polymer concentrations over a period of one minute are presented in figure 5.8. The gas and liquid superficial velocities are 15 m/s and 0.09 m/s respectively for all of the cases.

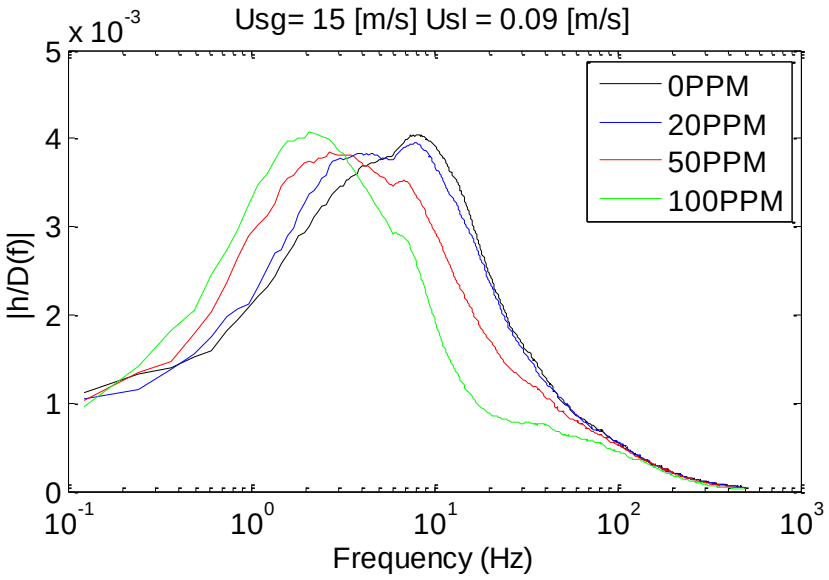

Figure 5.8: Frequency domain signals of liquid holdup data for different polymer concentrations.

As shown in figure 5.8 the dominant structures are moved towards the lower frequencies by increasing the polymer concentration. Of a particular interest are some high frequency (between 10 Hz and 100 Hz) contents that are damped significantly, by increasing the polymer concentration. Damping of the liquid phase turbulences might be a possible reason for that. Considering figures 5.6 and 5.8 damping of the small wavelength (high frequency) disturbances on the roll waves and on the liquid layer between the roll waves might also be the cause of damping of the high frequency contents as in figure 5.8. Frequency domain representations for different liquid flow rate are presented in appendix F.

5.4 Wave dynamics

In this section the focuses lies on the study of the long amplitude waves and the effects of DRPs on them. The average velocity of waves is calculated by measuring the average time required for waves to travel a certain distance between the two sets of conductance probes. In section 5.4.2 the frequency of the waves is measured by counting the number of waves passed a set of conductance probes and finally in section 5.4.3 the shape of the waves is described and the effects of DRPs on them are investigated.

5.4.1 Wave velocity

In this section the representative velocity of long amplitude waves is estimated by measuring the time lag between the wave registrations by two sets of probes. The cross-correlation function is applied to estimate the similarity of two signals as a function of existing time lag between them. The cross-correlation function for discrete signals is explained in appendix D.

In order to gain a better estimation of the velocity of the roll waves, first these structures should be separated from the other small amplitude holdup fluctuations. This is performed by applying the frequency filter to the signals measured by each set of probes. At the flow rates utilized in this work, the long amplitude waves are not expected (based on visual observations, signals obtained from conductance probes and high speed camera recordings) to exist with a frequency higher than 10 Hz. As a result, a low pass frequency filter with a barrier at 20 Hz is applied to the signal obtained by each set of probes. Afterwards, the cross-correlation function is applied to find the time lag between the signals. This time lag is used as the representative of the time needed for waves to travel the distance between the probes. Then the representative velocity of the waves is measured by knowing the distance between the two sets of probes. More precise estimation of the wave velocity could be obtained by estimating the velocity of each wave separately and then averaging over these values.

The wave velocities for different polymer concentrations and constant gas superficial velocity of 9 m/s are shown in figure 5.9:

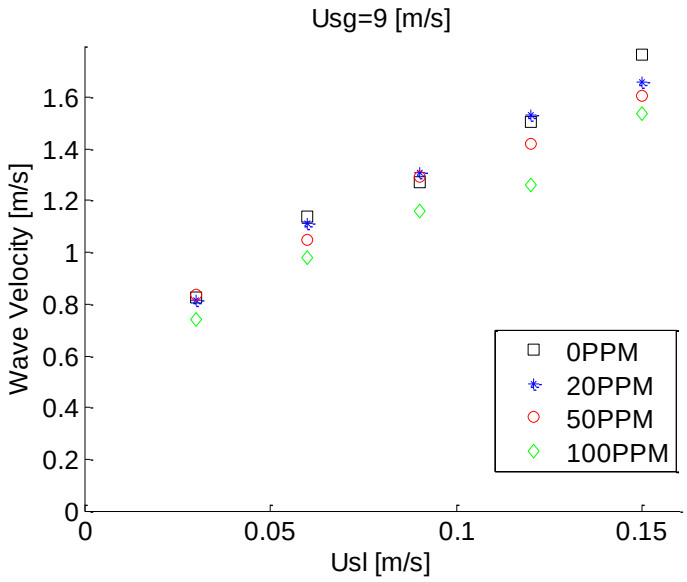

Figure 5.9: Measurements of roll waves' velocity for various liquid flow rates and polymer concentrations at the constant gas superficial velocity of 9 m/s.

As presented in figure 5.9 the representative velocity of waves increases by increasing the liquid flow rates (same trend were observed by increasing the gas velocity). Higher actual gas velocity as a consequent of an increase in liquid/gas flow rate applies higher shear force on the back of the waves resulting in an increase in their velocity.

On the other hand, increasing the polymer concentration decreases the representative velocity of the waves which could be due to reduction in interfacial shear stress (see chapter 6). It might be argued that the decrease in the interfacial shear stress is associated with damping of interfacial disturbances and reduction in interfacial friction causes an increase in slip velocity between the two phases resulting in an increase in liquid holdup and a decrease in the wave velocity.

It is shown in figures 5.9 that the average velocity of roll waves increases by increasing the liquid flow rate. However, the average wave velocity will always be small in comparison with the gas actual velocity (about 0.1 to 0.2 times of the actual gas velocity). The representative wave velocities for different gas and liquid flow rates are presented in appendix G.

5.4.2 Wave frequency

The frequency of the long amplitude waves is calculated by counting the number of large amplitude structures in a tracings of time variations of h/D . First a low pass frequency filter (with a barrier at 20 Hz) is applied to the tracing of liquid height variations in time to separate the roll waves from the other lower amplitude (high frequency) disturbances. Afterwards, the number of local maximums is counted and registered as the number of roll waves. The frequency of roll waves is obtained by dividing the number of roll waves by the measurement time. The wave frequencies for different polymer concentrations and constant gas superficial velocity of 9 m/s are shown in figure 5.10.

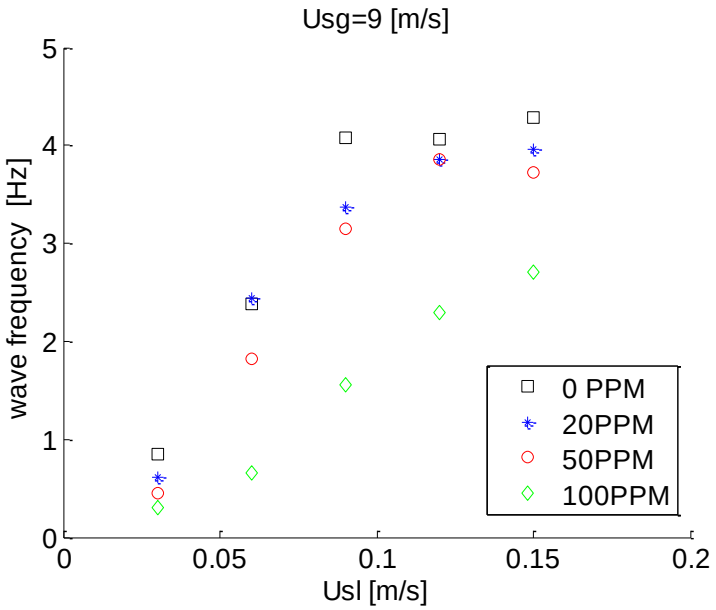

Figure 5.10: Frequency of roll waves for various liquid flow rates and polymer concentrations at a constant gas superficial velocity of 9 m/s.

In Figure 5.10 it is shown that the roll wave frequency is increased by increasing the liquid flow rate. As it is presented in figure 5.10 the frequency of roll wave is reduced after the addition of polymers. Addition of polymers caused lower roll wave frequency and velocity which can be interpreted as the lower level of momentum exchange between the gas and liquid phases and less interfacial shear stress

5.4.3 Wave shape

Visual observations and videos recorded from the high speed camera show that not only the velocity and the frequency of the roll waves are changed but also their shape is influenced by the polymers. Figures 5.11 and 5.12 present the typical shape of roll waves for pure water and the 100 ppm polymeric solution at the liquid superficial velocity of 0.09 m/s and the gas

superficial velocity of 9 m/s. These pictures are obtained by collecting the consecutive frames. The videos are recorded at a rate of 250 frames per second which is equal to the time interval of 4 ms between the frames. To clearly present the movement of the waves one out of each four consecutive frames is shown in figures 5.11 and 5.12. Consequently, the time interval between the frames is 16 ms.

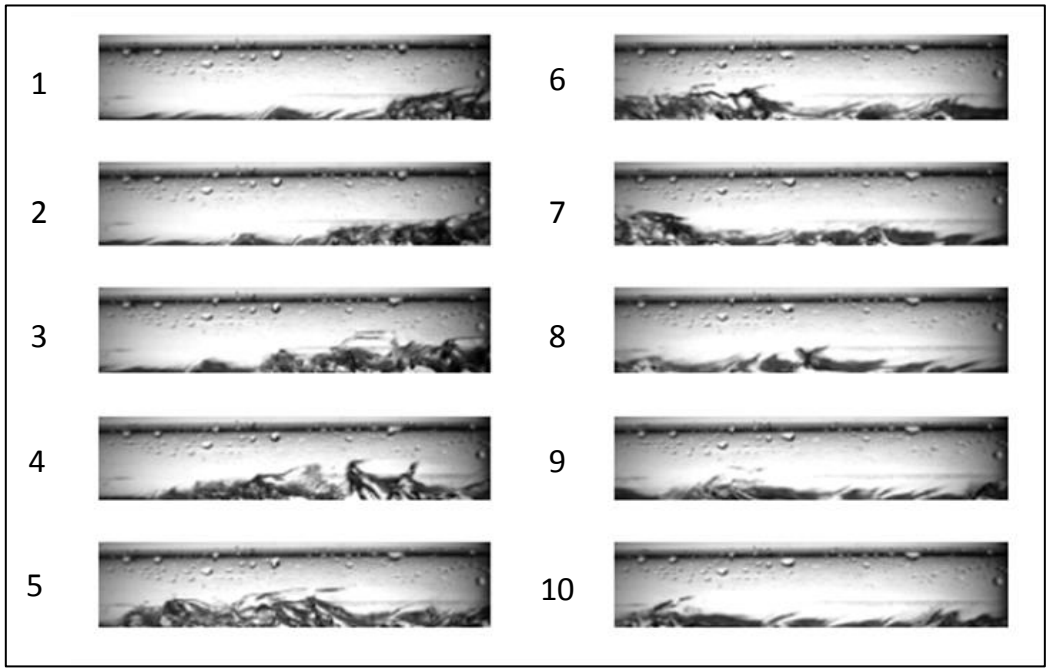

Figure 5.11: Roll wave for air-water flow at the liquid superficial velocity of 0.09 m/s and gas superficial velocity of 9 m/s (the time difference between the frames is 0.016 s) .

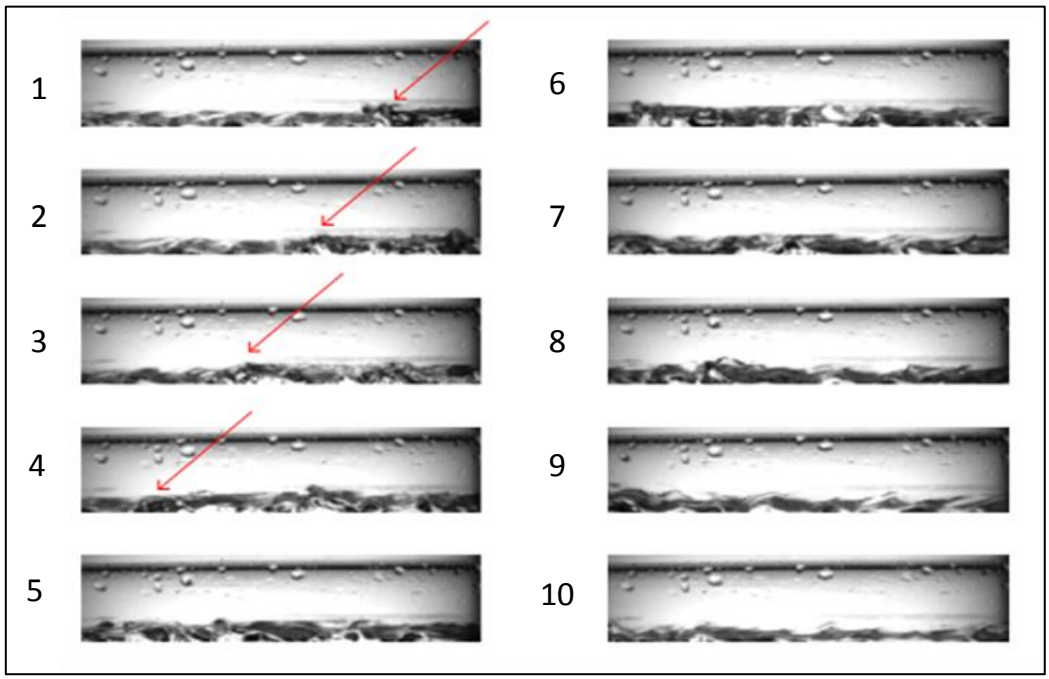

Figure 5.12: Roll wave for air and 100 ppm polymeric solution flow at the liquid superficial velocity of 0.09 m/s and gas superficial velocity of 9 m/s(the time difference between the frames is 0.016 s).

As shown in figures 5.11 and 5.12 the shapes of the roll waves clearly change after the addition of polymers. The surface of roll wave shown in figure 5.12 (for polymeric solution) is much smoother than the one presented in figure 5.11 (for water) (this could also be seen in figure 5.6). Several small droplets can be seen in figure 5.11 at the top of the roll wave, which are not seen in figure 5.12. These droplets are separated from the crest of the wave and carried by the gas phase for a limited time and then deposited into the liquid phase. The droplet that is entrained initially has a velocity equal to the wave velocity (separated from the wave). The energy required to accelerate the droplet into gas stream is eventually dissipated when the droplet is deposited into the liquid phase. The energy dissipated due to the entrainment-deposition processes of droplets has a considerable contribution to the total pressure drop (Fernandes et al. 2004). As a result, reducing the number of small droplets when the polymers are added might also have a contribution to the reduction observed in the pressure losses.

Moreover, the wavelength of the roll waves is clearly increased by the addition of the polymers and there are less sharp corners at the surface of the roll waves when the polymers are present. This can be illustrated by comparing figures 5.11 and 5.12. The damping small wavelength disturbances were suspected to be the underlying reason for damping of the high frequency contents at the frequency domain representation of the holdup tracings(see figure 5.8) . It can also be seen in figure 5.15 that the height of the liquid film in front of the roll waves is much higher when the polymers are added to the flow.

5.5 Conclusions

As presented in this chapter, Addition of drag reducing polymer reduces the pressure losses of stratified gas-liquid flows and the drag reduction increases by increasing the polymer concentration. The fact that drag reductions up to 55% are obtained for the polymer concentrations as low as 100 (while the surface tension of a polymeric solution and water are roughly equal for these concentrations) suggest that surface tension does not play an important role in the drag reduction of the stratified gas-liquid flows.

Moreover, considering an increase in drag reduction by increasing the gas/liquid flow rates, the interactions between the polymers and the turbulences (as a result of non-Newtonian behavior of polymers e.g. shear thinning and viscoelastic) might have a contribution to the observed drag reduction.

It has been observed that the addition of the polymer causes a reduction in the interfacial surface area by reducing the curvature of the interface. Decreasing the interfacial area reduces the contribution of interfacial shear stress in pressure losses and might lead to a reduction in frictional losses.

The addition of polymers increases the liquid holdup. It is assumed that increasing the slip velocity at the interface as a result of reduction in the interfacial shear stress is the main reason for that.

The Analysis made on the tracings of the time variations of the liquid height showed that the interfacial disturbances are significantly damped by addition of polymers. The reduction in interfacial shear stress might be associated with damping of the interfacial disturbances.

Decreasing the interfacial shear stress reduces the force applied by the gas phase on the roll waves and causes a reduction in their velocity and frequency. Moreover, high speed camera

recordings showed that the shapes of the roll waves are also affected by addition of polymers. Their wavelength is longer and their surface is smoother after the addition of polymers.

Chapter 6: Modeling

According to the experimental results obtained in chapter 5, the reduction of interfacial shear stress might play an important role in the observed drag reduction. Although the interfacial shear stress is not measured directly in the experiments, it can be estimated using the one-dimensional momentum balance in which semi-empirical correlation is used to estimate the gas-wall shear stress. In section 6.1 one-dimensional momentum balance is explained. In order to assess the validity of semi-empirical correlations needed to calculate the interfacial shear stress, a comparison is made between the pressure drops measured in the experiments without polymers and those predicted by a recent model presented by Tzotzi & Andritsos (2013). In section 6.2 one dimensional momentum balace of gas phase is used to quantitatively investigate the effect of DRPs on interfacial shear stress. In section 6.3 a model is proposed to assess the contribution of damping the interfacial disturbances and reduction in the curvature of interface on the drag reduction of stratified gas-liquid flows. Finally the main conclusions of this chapter are presented in section 6.4.

6.1 One-dimensional momentum balance

Commonly the one-dimensional momentum balances of both phases are applied to predict the pressure drop in gas-liquid stratified flows. The pressure gradient for two-phase flow of air and water in horizontal pipes comprises of different frictional component shown in figure 6.1. In this approach, it is assumed that the interface is flat, the effects of all interactions between the two phases are lumped in the Interfacial shear stresses, and all of the three-dimensional effects are neglected. In the case with fully developed stratified flow the one-dimensional momentum balance can be written as:

$$-A_G\left(\frac{dP}{dL}\right)_G - \tau_{WG}S_G - \tau_i S_i = 0 \qquad \textit{Eq.6.1}$$

$$-A_L\left(\frac{dP}{dL}\right)_L - \tau_{WL}S_L + \tau_i S_i = 0 \qquad \textit{Eq.6.2}$$

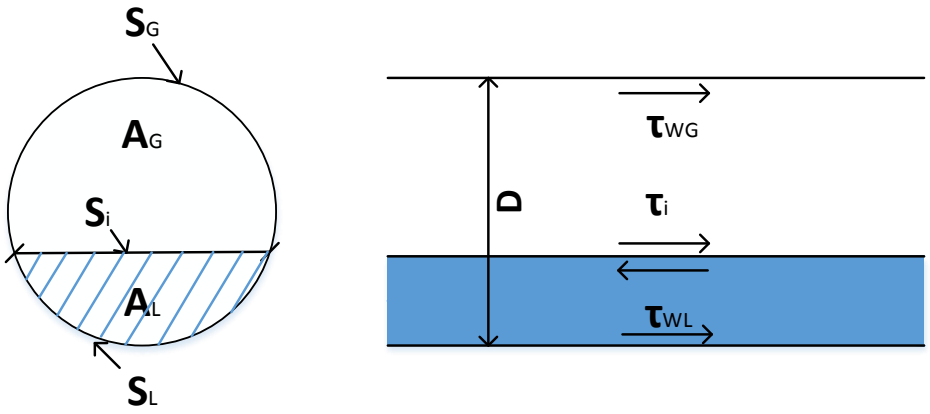

Figure 6.1: Geometrical and physical variables in stratified gas-liquid flows in horizontal pipes.

The geometrical parameters S_G, S_L, S_i, A_G, A_L and frictional stresses are shown in fig 1.6. Equation 6.1 represents the balance between the pressure forces in the gas space and the frictional stress between the gas and solid boundary of the pipe τ_{WG}, and the resisting stress at the gas-liquid interface τ_i. Equation 6.2 is a balance between pressure forces, the drag force induced by gas on liquid at the interface and the resisting stress at the liquid-wall boundary. The parameter τ_i strongly depends on the shape of the gas-liquid interface. Consequently, sufficient understanding of the liquid film morphology is essential for estimating the resisting stress at the gas-liquid interface.

Tzotzi & Andritsos (2013) introduced the latest model to estimate the pressure drop of the stratified gas-liquid flows. Their model is essentially the one-dimensional model based on the momentum balance for each phase(Tzotzi & Andritsos 2013). The main contribution of Tzotzi & Andritsos is on the development of new semi-empirical equations to predict the transition to 2-D waves and long amplitude waves (roll waves) sub-regions. They also provided empirical correlations to estimate the interfacial friction factor for different stratified flow regimes as a function of the gas-wall friction factor and the gas superficial velocity.

In this section the model provided by Tzotzi & Andritsos (2013) is shortly explained and the measured pressure losses (without polymers) in the experiments are compared with the values predicted by this model.

6.1.1 Gas-wall & liquid-wall shear stresses

The correlations derived by Taitel & Dukler (1976) to describe the gas-wall and liquid wall shear stresses are implemented in this model (Taitel & Dukler 1976). The gas-wall and liquid-wall shear stresses are defined as follows:

$$\tau_{GW} = f_{GW}\frac{\rho_G {U_G}^2}{2} \qquad \textit{Eq.6.3}$$

$$\tau_{LW} = f_{LW}\frac{\rho_L {U_L}^2}{2} \qquad \textit{Eq.6.4}$$

Where U_G, U_L are actual gas and liquid velocities and the terms f_{gw}, f_{lw} (in a smooth pipe) are calculated from equations 6.5 and 6.6, based on the actual Reynolds number of each phase:

$$f_{GW} = C_G Re_G^{-m} \qquad \textit{Eq.6.5}$$

$$f_{LW} = C_L Re_L^{-n} \qquad \textit{Eq.6.6}$$

For turbulent flow ($Re > 4000$), $C = 0.046$ and $m, n = 0.2$ and for laminar flow ($Re < 4000$), $C = 16$ and $m, n = 1$. The Reynolds numbers and the hydraulic diameters are written as:

$$Re_G = \frac{D_G U_G}{\upsilon_G} \qquad \textit{Eq.6.7}$$

$$Re_L = \frac{D_L U_L}{\upsilon_L} \qquad \textit{Eq.6.8}$$

$$D_G = \frac{4A_G}{S_G + S_i} \qquad \textit{Eq.6.9}$$

$$D_L = \frac{4A_L}{S_l} \qquad \textit{Eq.6.10}$$

The geometrical variables are shown in figure 6.1.

6.1.2 Interfacial shear stress

The interfacial shear stress is defined in equation 6.11 where the interfacial friction factor is related to the dominant stratified regime and the superficial gas velocity:

$$\tau_i = f_i \frac{\rho_G (U_G - U_L)^2}{2} \qquad \textit{Eq.6.11}$$

Where f_i is the interfacial friction factor. The transitions to 2-D waves and long amplitude waves for the stratified air-water flows are predicted by equations 6.12 and 6.13 respectively(Tzotzi & Andritsos 2013):

$$U_{GS,2-D} \geq \frac{1}{1.95} \ln\left(\frac{0.8}{U_{LS,2-D}}\right) \qquad \textit{Eq.6.12}$$

$$U_{GS,KH} \geq \frac{1}{0.65} \ln\left(\frac{1.39}{U_{LS,KH}}\right) \qquad \textit{Eq.6.13}$$

The ratio of the interfacial friction factor to the gas-wall friction factor is calculated with respect to the dominant stratified sub-region and the gas superficial velocity(Tzotzi & Andritsos 2013):

$$\frac{f_i}{f_{Gw}} = 1 \qquad for\ U_{GS} < U_{GS,2-D} \qquad \textit{Eq.6.14}$$

$$\frac{f_i}{f_{Gw}} = 1 + 0.35 \left(\frac{h}{D}\right)^{0.5} \left(U_{GS} - U_{GS,2-D}\right) \quad for\ U_{GS,2-D} \leq U_{GS} \leq U_{GS,KH} \qquad \textit{Eq.6.15}$$

$$\frac{f_i}{f_{Gw}} = 2\left(\frac{h}{D}\right)^{0.1} + 4\left(\frac{h}{D}\right)^{0.5} \left(U_{GS} - U_{GS,2-D}\right) \qquad for\ U_{GS} > U_{GS,KH} \qquad \textit{Eq.6.16}$$

6.1.3 Calculation procedure

An iterative procedure is proposed to estimate the pressure drop with respect to the known gas, liquid superficial velocities, and the fluid properties. The proposed method starts with assuming an initial value for $\left(\frac{h}{D}\right)$, and then calculates the geometrical properties as presented in equations 6.17 to 6.22:

$$\gamma = 2\cos^{-1}\left(1 - \frac{2h}{d}\right) \qquad \textit{Eq.6.17}$$

$$\frac{S_i}{D} = \sin\left(\frac{\gamma}{2}\right) \qquad \textit{Eq.6.18}$$

$$\frac{S_L}{D} = \frac{\gamma}{2} \qquad \textit{Eq.6.19}$$

$$\frac{S_L}{D} = \pi - \frac{\gamma}{2} \qquad \textit{Eq.6.20}$$

$$\frac{A_L}{A} = \frac{\gamma - \sin(\gamma)}{2\pi} \qquad \textit{Eq.6.21}$$

$$\frac{A_G}{A} = 1 - \frac{A_L}{A} \qquad \textit{Eq.6.22}$$

The actual gas and liquid velocities (U_G, U_L) are calculated based on the geometrical properties and the superficial velocities. Afterwards, the Reynolds number corresponding to each phase is calculated from equations 6.7 and 6.8. Knowing the Reynolds numbers, the gas-wall and liquid-wall friction factors and the shear stresses can be calculated by applying equations 6.3-6.6.

Interfacial friction factor and shear stress are evaluated with respect to the dominant stratified flow regime by implementing the adequate equations from equations 6.11 to 6.16.

The pressure drop across the pipe length for the gas and the liquid phases are calculated from equations 6.1 and 6.2 respectively and the procedure is repeated for different values of $\left(\frac{h}{D}\right)$ until the difference between the pressure drops of two phases is minimized[5]. Since there is only a single real value of $\left(\frac{h}{D}\right)$ (between zero and one) for which the pressure drop in two phases are equal, the mathematical methods such as Newton-Raphson and Regula-falsi can be used to reach a solution in a faster way. It claimed by Tzotzi & Andritsos (2013) that this model is generally capable of predicting the pressure drop of stratified gas-liquid flows within 30% of accuracy(Tzotzi & Andritsos 2013).

In Figure 6.2 pressure drop measured in experiment for the entire range of gas and liquid flow rates and without polymers are compared with ones predicted by the aforementioned model:

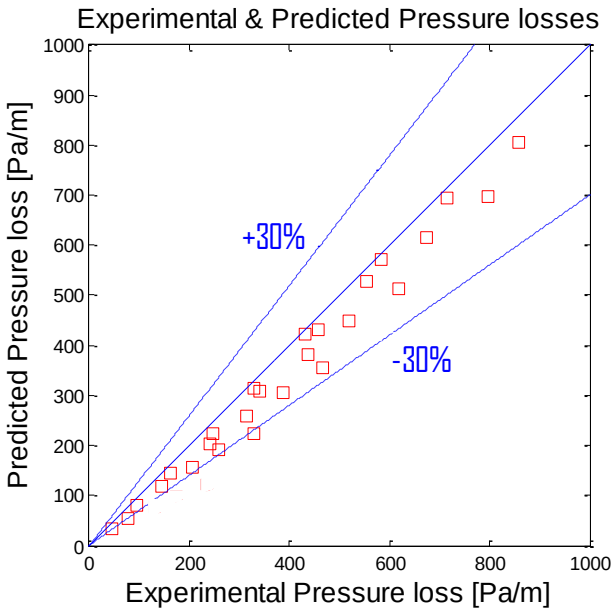

Figure 6.2: Comparison between the predicted pressure losses by Tzotzi & Andritsos model and measured pressure losses.

As it is presented in figure 6.2, the pressure losses measured in the experiments are slightly larger than the values predicted by the model. However, they are within the acceptable range of the model. This shows that using the one-dimensional momentum balance assumption with the semi-empirical correlation used in this model to predict the gas-wall friction factor, might be a sufficiently accurate way to calculate the interfacial shear stress of the stratified flow in the experimental setup used in this work.

[5] The maximum error between these values was less than 2 % of the pressure drop in our calculations.

6.2 Interfacial friction

In this section the one-dimensional momentum balance is used to calculate the interfacial shear stresses for stratified flows with and without polymers. Since the interfacial shear stress is not measured directly in this study, measured parameters are combined with the one-dimensional momentum balance (see section 6.1) to calculate the interfacial stress and friction factor. First the mean liquid holdup (measured in the experiments) is used to calculate the average actual gas velocity from equation 1.5. Then considering the fact that polymers are only present in the liquid phase and the gas-wall friction factor is not affected by them, equations 6.3 and 6.5 are utilized to calculate the gas-wall friction factor and shear stress. Comparison made in section 6.1 shows that these equations can be used to estimate the gas-wall shear stress of the stratified flow in the experimental setup used in this study.

Knowing the gas-wall shear stress and the pressure drop - which is directly measured in the experiments - it is possible to estimate the interfacial shear stress and friction factor, using equations 6.1 and 6.11. The interfacial shear stress and the ratio of pressure loss caused by interfacial friction and gas-wall friction for different polymer concentrations for the superficial gas velocity of 9 m/s are shown in figures 6.3 and 6.4:

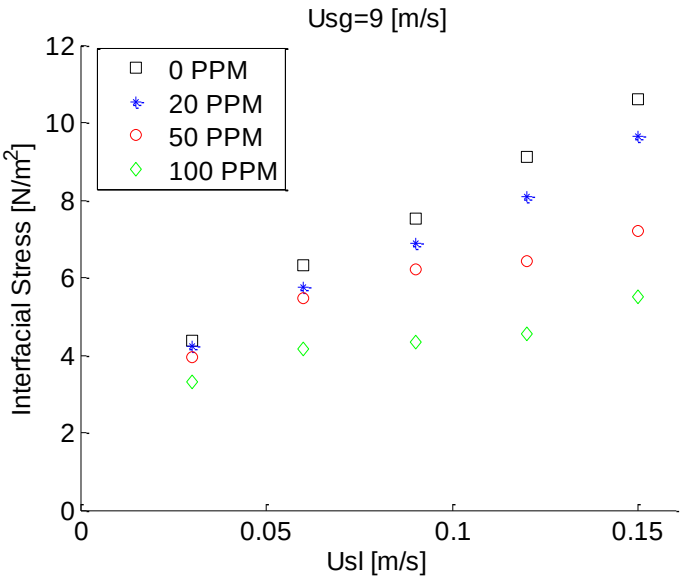

Figure 6.3: Effect of polymers on τ_i for constant Usg= 9 m/s.

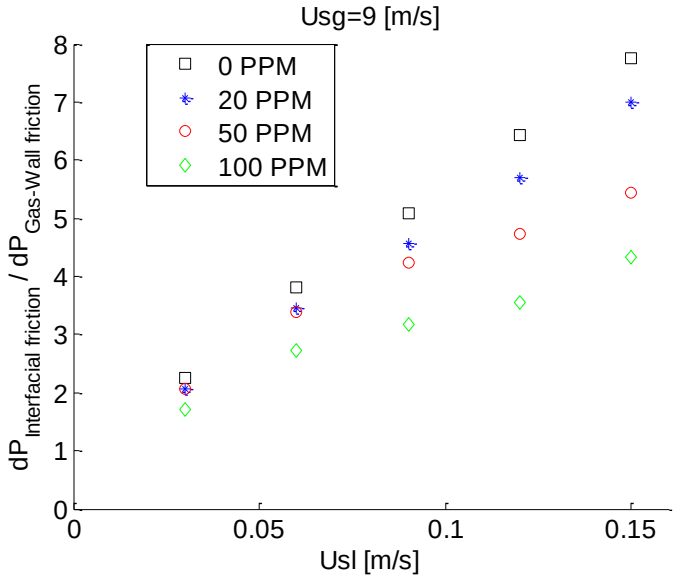

Figure 6.4: Effect of polymers on dP_i/dP_{GW} for constant Usg= 9 m/s.

As shown in figure 6.3 the interfacial shear stress is significantly reduced by increasing the polymer concentration. The interfacial shear stress is increased by increasing the liquid/gas flow rates. That is due to the fact that increasing either one of them causes an increase in the gas actual velocity and increases the disturbances at the interface.

The role of the interfacial friction and gas-wall friction in the total pressure drop are compared in figure 6.4. Data presented in this figure shows that the contribution of interfacial shear stress on the frictional pressure losses is significant. In absence of polymers, the ratio of dP_i/dP_{GW} increases from 2 for the superficial liquid velocity of 0.03 m/s to up to 8 for the highest liquid velocity. While the contribution of the interfacial shear stress to the frictional pressure losses is considerably reduced after the addition of the polymers. The interfacial friction factors and interfacial pressure drops for different gas and liquid velocities are presented in appendix H.

6.3 Post processing Model

In previous chapters it has been mentioned that the addition of the drag reducing polymers to the stratified air-water flows affect several features of flows including the entrainment rate, the curvature of the interface, the average liquid holdup, and the interfacial disturbances (see chapter 5). Damping of the interfacial disturbances and the reduction in the curvature of the interface might have a considerable contribution to the drag reduction of the stratified gas-liquid flows. In this chapter a model is introduce to assess the contribution of these two factors to the drag reduction of the stratified flows. Method used to consider the effect of interfacial disturbances (roughness model) and the curvature of the interface (double-circle model) are introduced in sections 6.3.1 and 6.3.2 respectively. The drag reductions calculated by the model are compared with the values measured in the experiment for specific cases (section 6.3).

6.3.1 Roughness model

In order to take into account the effect of interfacial disturbances on the interfacial shear stress, the gas-liquid interface is modeled as a rough wall and the gas is assumed to flow between this surface and the pipe perimeter. The interfacial friction factor is calculated based on the equivalent sand roughness of the interface. Fernandez (1984) introduced a modified rms[6] of interfacial height considering the part of the waves that emerges in the viscous sub-layer:

$$h' = \Delta h \sqrt{2\left[1 - \left(\frac{56\nu_G}{u_i^* D_G}\right)^2\right]} \qquad \text{Eq.6.23}$$

Where u_i^* is the frictional velocity at the interface, D_G *and* ν_G are the gas phase hydraulic diameter and kinetic viscosity, and Δh is the rms value of the liquid height fluctuations(Fernandez 1984). Fernandez (1984) showed that the modified rms value of the interfacial height can be used as a representative of the interface sand roughness(Fernandez 1984). The rms value of the liquid height fluctuation is calculated from the measured time variation of h/D at the center of pipe using conductance probes. The interfacial friction factor is calculated from the Colebrook correlation:

$$\frac{1}{\sqrt{f_i}} = 3.48 - 4\log\left(\frac{2h'}{D_G} + \frac{9.35}{Re_G\sqrt{f_i}}\right) \qquad \text{Eq.6.24}$$

6.3.2 Double-circle model

Visual observations made in this study and the data published by Cav & Brill (1997) showed that when the long amplitude waves and atomization are the dominant stratified regime of air-water flows (without polymers) the interface has a significant concave down curvature(Cav & Brill 1997). Cav & Brill (1997) proposed a double circle model to take into account the curvature of the interface. This model is shown in figure 6.5:

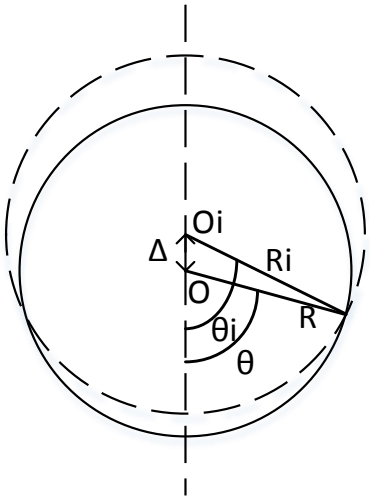

Figure 6.5: Double circle method proposed by Cav & Brill (1997).

The geometrical properties of stratified flow implementing the double circle model are calculated from equations 6.25 to 6.29:

[6] Root mean square.

$$S_G = (\pi - \theta)D \quad \text{Eq.6.25}$$

$$S_L = \theta D \quad \text{Eq.6.26}$$

$$S_i = \theta_i D_i \quad \text{Eq.6.27}$$

$$A_G = (1 - H_L)\frac{\pi D^2}{4} \quad \text{Eq.6.28}$$

$$A_G = H_L \frac{\pi D^2}{4} \quad \text{Eq.6.29}$$

Where θ *and* θ_i are the film wetted angles of circles O *and* O_i, D *and* D_i are the diameters of circles O *and* O_i and H_L is the liquid holdup. The parameters θ_i *and* D_i can be calculated from θ *and* D by applying the geometrical correlations presented in equations 6.30 and 6.31:

$$D_i = \frac{sin\theta}{sin\theta_i} D \quad \text{Eq.6.30}$$

$$\theta_i = \left(\frac{sin\theta_i}{sin\theta}\right)^2 (\theta + \frac{sin^2\theta}{tg\theta_i} - \frac{sin2\theta}{2} - \pi H_L) \quad \text{Eq.6.31}$$

Hart (1989) proposed a correlation, based on the extensive experimental data, to relate the wetted wall fraction to the liquid holdup and modified Froude number:

$$\frac{\theta}{\pi} = 0.53{\alpha_L}^{0.374} + 0.26Fr^{0.58} \quad \text{Eq.6.32}$$

$$Fr = \frac{\rho_L U_L^2}{(\rho_L - \rho_G)gD} \quad \text{Eq.6.33}$$

Where Fr is the modified Froude number and α_L is the liquid holdup(Hart 1989).

6.3.3 Pressure drop calculation

In order to assess the contribution of the damping of the interfacial disturbances and the reduction in the curvature of the interface, one-dimensional momentum balance is used to calculate the pressure drop with and without polymers. In this calculation the interfacial shear stress is calculated based on the equivalent sand roughness of the interface which is calculated from the time variation of h/D at the center of the pipe. Moreover, the length of the gas-liquid interface (S_i) is calculated from the double-circle model in absence of polymers and when polymers are added this value is calculated based on the flat interface assumption. The assumption of the flat interface is only valid for high polymer concentrations. Hence, in this section only the data for the 100 ppm solution are used. Moreover, since the effect of entrainments is not considered in the proposed model, it is not possible to use the data for the atomization regime. Based on the model proposed above, the frictional pressure losses are calculated for the stratified flow of air-water and air-polymeric solution (100 ppm), and then the drag reduction is calculated from these values.

In Figure 6.6 a comparison is made between the drag reduction calculated by the proposed model and the values obtained during the experiments:

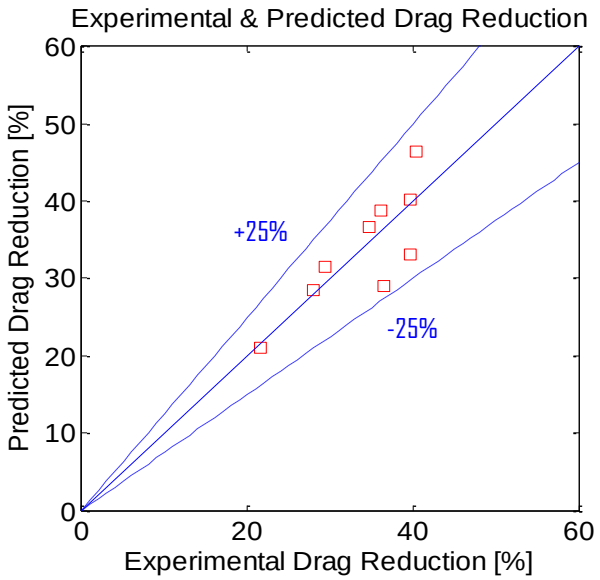

Figure 6.6: Comparison between the drag reduction calculated by the proposed model and values obtained during the experiments for 100 ppm solution.

As it is shown in figure 6.6 there is a good agreement between the drag reduction estimated by the model and the values obtained in the experiments. These results show that the reduction in the curvature of the interface and damping of the interfacial disturbance might have a considerable contribution to the observed drag reduction in the stratified flows after the addition of polymers.

6.4 Conclusions

The pressure losses measured for the stratified flows without polymers are compared with the ones predicted by the one-dimensional model proposed by Tzotzi & Andritsos (2013) for the entire range of gas and liquid flow rates. Suficient agreement between the measured and predicted values shows that the semi-empirical correlation used in this model (equations 6.3 and 6.5) can be implemented to predict the gas-wall shear stress of the experiments. Implementing this correlation and knowing the average holdup and pressure losses, the one-dimensional momentum balance of the gas phase is used to calculate the interfacial shear stress (with and without polymers). The results showed significant reduction in the interfacial shear stress after the addition of the polymers. It could be argued that the observed increased in the liquid holdup and decrease in the wave velocity and frequency after the addition of polymers (see chapter 5) are associated with the reduction of the interfacial shear stress.

In order to assess the contribution of the damping the interfacial disturbances and reduction of the curvature of the interface on the pressure losses, a model is proposed. Using this model, drag reductions close to the values measured in the experiments are obtained. These results could be interpreted by arguing that the polymers damp the interfacial disturbances and reduce the curvature of the interface. In this way they reduce the frictional pressure losses associated with interfacial shear stress by reducing the interfacial shear stress and by reducing the interfacial area.

Chapter 7: Conclusions & Recommendations

A summary of the conclusions and recommendations from this work is presented in this chapter. The main conclusions of this study are presented in section 7.1. Thereafter, based on the aforementioned conclusions, number of recommendations for the future works is described.

7.1 Conclusion

The main goals of this work include: (i) improving the understanding of the influences of drag reducing polymers on horizontal gas-liquid stratified flows and how they are affecting the pressure losses and fluctuations; and (ii) investigating the effects of drag reducing polymers on the interfacial phenomena and how these effects are related to the reduction observed in pressure losses and in the fluctuations.

Rheological measurements showed that the Addition of polymers to water results in a viscoelastic behavior proving that the polymer molecules are capable of storing and then releasing the energy after an applied shear force is removed. It is argued that this behavior allows polymers to suppress the turbulences and store their energy where the shear forces are higher and then releasing this energy where shear forces are lower. Considering an increase in the drag reduction of stratified flow by increasing the liquid Reynolds number and polymer concentration, the interactions between the polymers and turbulences (as a result of non-Newtonian behavior of polymers e.g. shear thinning and viscoelastic) might have a contribution to the observed drag reduction.

The static and dynamic surface tensions of water are not considerably affected by the addition of the polymers. Drag reductions up to 55% are obtained for the stratified flows with the polymer concentrations as low as 100 ppm accordingly, it is argued that surface tension does not play an important role in the drag reduction of stratified gas-liquid flows with these concentrations.

The interfacial disturbances are significantly damped and the liquid holdup is increased by the addition of polymers. DRPs also cause a decrease in interfacial shear stress. The pronounced increase in the liquid holdup is caused by the decrease in the interfacial shear stress.

Decreasing the interfacial shear stress reduces the force applied by the gas phase on the roll waves and causes a reduction in their velocity and frequency. After the addition of polymers, the amplitude of roll waves decreases while their wavelength increases. These roll waves - in comparison with the larger amplitude smaller wavelength roll waves observed in the absence of polymers - are less likely to form slugs. According to that it is suggested that the drag reducing polymers might shift the transition to the slug flow to the larger liquid flow rates.

High speed camera recordings showed that the addition of DRPs into the stratified flow suppresses the entrainment of droplets into the gas phase. The reduction in entrainment level might have a contribution to the drag reduction of stratified flows.

The high frequency waves on the roll waves and on the stratified flow between them are significantly damped after the addition of polymers. It is suggested that the reduction in the interfacial shear stress is associated, mainly, with damping of the interfacial disturbances. Moreover, the addition of polymer causes a reduction in the interfacial surface area by reducing the curvature of the interface. Motivated by these, a model is proposed to investigate the contribution of damping the interfacial disturbances (roughness of the interface) and reducing

the interfacial surface area to the drag reduction. The experimental data is used to determine the adequate values for the roughness parameter and the liquid holdup. Drag reductions close to the values measured in experiments are calculated by the model. These results are interpreted by arguing that the damping of the interfacial disturbances and reducing the interfacial area after the addition of polymers, reduces the momentum exchange between the gas and liquid phases and have a considerable contribution to the drag reduction of stratified gas liquid flows.

7.2 Recommendations

To investigate relevant viscoelastic behavior of the DRPs at the turbulent flows, the oscillation test should be conducted at different frequencies which are corresponding to the different turbulent scales.

The Design and implementation of an optical insert to allow for flow visualization from inside the pipe will increase the quality of the information extracted from the recorded videos. One of the limitations of the conductance probes method and flow visualization from outside of the pipes is that none of them is capable of capturing the small amplitude structures such as ripples and small droplets with sufficient resolution. Designing an adequate optical insert and flow visualization from inside may help while dealing with smaller structures.

The considerable decline in the Reynolds shear stresses has been mentioned as one of the most important reasons in the single phase drag reduction. Sufficient information regarding the Reynolds shear stresses can be obtained by applying the PIV (particle image velocimetry) . The PIV measurements can also reveal essential information regarding the interfacial and liquid-wall shear stresses as well as the actual velocity of different part of the waves.

An automated image processing technique to detect the roll waves and their properties could be used to facilitate the extraction of the information from the recorded videos.

Quantitative and detailed study of the entrainments was out of the scope of this work. The separation and deposition of droplets have a significant influence on the pressure losses along the pipe. Sufficient understanding from the entrainments and how the addition of polymers affects them could be of great help to improve the proposed model to estimate the drag reduction in all the stratified sub-regions.

Based on the results obtained in this study it is expected that the addition of DRPs postponed the transition to slug flow to greater liquid flow rates. The detailed investigation of the effect of drag reducing polymers on the transition to slug flow could be the next step to move towards the application of the drag reducing polymer as a solution for the slug induced problems in oil and gas industry.

In the field applications the typical size of the pipes larger than 5 cm. This work proves the benefit of using the drag reducing polymers in the pipe sizes smaller than this range. The next stage of the research could be investigating the effect of DRPs in larger pipe sizes. Water and air are used in this study as the liquid and gas phases which are different in properties with the fluids that are present in the oil and gas industry. Conducting the similar study with the natural gas and condensates and at the harsh field conditions can improve the understanding the effect of DRPs at the real world applications.

Bibliography

Al-Sarkhi, A. & Hanratty, T.J., 2001. Effect of drag-reducing polymers on annular gas–liquid flow in a horizontal pipe. *International Journal of Multiphase Flow*, 27(7), pp.1151–1162. Available at: http://www.sciencedirect.com/science/article/pii/S0301932200000719 [Accessed June 9, 2014].

Al-sarkhi, A., Nakla, M. El & Ahmed, W.H., 2011. Friction factor correlations for gas–liquid/liquid–liquid flows with drag-reducing polymers in horizontal pipes. *International Journal of Multiphase Flow*, 37(5), pp.501–506. Available at: http://www.sciencedirect.com/science/article/pii/S0301932211000255 [Accessed June 9, 2014].

Al-sarkhi, A. & Soleimani, A., 2004. Effect of Drag Reducing Polymers on Two-Phase Gas–Liquid Flows in a Horizontal Pipe. *Chemical Engineering Research and Design*, 82(12), pp.1583–1588. Available at: http://www.sciencedirect.com/science/article/pii/S0263876204726593 [Accessed June 9, 2014].

Andritsos, N. & Hanratty, T.J., 1987. Interfacial instabilities for horizontal gas-liquid flows in pipelines. *International Journal of Multiphase Flow*, 13(5), pp.583–603. Available at: http://www.sciencedirect.com/science/article/pii/0301932287900371 [Accessed June 9, 2014].

Baker, 1954. simultaneous flow of oil and gas. *Oil Gas Journal*.

Bryanston-Cross, P.J. & Epstein, A., 1990. The application of sub-micron particle visualisation for PIV (Particle Image Velocimetry) at transonic and supersonic speeds. *Progress in Aerospace Sciences*, 27(3), pp.237–265. Available at: http://www.sciencedirect.com/science/article/pii/0376042190900088 [Accessed June 9, 2014].

Cav, X.D. & Brill, J.P., 1997. Gas-Liquid Stratified-Wavy Flow in IHorizontal Pipelines. , 1(December 1997).

Daas, M. & Bleyle, D., 2006. Computational and experimental investigation of the drag reduction and the components of pressure drop in horizontal slug flow using liquids of different viscosities. *Experimental Thermal and Fluid Science*, 30(4), pp.307–317. Available at: http://www.sciencedirect.com/science/article/pii/S089417770500097X [Accessed June 9, 2014].

Fernandes, R.L.., Jutte, B.. & Rodriguez, M.., 2004. Drag reduction in horizontal annular two-phase flow. *International Journal of Multiphase Flow*, 30(9), pp.1051–1069.

Available at: http://linkinghub.elsevier.com/retrieve/pii/S0301932204000771 [Accessed August 15, 2014].

Fernandes, R.L.J. et al., 2009. Experimental Study of DRA for Vertical Two-Phase Annular Flow. *Journal of Energy Resources Technology*, 131(2), p.023002. Available at: http://energyresources.asmedigitalcollection.asme.org/article.aspx?articleid=1414907 [Accessed June 9, 2014].

Fernandez, F., 1984. Etude des interactions dynamiques en écoulement diphasique stratifié. In *INP Toulouse*.

Fontaine, a. a., Petrie, H.L. & Brungart, T. a., 2006. Velocity profile statistics in a turbulent boundary layer with slot-injected polymer. *Journal of Fluid Mechanics*, 238(-1), p.435. Available at: http://www.journals.cambridge.org/abstract_S0022112092001770.

Gai, H., 1990. *Ultrasonic techniques for flow imaging : front-end transducers, image reconstruction algorithms and system design.* University of Manchester.

Haandrikman, G. et al., 1999. Slug control in flowline/riser systems. In *Proc 2nd Int Conf*.

Hart, J., 1989. J. HART, P. J. HAMERSMA'[" and J. M. H. , 15(6), pp.947–964.

Havre, K., Stornes, K.O. & Stray, H., 2000. *Taming slug flow in pipelines*,

Katerpallir, S. & White, C., 2000. The onset of drag reduction by dilute polymer additives, and the maximum drag reduction asymptote. *J. Fluid Mech*, 409, pp.149–164.

Kawaji, M., 1998. Two-phase flow measurements using a photochromic dye activation technique. *Nuclear Engineering and Design*, 184(2-3), pp.379–392. Available at: http://www.sciencedirect.com/science/article/pii/S0029549398002106 [Accessed June 9, 2014].

Koskie, J.E., Mudawar, I. & Tiederman, W.G., 1989. Parallel-wire probes for measurement of thick liquid films. *International Journal of Multiphase Flow*, 15(4), pp.521–530. Available at: http://www.sciencedirect.com/science/article/pii/0301932289900517 [Accessed June 9, 2014].

Lin, P.Y. & Hanratty, T.J., 1987. EFFECT OF PIPE D I A M E T E R ON FLOW PATTERNS F O R A I R - W A T E R FLOW IN H O R I Z O N T A L. , 13(4), pp.549–563.

Lin, P.Y. & Hanratty, T.J., 1986. Prediction of the initiation of slugs with linear stability theory. *International Journal of Multiphase Flow*, 12(1), pp.79–98. Available at: http://linkinghub.elsevier.com/retrieve/pii/0301932286900054.

Lumley, L., 1948. DRAG REDUCTION BY ADDITIVESl. , 656(33), pp.367–384.

Min, T. et al., 2003. Drag reduction by polymer additives in a turbulent channel flow. *Journal of Fluid Mechanics*, 486, pp.213–238. Available at: http://www.journals.cambridge.org/abstract_S0022112003004610 [Accessed August 5, 2014].

Oliver, D.R. & A.Young, H., 1968. Two-phase non-Newtonian flow. *Trans. Inst. Chem. Engrs*.

Rosehart, R.G., Scott, D.S. & Rhodes, E., 1972. Gas-liqud slug flow with drag-reducing polymer solutions. *AIChE Journal*, 18(4), pp.744–750. Available at: http://doi.wiley.com/10.1002/aic.690180414 [Accessed June 9, 2014].

Runge, T. & Andersen, M., 2007. Analyzing Multiphase Flow in Horizontal and Deviated Wells. *Oilfield Review Interactive*, (4), pp.1–9.

Soleimani, A., Al-Sarkhi, A. & Hanratty, T.J., 2002. Effect of drag-reducing polymers on pseudo-slugs––interfacial drag and transition to slug flow. *International Journal of Multiphase Flow*, 28(12), pp.1911–1927. Available at: http://www.sciencedirect.com/science/article/pii/S0301932202001106 [Accessed June 9, 2014].

TABOR, M., 1986. A Cascade Theory of Drag Reduction . *EUROPHYSICS LETTERS*, 519.

Taitel, Y. & Dukler, A.E., 1976. A theoretical approach to the Lockhart-Martinelli correlation for stratified flow. *Int. J. Multiphase Flow*, (2), pp.591–595.

Toms, B., 1948. Some observations on the flow of linear polymer solutions through straight tubes at large Reynolds numbers. In *Rheological Congress*.

Den Toonder, J.M.J., 1996. *Drag Reduction by Polymer Additives in a Turbulent Pipe Flow: Laboratory and Numerical Experiments*.

Tzotzi, C. & Andritsos, N., 2013. Interfacial shear stress in wavy stratified gas–liquid flow in horizontal pipes. *International Journal of Multiphase Flow*, 54, pp.43–54. Available at: http://www.sciencedirect.com/science/article/pii/S0301932213000451 [Accessed June 9, 2014].

Virk, P.S. et al., 1967. The Toms phenomenon: turbulent pipe flow of dilute polymer solutions. *Journal of Fluid Mechanics*, 30(02), p.305. Available at: http://www.journals.cambridge.org/abstract_S0022112067001442.

Warholic, M.D., Massah, H. & Hanratty, T.J., 1999. Influence of drag-reducing polymers on turbulence: effects of Reynolds number, concentration and mixing. *Experiments*

in Fluids, 27(5), pp.461–472. Available at: http://link.springer.com/10.1007/s003480050371.

White, C.M. & Mungal, M.G., 2008. Mechanics and Prediction of Turbulent Drag Reduction with Polymer Additives. *Annual Review of Fluid Mechanics*, 40(1), pp.235–256. Available at: http://www.annualreviews.org/doi/abs/10.1146/annurev.fluid.40.111406.102156 [Accessed June 9, 2014].

White, C.M., Somandepalli, V.S.R. & Mungal, M.G., 2004. The turbulence structure of drag-reduced boundary layer flow. *Experiments in Fluids*, 36(1), pp.62–69. Available at: http://link.springer.com/10.1007/s00348-003-0630-0 [Accessed May 26, 2014].

Xu, L. et al., 1997. Application of ultrasonic tomography to monitoring gas/liquid flow. *Chemical Engineering Science*, 52(13), pp.2171–2183. Available at: http://www.sciencedirect.com/science/article/pii/S0009250997000432 [Accessed June 9, 2014].

Acknowledgements

I take this opportunity to express my deep regards to people who have helped my through this project. First and foremost I offer my sincerest gratitude to my supervisors: Prof. dr. Ir. B. J. Boersma, Dr.ir Jos van 't Westende and Pejman Shoeibi Omrani who have supported, monitored, guided and encouraged me throughout this project while allowing me to do the work on my own way.

Andries aided me with installing my setup and running the equipment at fluid flow laboratory at TNO and Evert provided me with useful guidance for building the conductance probes and related electronics. I am completely grateful for all their helps and supports.

Many thanks go out to the team of Daniel at TNO, Eindhoven who helped me with surface tension and viscosity measurements.

I would like to express my profound regards to Pooria who has helped me with the signal processing and was always there for me as a colleague and as a friend.

During the project, I could always rely on my best friends Arash and Saman when I needed some time off or motivation to go on.

At last but not least, I would like to thank my family for supporting me spiritually through my life.

Appendices

Appendix A: Conductance Probes

A.1 Circuit specifications

The conduction is measured at a frequency of 100 kHz with a sinusoidal shape. Therefore, an AC-generator is used and connected to the 'Carrier Input' as shown in figure A.1. Capacitor C1 blocks any DC-signal that could still be present in the AC-generator. Part B acts as buffer amplifier to drive the probe wires with a fixed AC-voltage and from a low impedance source.

Part G is a galvanic separation, taking care that the probe wires are completely electrically floating and not influenced by any ground potential in the circuit or unbalance in the conduction from each wire to the fluid.

Part C is a current-to-voltage converter which converts the 100 kHz current in the probe wires, into a 100 kHz voltage at the output. As a result this output voltage is a direct measure of the 100 kHz current in the probe wires. In other words the *amplitude of the* 100 kHz *output voltage* of part C is a direct measure for the conductance.

Part R is a rectifier to convert this 100 kHz conductance signal in a 100 kHz rectified signal.

Finally, part F is a higher order 10 kHz low-pass filter that removes the 100 kHz ripple from the conductance signal .Consequently, at the output an approximately DC-voltage is found representing the measured conductance between the probe wires.

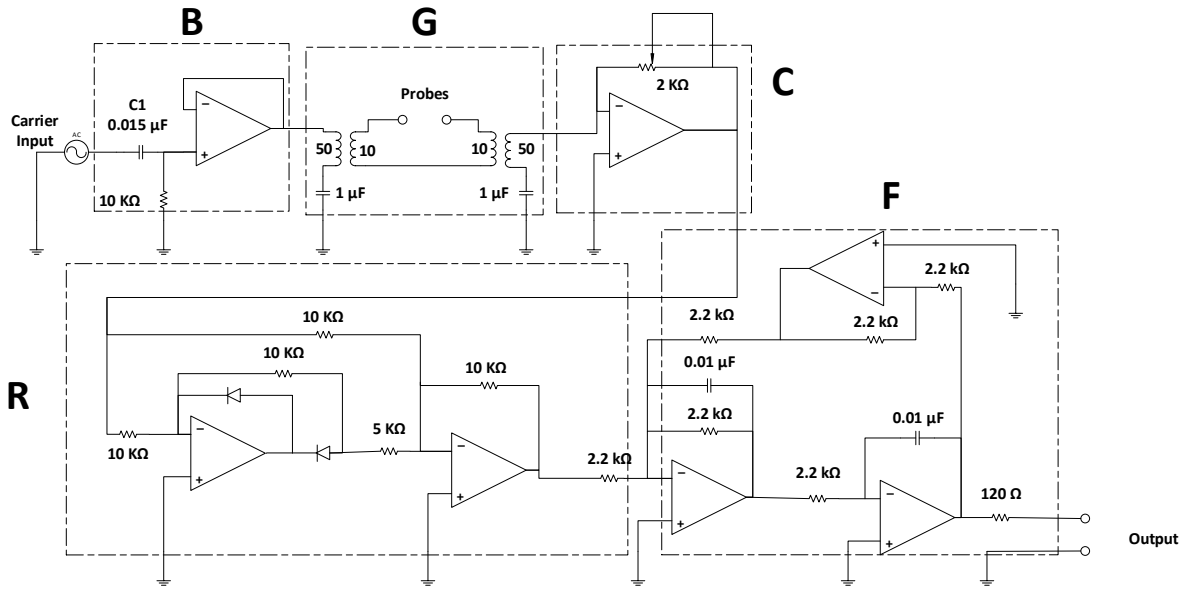

Figure A.1: Representation of the electrical circuit applied for liquid height measurement.

A.2 Linearity of electrical response

Linearity of the output voltage with respect to the existence conductivity between the probed is an important feature of the circuit. The nonlinear respond could mostly arias from insufficient galvanic separation at part G or electrical resistance at either sides of the transformer. To

prevent such effect, special type of transformer is utilized in this experiment. This type of transformer is formed by two coils of wire with extremely low internal resistance. In this way the only resistance that can affect the output voltage is the resistance of the liquid between the conductance probes.

The linearity of the electrical response of the circuit is assessed by placing various known resistances between the probes and by measuring the output response of the circuit to these resistances. To do so, first the exact value of each resistance is measured by an ohmmeter. The results of these measurements are presented in figure A.2.

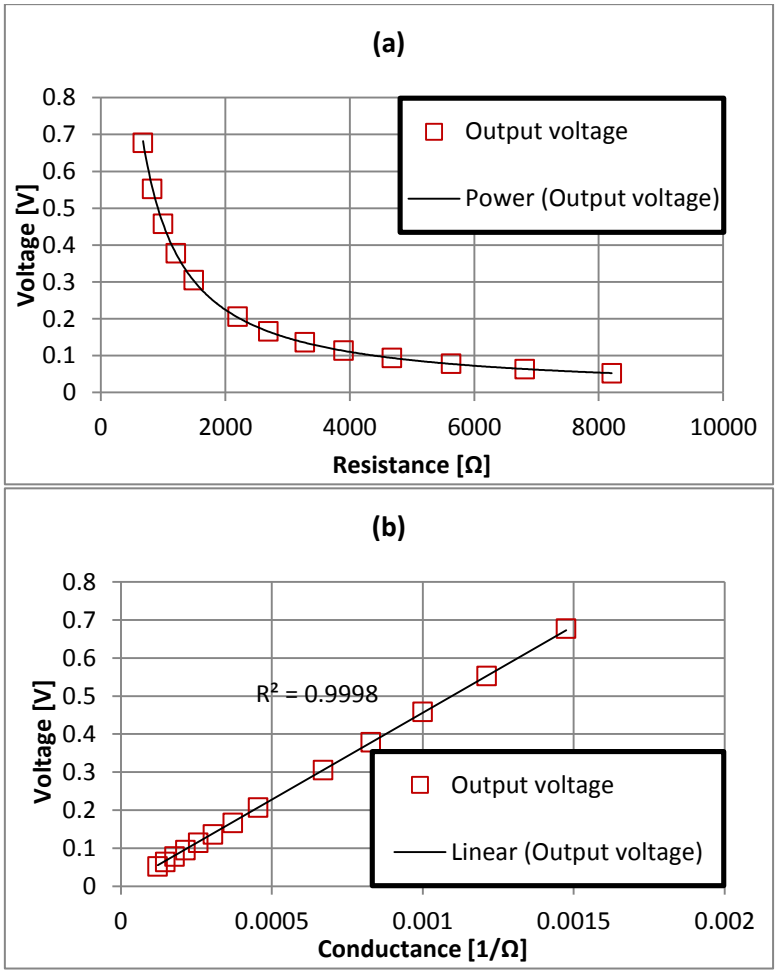

Figure A.2: Electrical response of the circuit to various (a) resistance, (b) conductance.

As it is shown in figure A.2, the designed electrical equipment reposes almost perfectly linear with variation of conductance. It should be mentioned that the range of the resistances used in this test was defined by the range of resistances expected in the experiment. This range was achieved by measuring the electrical resistance between the probes when the pipe is filled with water and when there a limited amount of water between the probes.

A.3 Calibration

Altogether, three sets of electrical circuits are made. Two of them to be utilized for measuring the liquid film thickness at the test section and on to be used with reference set of probes. Considering the fact that each of the components implemented in these circuits has it owns tolerance, it is crystal clear that the circuits will not work exactly the same.

In order to compensate this problem, a potentiometer is placed in the part C. By adjusting the impedance of this potentiometer it is possible to compensate for the circuits' differences and any other imperfections in installation of the probes inside the tube. To calibrate the liquid height measuring probes the following steps are taken:

1. The total volume of the test section is measured[7].
2. The measured volume is Compered with the one calculated from geometrical calculation.
3. The total height of the cross section is divided into 10 parts.
4. The corresponding liquid volume with respect to each liquid level is calculated.
5. The calculated volume of water is injected to the test section and the output signal for each case is measured.

It should be mentioned that the output signal in this case refers to the dimensionless signal (output voltage divided by the reference probe voltage) of the test section probes. This signal is a direct indication of dimensionless liquid level (h/D).In figure A.3 the calibration curve for each set of test section's probes is presented:

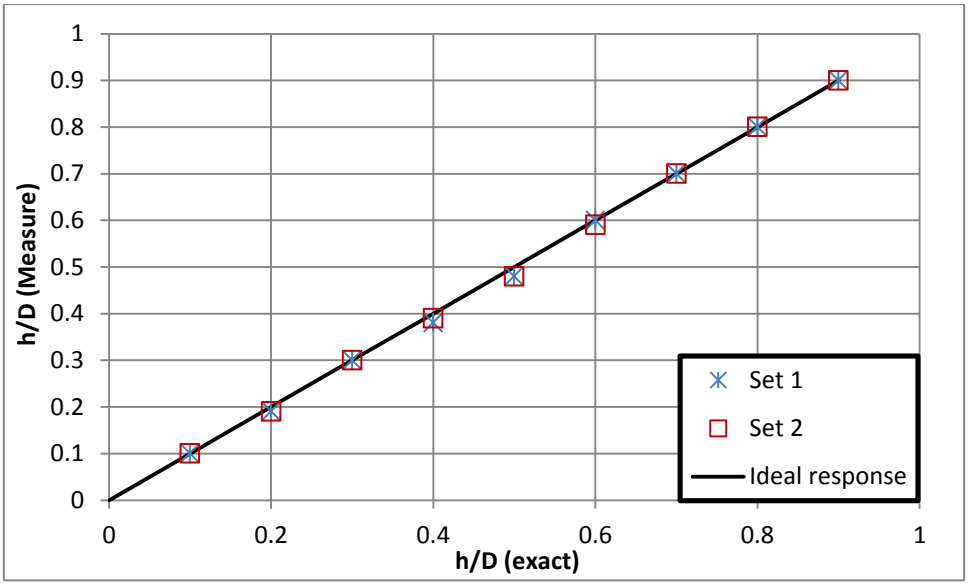

Figure A.3: Calibration curve for liquid height measuring probes.

The data presented in figure A.3 shows that there is a good agreement between the exact value of liquid height and the measured liquid height by the conductance probes. The mean value of

[7] This can be done by filling the test section with water and then measure the volume of the water.

the error for the measured height is less than 1% of the pipe diameter which is about 0.2 mm. This range of precision is sufficient for the purpose of this work.

Appendix B: High speed camera specifications

The eco414MVGE type camera from SVS-VISTEK is utilized for the flow visualization from outside of the pipe the camera specifications are presented in table B.1:

Table B.1: High speed camera specifications.

Camera Specifications	
Manufacturer	SVS-Vistek
Color/Mono	Color
Analog/Digital	Digital
Interface	GigE Vision
Horizontal Resolution	656
Vertical Resolution	492
Sensor Size	1/2"
Bit Depth	14
Sensor Type	Sony ICX414AL CCD
Pixel Size (µm)	9.9 x 9.9
Trigger Input	Yes
Camera In/Out	Yes
Lens Mount	CS-Mount

Appendix C: Single Phase experimental setup

A flexible hose with the inner diameter of 6 mm and length of 3.6 m was used as the main test section. The hose is fixed on an experimental table to ensure that it is levelled horizontally. Two pressure transducers are installed, two meters away from each other, and the pressure drop is calculated by subtracting the values measured by each of them. In order to ensure that the master solution and water are fully mixed and a homogeneous fully developed flow will reach the test section a long flexible pipe with same diameter is placed upstream the test section. The same facility as the one described in chapter 4 is utilized to supply the water and the master solution to the experimental setup.

Appendix D: Cross correlation function for discrete signals

The cross-correlation function for discrete signals is shown below:

$$(f * g)(n) \stackrel{\text{def}}{=} \sum_{m=-\infty}^{\infty} f^*[m]g[m+n]$$

In above equation f and g are the signals that their similarity should be assessed based on the time lag n.

This function shifts the "g" along the x-axis and calculating the integral of the product of "f" and "g" at each position. When the two functions are matched their negative parts are aligned, consequently their product would be positive with a great contribution to the integral. Moreover, at this situation the peaks are also aligned which also increases the value of integral. Hence, the best match is a result of the time lag for which the integral of the product has its maximum value.

Appendix E: Measured pressure losses

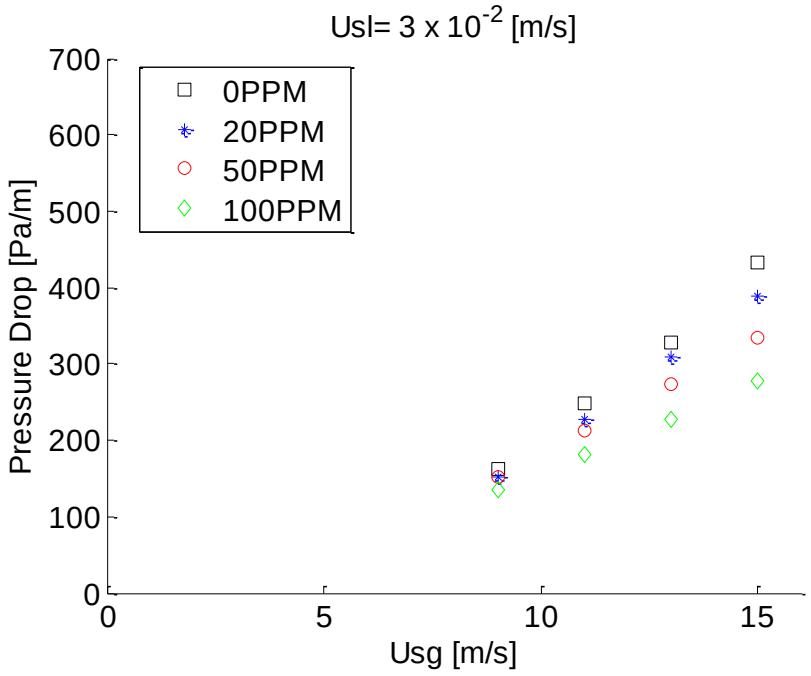

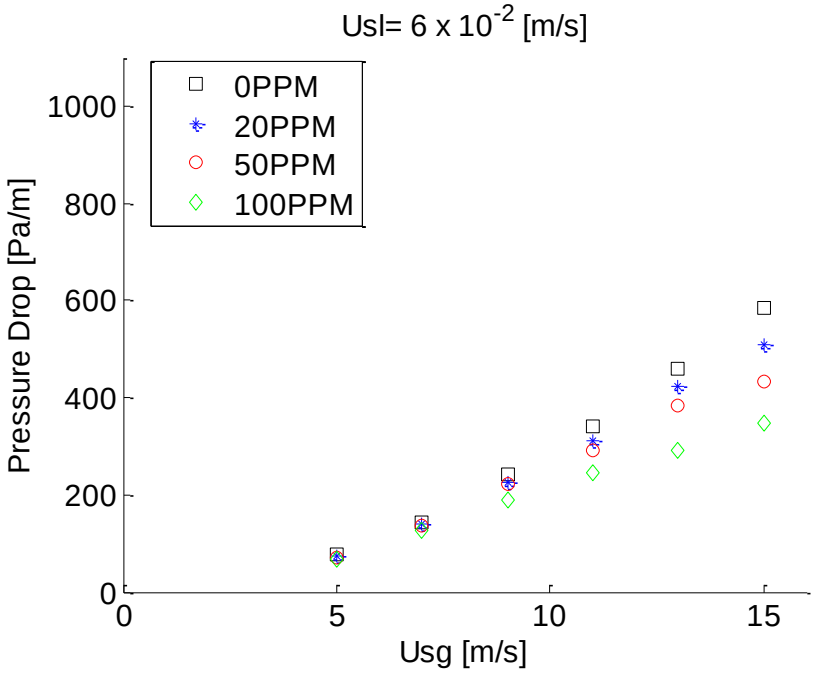

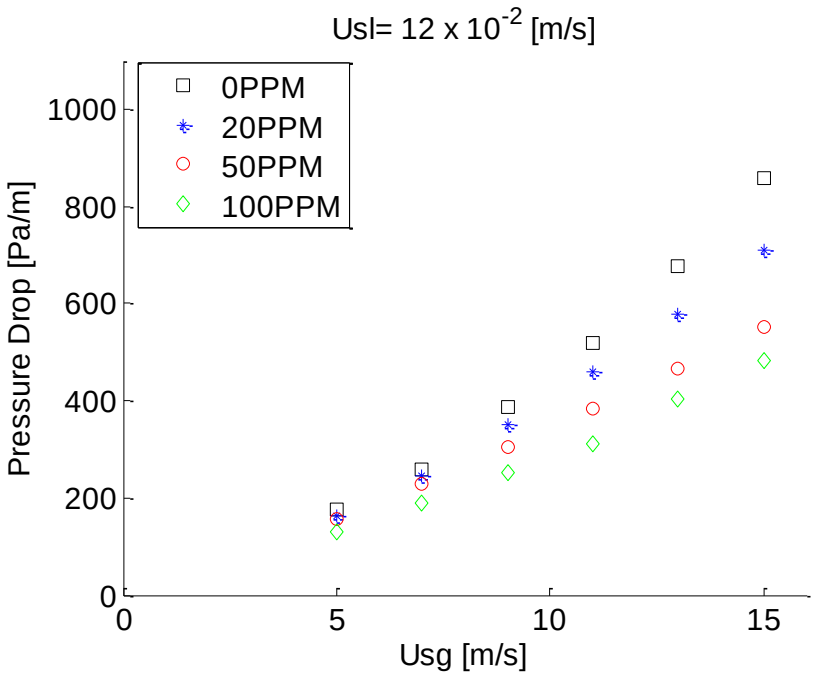
Usl= 12 x 10^-2 [m/s]
0PPM
20PPM
50PPM
100PPM
Pressure Drop [Pa/m]
Usg [m/s]
0
200
400
600
800
1000
0
5
10
15

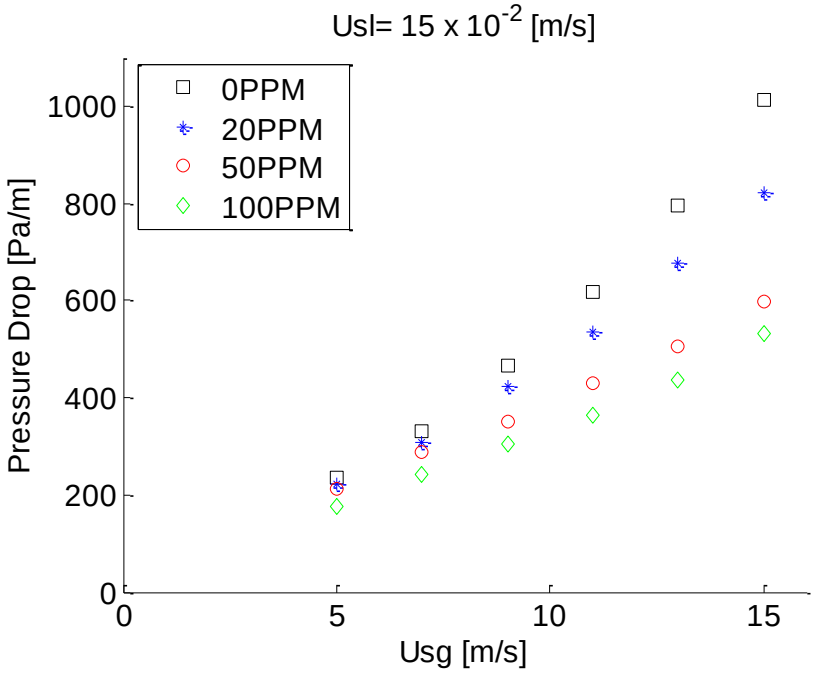
Usl= 15 x 10^-2 [m/s]
0PPM
20PPM
50PPM
100PPM
Pressure Drop [Pa/m]
Usg [m/s]
0
200
400
600
800
1000
0
5
10
15

Appendix F: Frequency domain signals

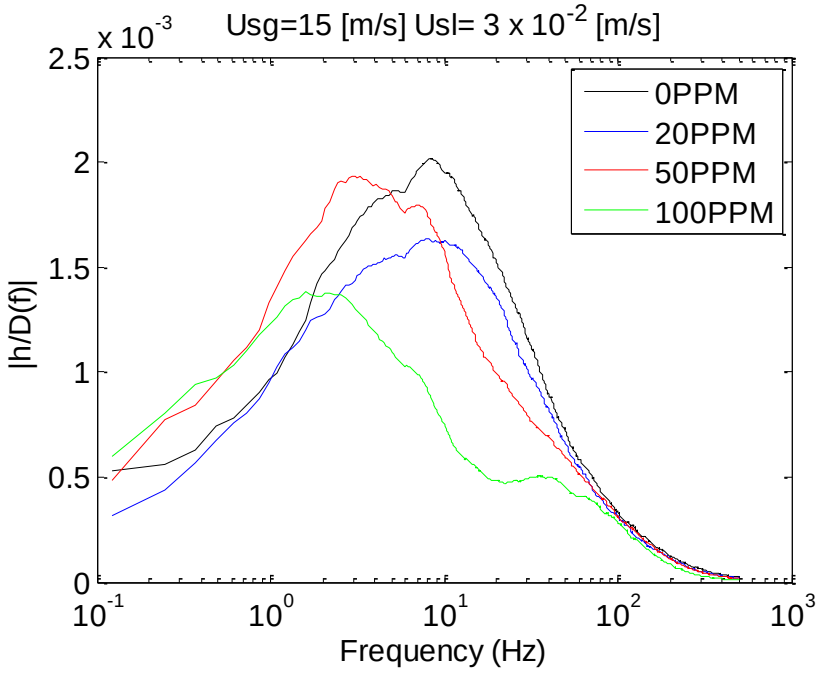

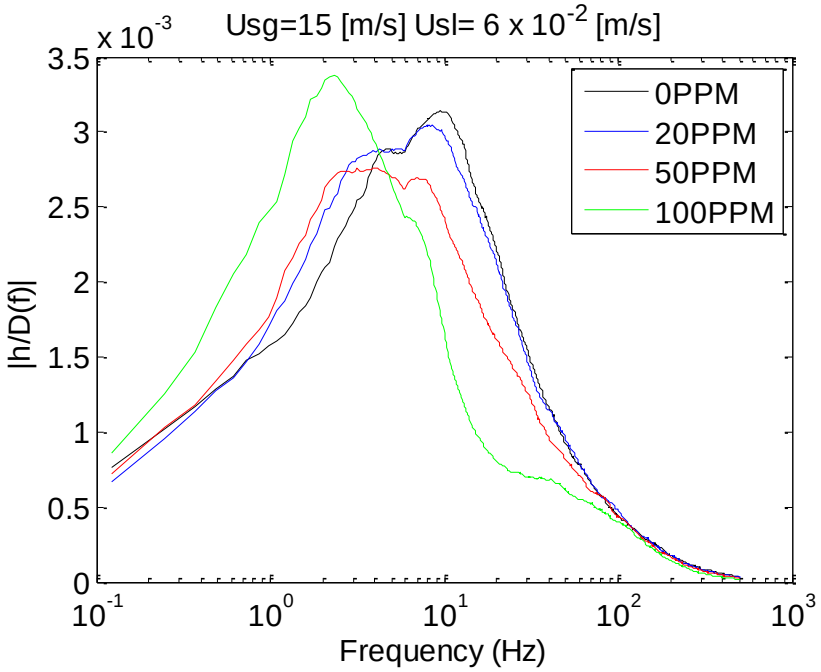

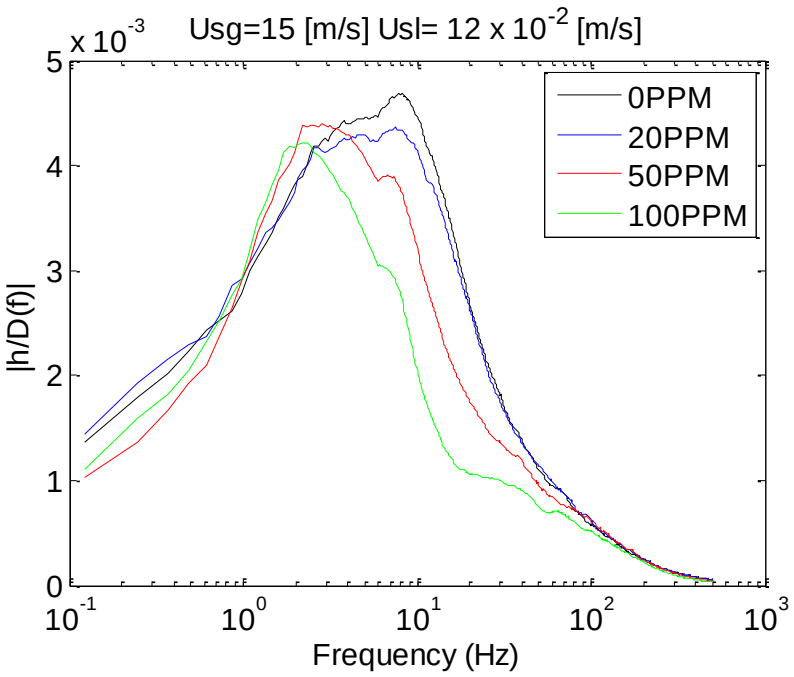
x 10^-3
Usg=15 [m/s] Usl= 12 x 10^-2 [m/s]
0PPM
20PPM
50PPM
100PPM
|h/D(f)|
Frequency (Hz)

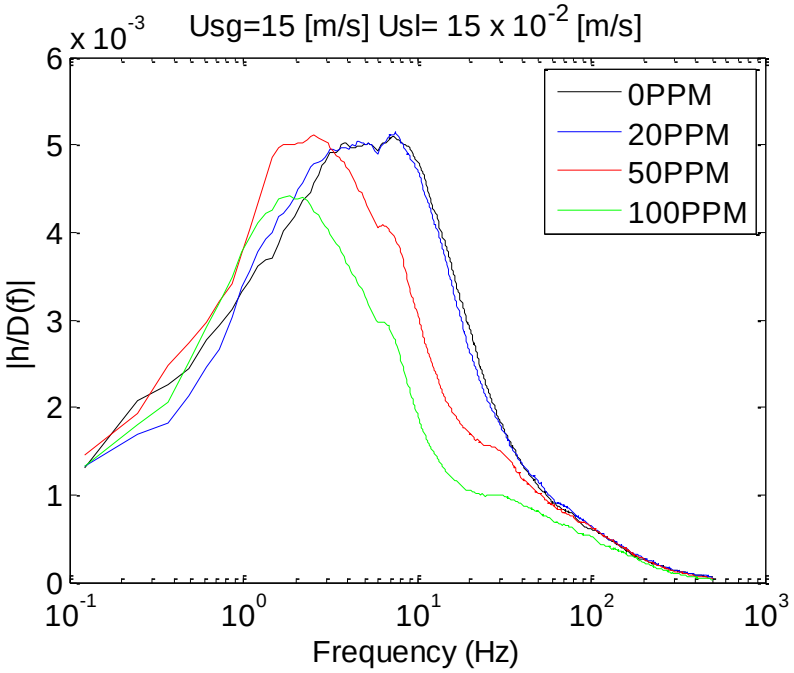
x 10^-3
Usg=15 [m/s] Usl= 15 x 10^-2 [m/s]
0PPM
20PPM
50PPM
100PPM
|h/D(f)|
Frequency (Hz)

Appendix G: Wave velocity & frequency

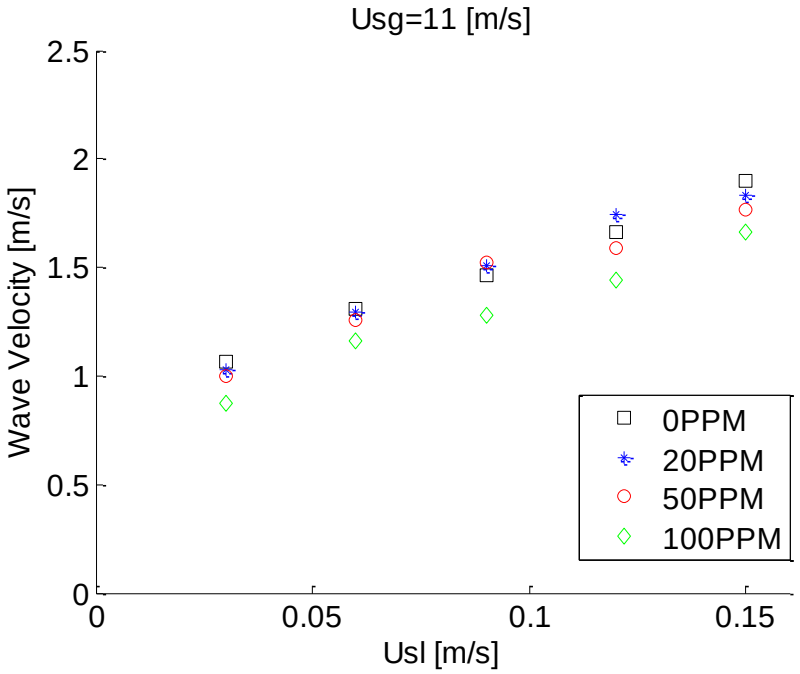

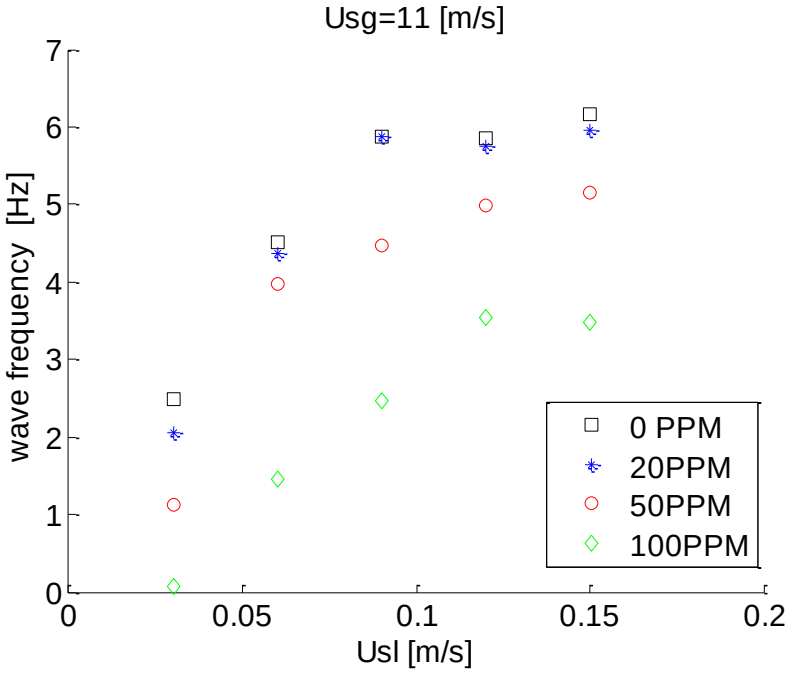

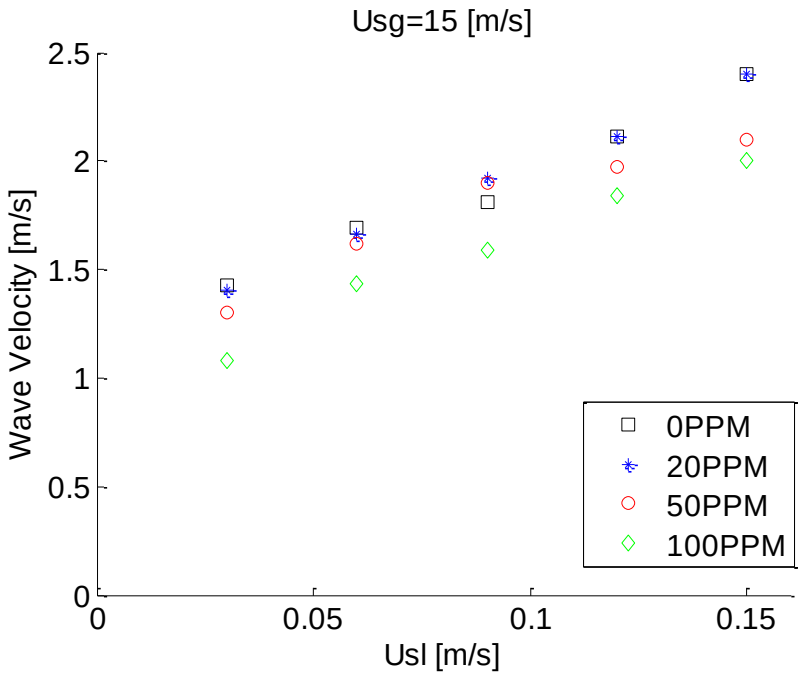
Usg=15 [m/s]
Wave Velocity [m/s]
Usl [m/s]
0PPM
20PPM
50PPM
100PPM

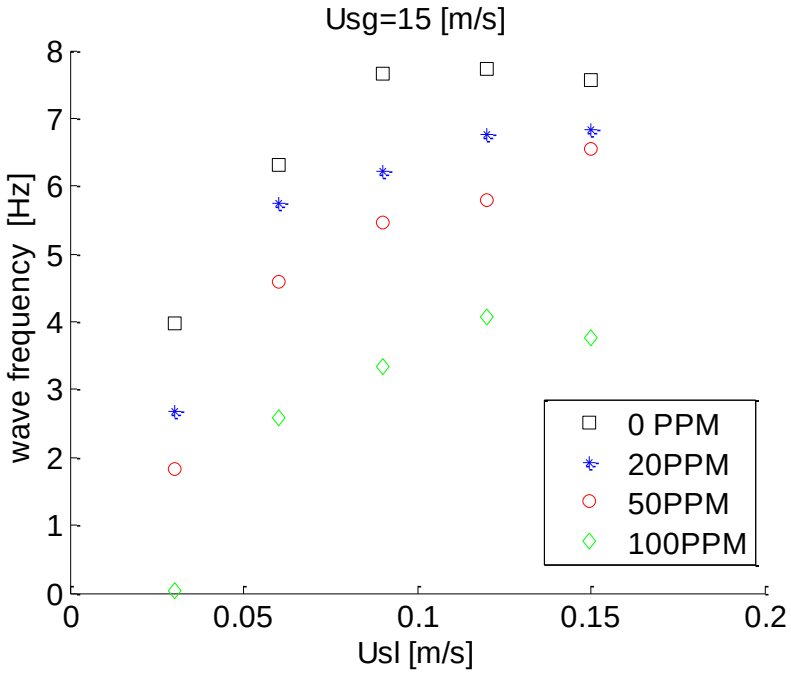
Usg=15 [m/s]
wave frequency [Hz]
Usl [m/s]
0 PPM
20PPM
50PPM
100PPM

Appendix H: Interfacial shear stress & Pressure drop fraction

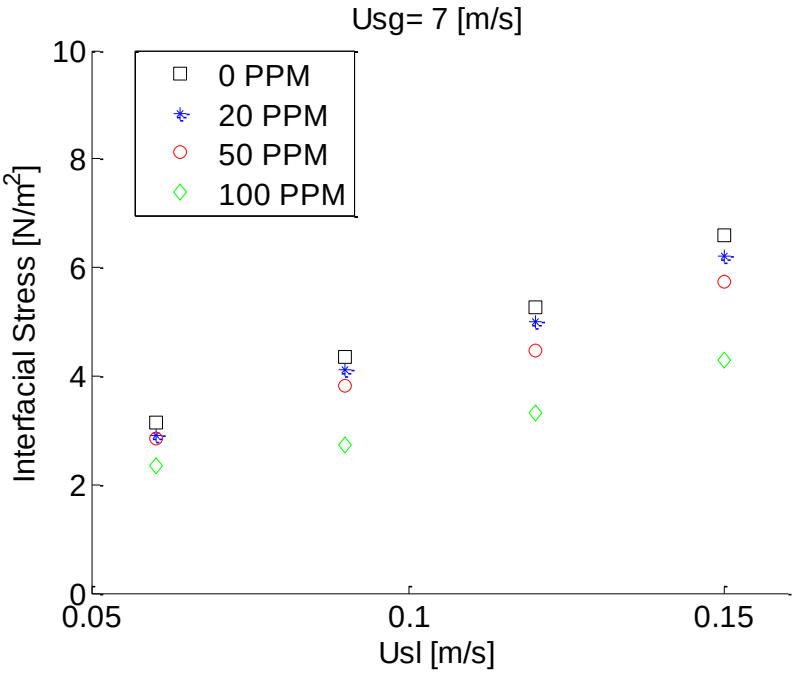

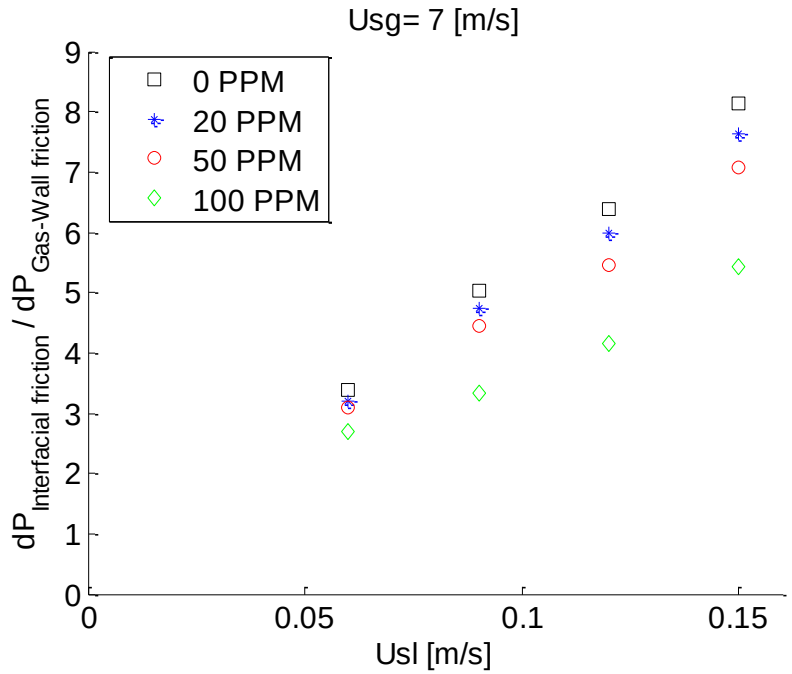

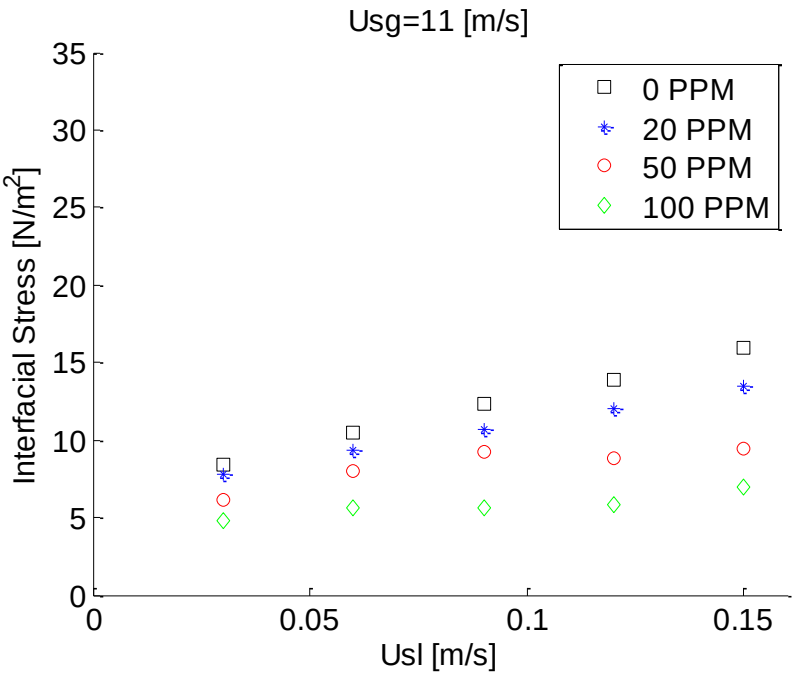
Usg=11 [m/s]
Interfacial Stress [N/m2]
Usl [m/s]
0 PPM
20 PPM
50 PPM
100 PPM
0
5
10
15
20
25
30
35
0
0.05
0.1
0.15

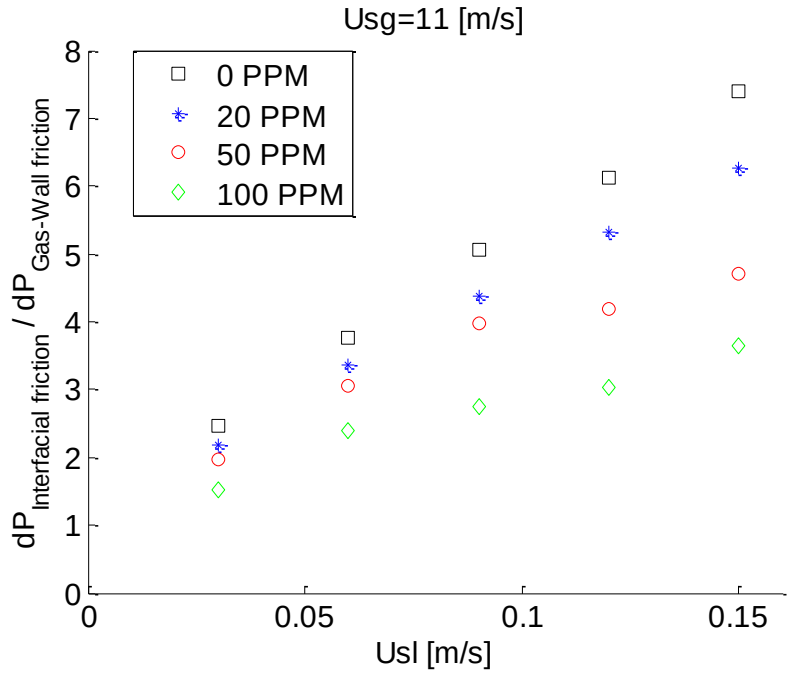
Usg=11 [m/s]
dP Interfacial friction / dP Gas-Wall friction
Usl [m/s]
0 PPM
20 PPM
50 PPM
100 PPM
0
1
2
3
4
5
6
7
8
0
0.05
0.1
0.15

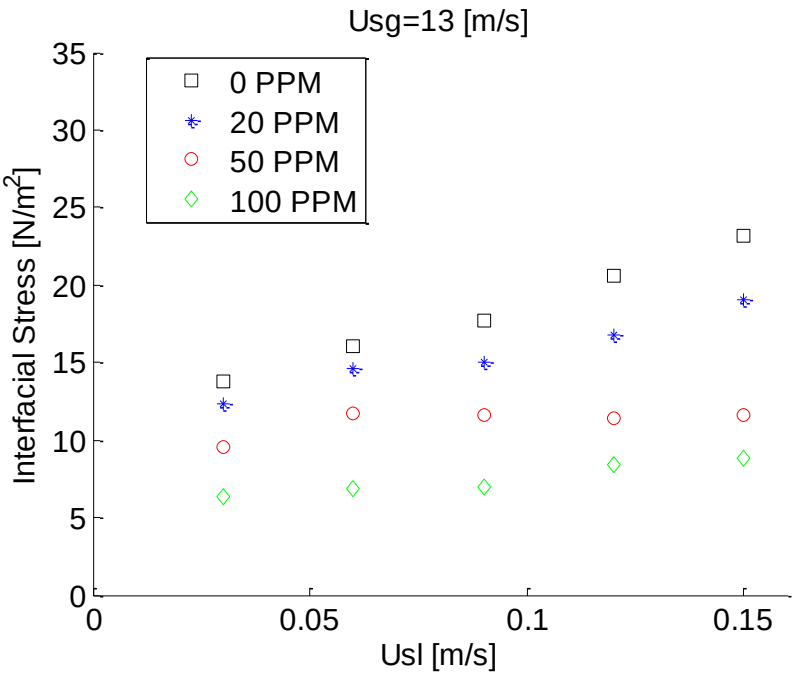
Usg=13 [m/s]
0 PPM
20 PPM
50 PPM
100 PPM
Interfacial Stress [N/m2]
Usl [m/s]
0
5
10
15
20
25
30
35
0
0.05
0.1
0.15

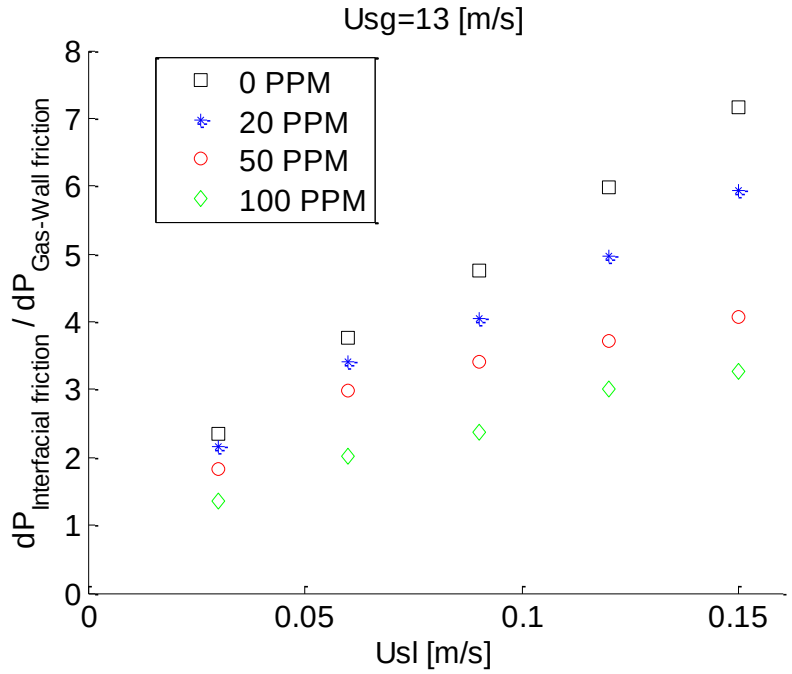
Usg=13 [m/s]
0 PPM
20 PPM
50 PPM
100 PPM
dP Interfacial friction / dP Gas-Wall friction
Usl [m/s]
0
1
2
3
4
5
6
7
8
0
0.05
0.1
0.15

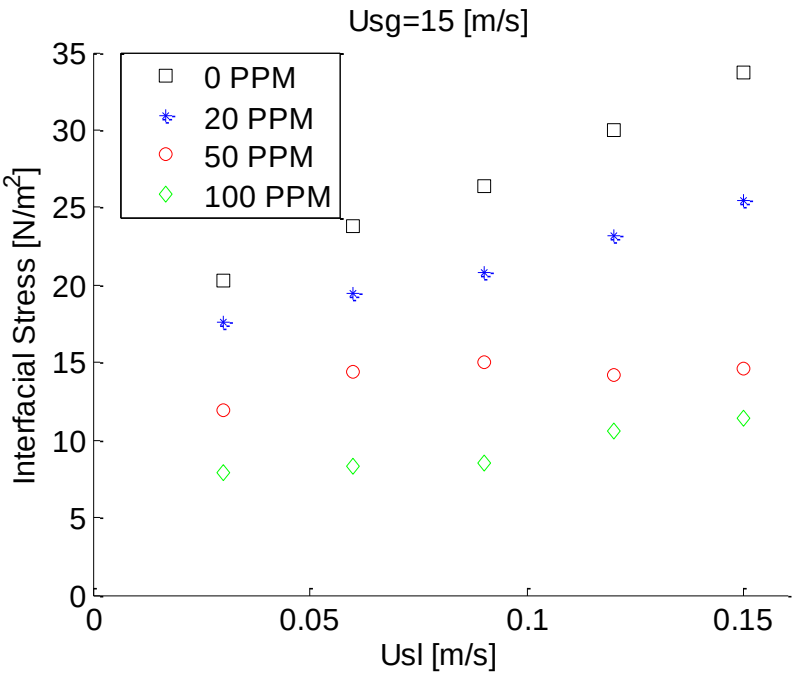
Usg=15 [m/s]
0 PPM
20 PPM
50 PPM
100 PPM
Interfacial Stress [N/m2]
Usl [m/s]
0
5
10
15
20
25
30
35
0
0.05
0.1
0.15

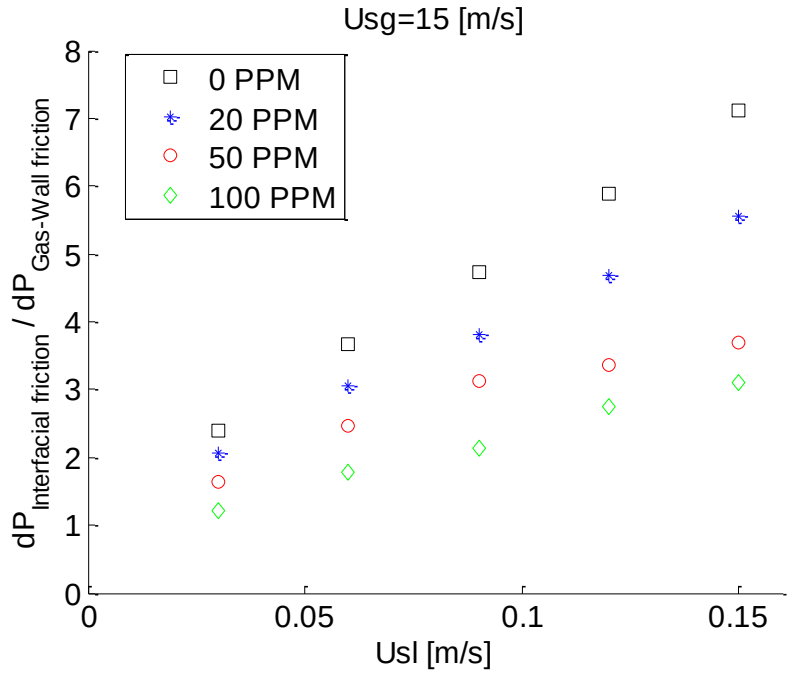
Usg=15 [m/s]
0 PPM
20 PPM
50 PPM
100 PPM
dP Interfacial friction / dP Gas-Wall friction
Usl [m/s]
0
1
2
3
4
5
6
7
8
0
0.05
0.1
0.15